(NASA-CR-134849) DEMONSTRATION OF SHORT-HAUL AIRCRAFT AFT NOISE REDUCTION TECHNIQUES ON A TWENTY INCH (50.8 cm) DIAMETER FAN, VOLUME 1 (General Electric Co.) 131 p HC A07/MF A01 CSCL 21E G3/07

N80-15083

Unclas 33460

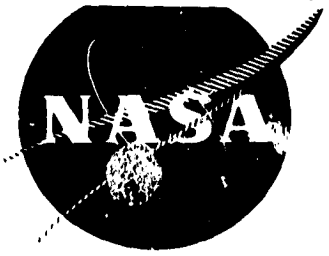

Demonstration of Short-Haul Aircraft Aft Noise Reduction Techniques on a Twenty Inch (50.8 cm) Diameter Fan

Volume I

By

D. L. Stimpert
R. A. McFalls

prepared for

NATIONAL AERONAUTICS AND SPACE ADMINISTRATION

NASA-Lewis Research Center
NAS3-18021

TABLE OF CONTENTS

TABLE OF CONTENTS (Concluded)

LIST OF FIGURES

LIST OF FIGURES (Continued)

LIST OF FIGURES (Continued)

LIST OF FIGURES (Concluded)

LIST OF TABLES

SECTION I

SUMMARY

A scale model test was conducted using a twenty inch (50.8 cm) diameter, low tip speed, low pressure ratio fan to assess the effect of source noise reduction techniques and advanced suppression concepts on aft radiated noise.

Source noise reduction techniques included the effects of spacing, effects of vane-blade ratio on the second harmonic, and the effect of Mach number through the vane row. At 0.5 chord spacing it was demonstrated that the farfield second harmonic level was minimized at a vane-blade ratio of 1.87; but there was no significant difference between the various vane-blade ratios at 1.5 chord. No significant reduction in fan broadband noise levels was observed by decreasing the Mach number through the vanes; however, this may be due to the levels at wide spacing being controlled by rotor-turbulence noise and not rotor-stator interaction noise.

Aft suppression tests indicated low (12%) porosity faceplate designs achieved higher peak suppression and wider bandwidth than did high (27%) porosity designs. Variable depth treatment was shown to be somewhat more effective than constant thickness treatment. The amount of suppression achieved with variable depth treatment was somewhat dependent upon whether the panels were oriented thin-to-thick or thick-to-thin. Variations in duct Mach number up to a maximum of about 0.53 indicates no apparent flow noise contribution.

SECTION II

INTRODUCTION

General Electric Company is currently engaged in the Quiet, Clean Short-haul Experimental Engine (QCSEE) Program under Contract NAS3-18021 to NASA Lewis Research Center. A major objective of the QCSEE Program is to develop and demonstrate the technology required to meet the stringent noise requirements anticipated for commercial turbofan short-haul aircraft.

An extensive series of component tests are being conducted to enable a better assessment of the various engine noise sources and advanced suppression concepts. Among these is the Scale Model Fan Test Program which investigated aft radiated source noise reduction and aft duct treatment design.

The program was conducted in the General Electric Anechoic Chamber using a 20-inch (50.8 cm) diameter 1.2 pressure ratio, 700 feet per second (213 meters per second) tip speed fan provided by NASA Lewis.

Volume I of this report presents the test configurations, test facility, vehicle, and data acqusition and reduction systems plus selected comparisons and initial engineering analysis of the data. Volume II presents the 1/3 octave band data in the form of computer plots of the major configurations and obvious comparisons. The standard package of plots includes

- PNL versus angle at 2 fan speeds
- PWL versus frequency at 2 fan speeds
- SPL versus frequency at 2 aft angles and 2 fan speeds

In addition, the source noise data package includes the following plots:

- BPF SPL versus acoustic angle at 2 fan speeds
- 2nd harmonic versus acoustic angle at 2 fan speeds

Volume III presents all the 1/3 octave band model data for all configurations. The data are given for both a 17 foot (5.18 m) arc and extrapolated to a 200 foot (60.96 m) sideline.

A subsequent report will provide a more detailed engineering analysis of the results and the impact of those results on the design of the full size QCSEE engine.

SECTION III

TEST FACILITY

This test was conducted in the anechoic environment of the General Electric Corporate Research and Development Aero/Acoustic Facility in Schenectady, New York. An overview of the facility is shown in Figure 1. A photograph of the facility is presented in Figure 2. It is comprised of:

1. A 2500 HP drive system for speeds up to 26,000 RPM

2. An anechoic chamber approximately 35 feet (10.67m) wide by 25 feet (7.62m) long by 10 feet (3.05m) high designed for less than $\pm$ 1 dB standing wave ratio at 200 Hz. All walls, floor, and ceiling are covered with an array of 28 inch (71.1cm) polyurethane foam wedges.

3. Porous walls for minimum inflow distortion to the fan when measuring inlet radiated noise.

4. Ability to install the fan for evaluation of both forward and exhaust radiated noise.

5. Farfield noise measurement on a 17 foot (5.2m) arc from 0 to 110° relative to the inlet for inlet radiated noise and nominally 60° to 160° relative to the inlet when measuring exhaust radiated noise.

The sound field is set up with the center of the arc located assuming the source location to be at the inlet face during tests of inlet radiated noise levels. For the exhaust radiated measurements on this test the source was not located at the same point due to the long exhaust duct. Table I presents the corresponding angles and distances to each microphone for both the long and short duct configurations.

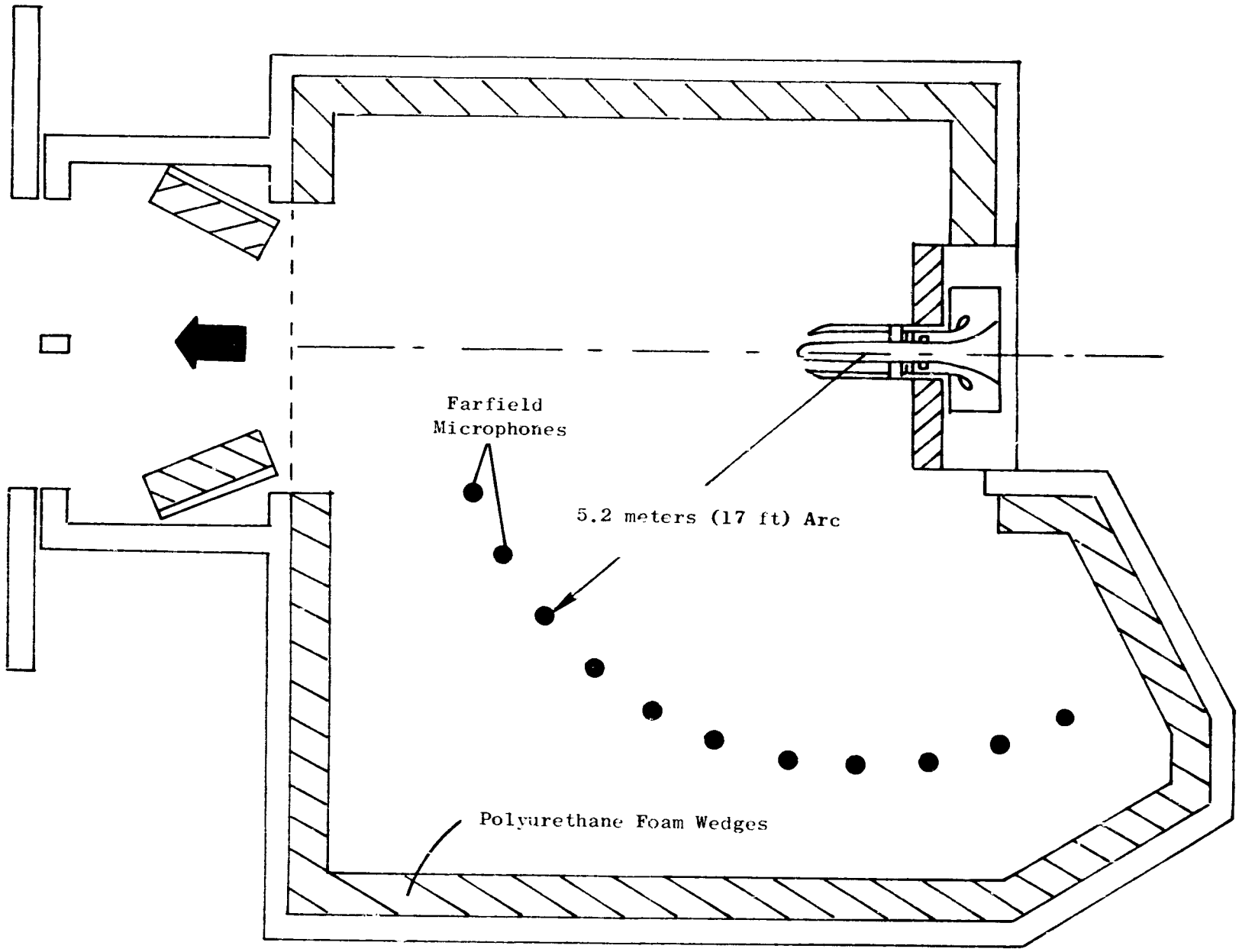

FIGURE 1 SCHEMATIC OF GENERAL ELECTRIC COMPANY ANECHOIC CHAMBER

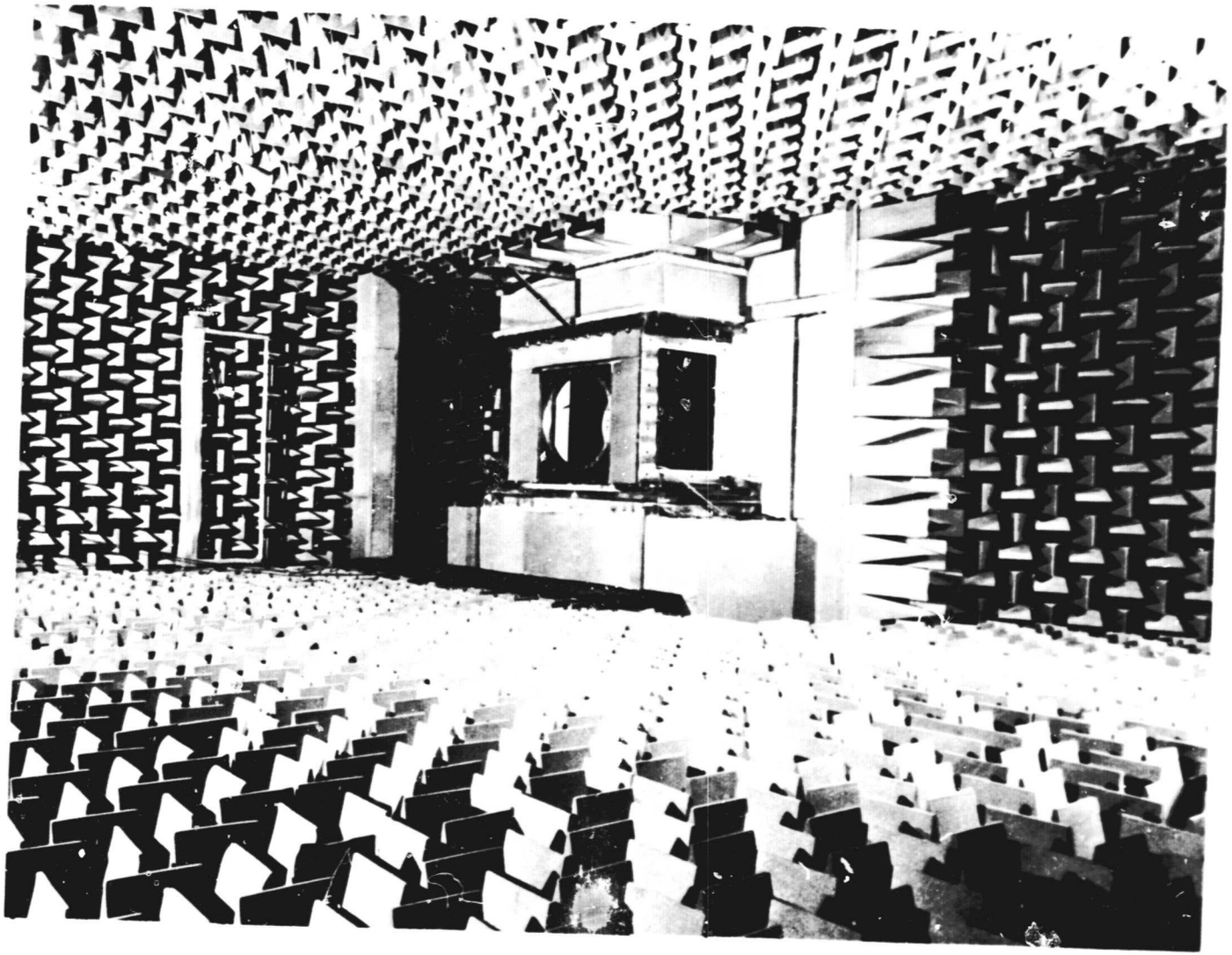

FIGURE 2 GENERAL ELECTRIC COMPANY ANECHOIC CHAMBER

TABLE I - FARFIELD MICROPHONE DISTANCES & ANGLES

- EXHAUST RADIATED NOISE
- ANGLES RELATIVE TO INLET

Nominal Distance Feet (Meters)	Angle Degrees	Short Duct Distance Feet (Meters)	Angle Degrees	Long Duct Distance Feet (Meters	Angle Degrees
17 (5.18)	160	16.58 (5.05)	159.3	14.41 (4.39)	156.2
17 (5.18	150	16.63 (5.07	148.9	14.65 (4.47)	144.5
17 (5.18)	140	16.69 (5.09)	138.6	14.97 (4.56)	133.1
17 (5.18)	130	16.77 (5.11)	128.4	15.36 (4.68)	122.0
17 (5.18)	120	16.86 (5.14)	118.1	15.79 (4.81)	111.2
17 (5.18)	110	16.96 (5.17)	108.0	16.26 (4.96)	100.7
17 (5.18)	100	17.07 (5.20)	97.9	16.74 (5.10)	90.5
17 (5.18)	90	17.18 (5.24)	87.9	17.23 (5.25)	80.7
17 (5.18)	80	17.29 (5.27)	78.9	17.70 (5.39)	71.1
17 (5.18)	70	17.39 (5.30)	68.1	18.15 (5.53)	61.7
17 (5.18)	60	17.49 (5.33)	58.2	18.55 (5.65(	52.5

SECTION IV

TEST HARDWARE

A schematic of the test vehicle is presented in Figure 3 and a vehicle installation drawing is shown in Figure 4. The airflow and noise source for these tests was a twenty inch (50.8 cm) diameter fan designated Rotor 55 which was supplied by NASA Lewis Research Center. Fan parameters are presented in Table II and the rotor, shown in the photograph in Figure 5, was mounted in a front drive configuration. The rotor blades were closed 6 degrees (.10 rad) from nominal for these tests due to a clutch cooling capacity limit.

Initial checkout and selected subsequent tests were conducted with the original vane row designed with Rotor 55 and which had 11 vanes. Two additional vane rows were manufactured. The first (hereafter referred to as the baseline vanes) was designed to enable investigation of the effects of vane/blade ratio from 1.63 to 2.07. The number of vanes selected for the baseline design was 25 and the chord length of these vanes was ratioed inversely (11/25) as the number of vanes to the chord of the original Stage 55 vanes. To vary the vane-blade ratio with these baseline vanes, inner and outer rings were manufactured to house from 25 to 31 (V/B = 1.67 to 2.07) baseline vanes. The effects of axial spacing between blade and vane row on noise was also evaluated with 28 baseline vanes.

The second vane row designed incorporated a flowpath with a larger annulus area through the vanes to investigate the effect of lowering the Mach number through the vanes. It was desirable to use a maximum annulus area opening consistent with not aerodynamically overloading the walls or vanes and to cover the anticipated area opening available within the existing ground rules or the QCSEE propulsion system. An acceptable predicted loading level resulted from an increased solidity, 31 vane configuration in conjunction with an 11% area increase at the OGV inlet. Also, since the baseline vanes would be tested in a 31 vane configuration, a direct performance comparison would be obtainable. Table III shows the design diffusion factors for the 25 and 31 vane low Mach configurations relative to the 25 and 31 vane baseline configuration. A modest loading increase in the hub of the low Mach vanes was predicted going from 35 baseline vanes to 31 low Mach vanes. Figure 6 compares the low Mach and baseline configuration flowpaths.

Both vane sets were designed using the same NACA 400 series airfoils employed in the original design. The radial distributions of t_m/c differed from the stage 55 vanes as indicated below:

	t_m/c		
	Tip	Pitch	Hub
Stage 55	.09	.09	.09
Baseline	.125	.081	.102
Low Mach	.115	.085	.115

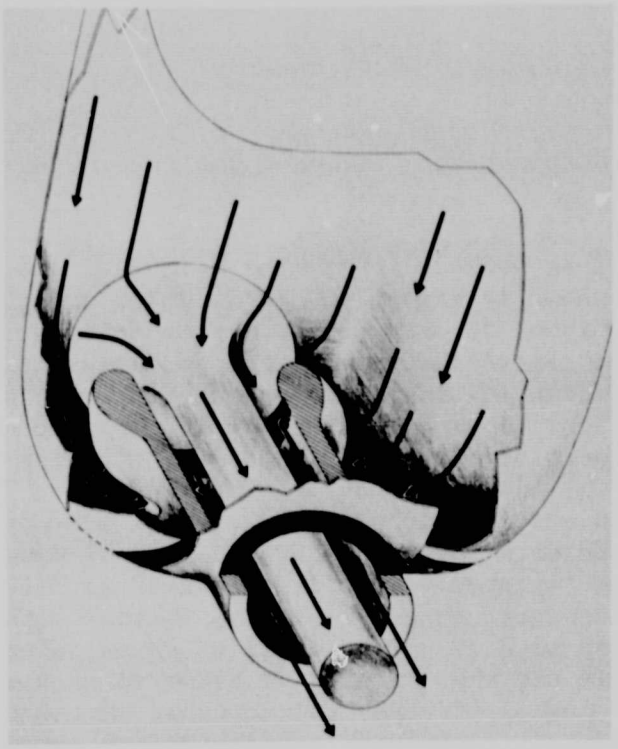

See Insert Above

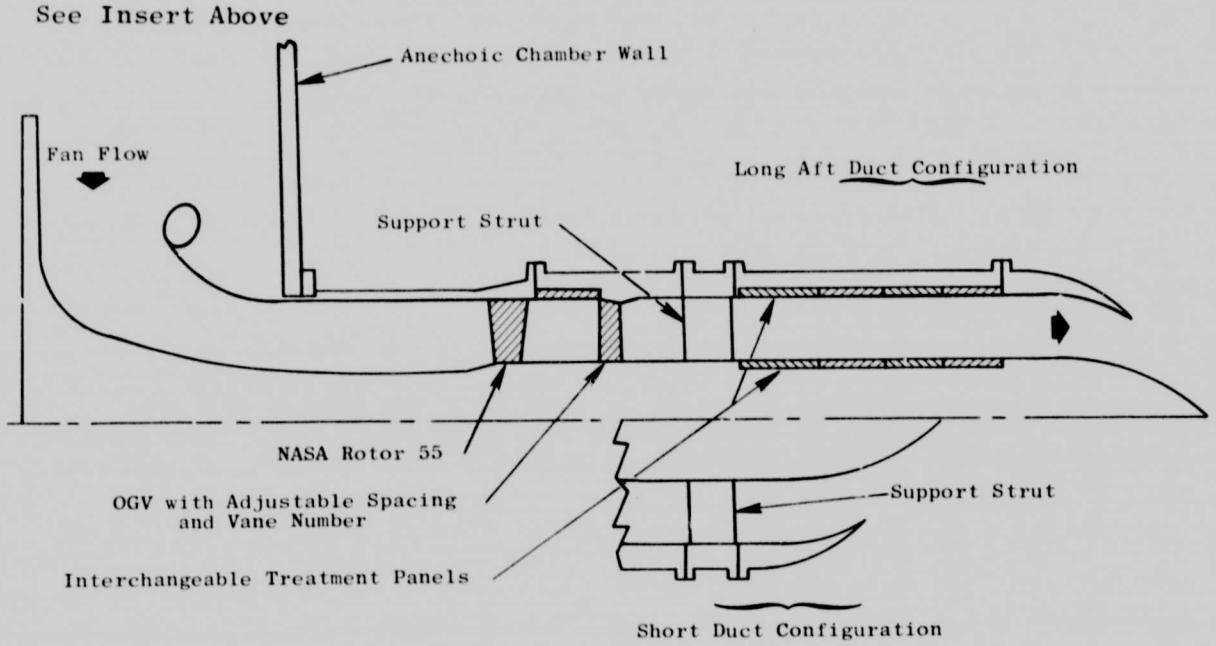

FIGURE 3 TEST VEHICLE SCHEMATIC

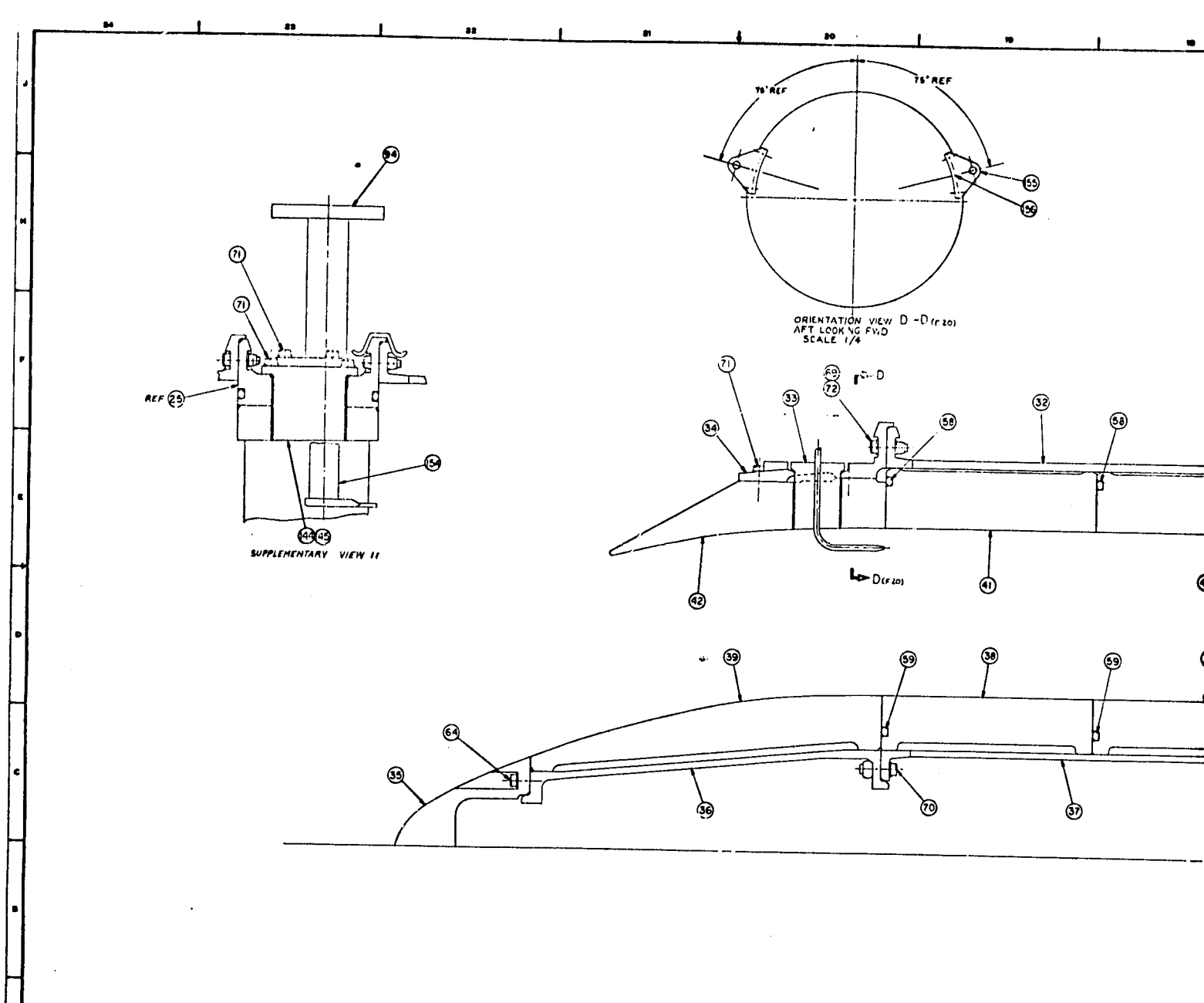

FIGURE 4 SCALE MODEL FAN TEST VEHICLE INSTALLATION DRAWING (SHEET 1 OF 2).

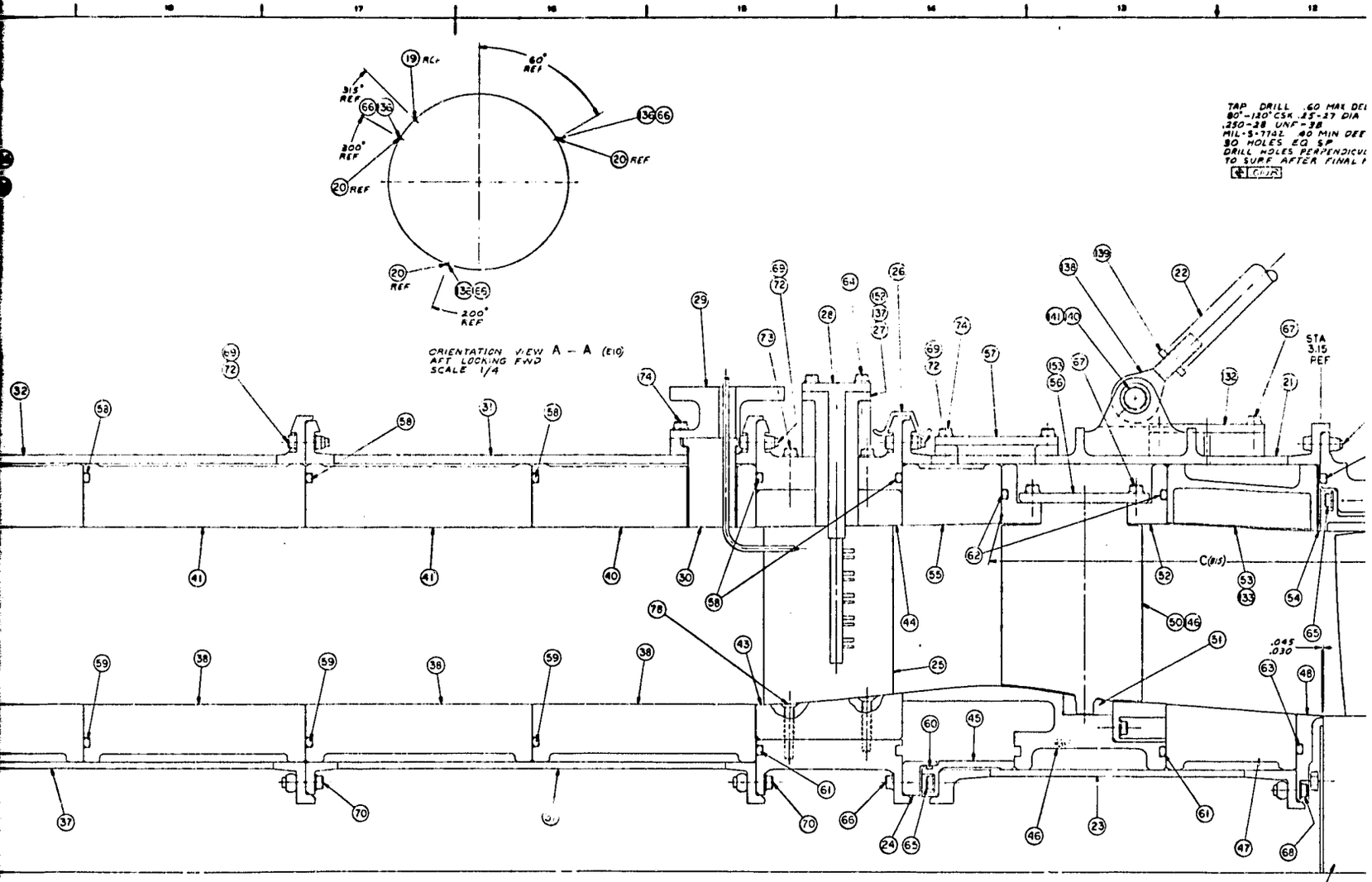

TAP DRILL .60 MAX DEP
80°–120° CSK .25-27 DIA
.250-28 UNF-3B
MIL-S-7742 .40 MIN DEP
30 HOLES EQ SP
DRILL HOLES PERPENDICU
TO SURF AFTER FINAL

ASSY IDENT NO	APPLICABLE SUPPLEMENTARY VIEWS OTHERWISE SAME AS ITEM 1	C (E13) REF
4013151-600G01	—	12.152
G02	3	10.146
G03	3	10.146
G04	3	10.146
G05	3	10.146
G06	3	10.146
G07	3	10.146
G08	3	10.146
G09	1	10.146
4013151-600G10	—	12.152

ASSY IDENT NO	APPLICABLE SUPPLEMENTARY VIEWS OTHERWISE SAME AS ITEM 1	C (E13) REF
4013151-600G11	2	8.277
G12	10	12.017
G13	3	10.146
G14	9	10.146
G15	8	10.146
G16	4	10.146
G17	5	10.146
G18	4	10.146
4013151-600G19	6	10.146

SIZE J | 4013151-600 | SHEET 1 REV

1 OF 2).

FOLDOUT FRAME 2

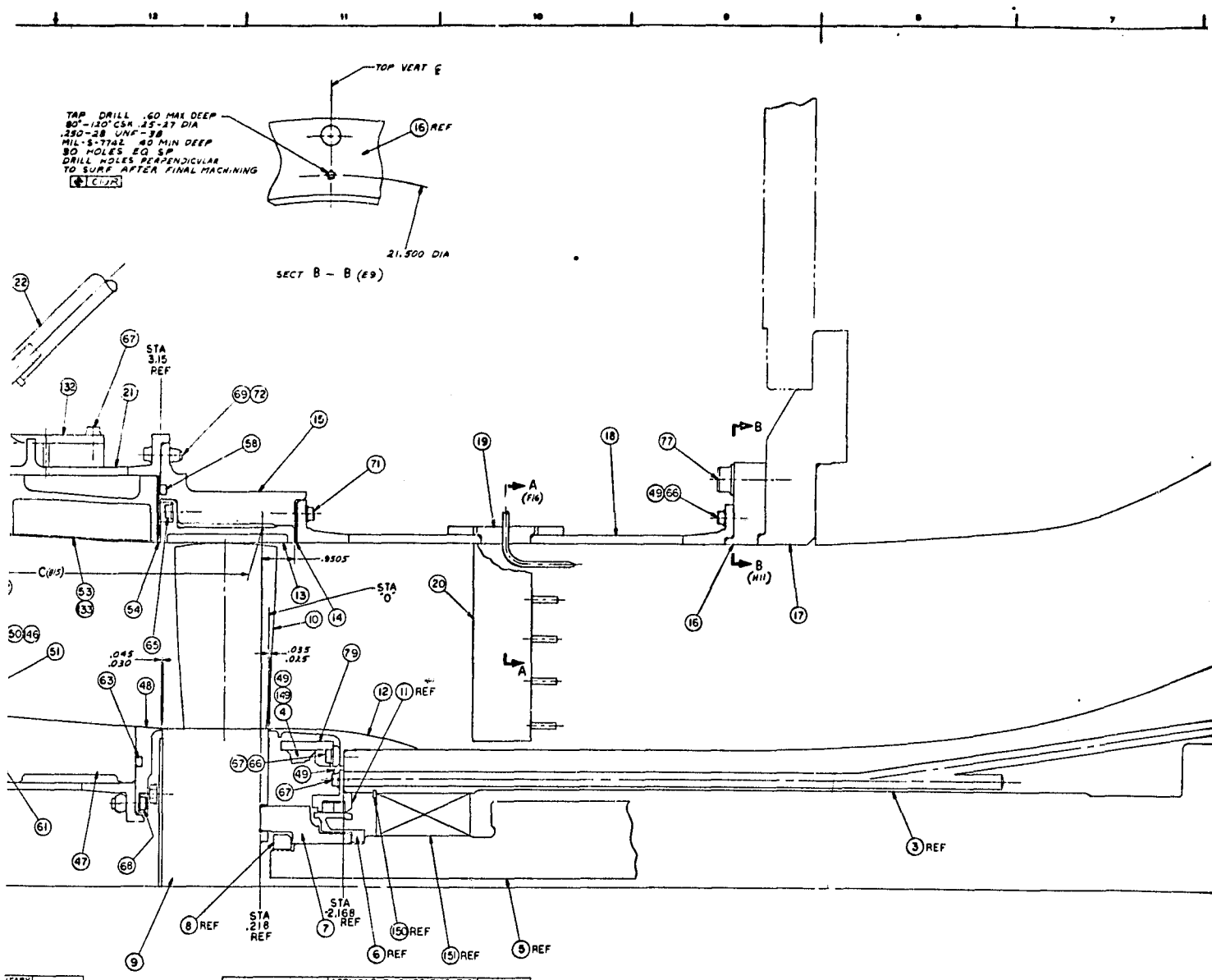

ITARY ME	C (E13) REF
	8.277
	12.017
	10.146
	10.146
	10.146
	10.146
	10.146
	10.146
	10.146

ASSY IDENT NO	APPLICABLE SUPPLEMENTARY VIEWS OTHERWISE SAME AS ITEM 1	C (E13) REF
4013151-600G20	7	10.146
G21	—	12.152
G22	8	10.146
G23	1	10.146
G24	—	12.152
G25	10	12.017
G26	3	10.146
G27	11	12.152
4013151-600G28	11	12.152

SIZE	DWG NO	SHEET	REV
J	4013151-600	1	

FOLDOUT FRAME 1

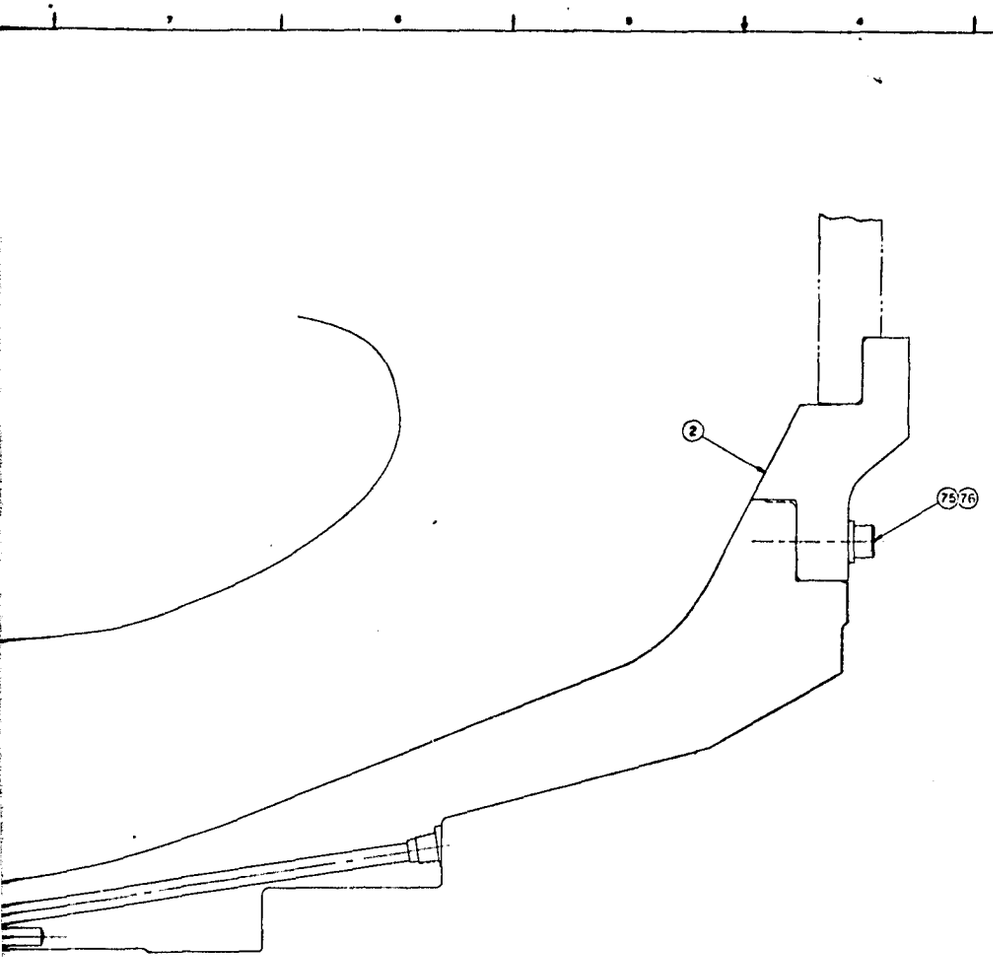

DUPLICATE TRACING

2 THICKNESS OF ITEM 54 (B12) TO BE ADJUSTED TO OBTAIN DIM C (E13)

4 MUST CONFORM TO:

P1T93 CL-A	(INTERPRETATION OF DWG)
P1T99 CL-A	(MACHINED FEATURES)
AS567	(LOCKWIRE)
P127F2 CL-A	(ASSEMBLY TORQUES)

TO BE CHG BY D-CID ONLY

ASSEMBLY — SEE SEPARATE PARTS LIST

GENERAL ELECTRIC AIRCRAFT ENGINE GROUP CINCINNATI, OHIO, U.S.A.

QCSEE

20 INCH SCALE MODEL

J 07482 4013151-600

SHEET 1 OF 2

4013151-600

FOLDOUT FRAME 2

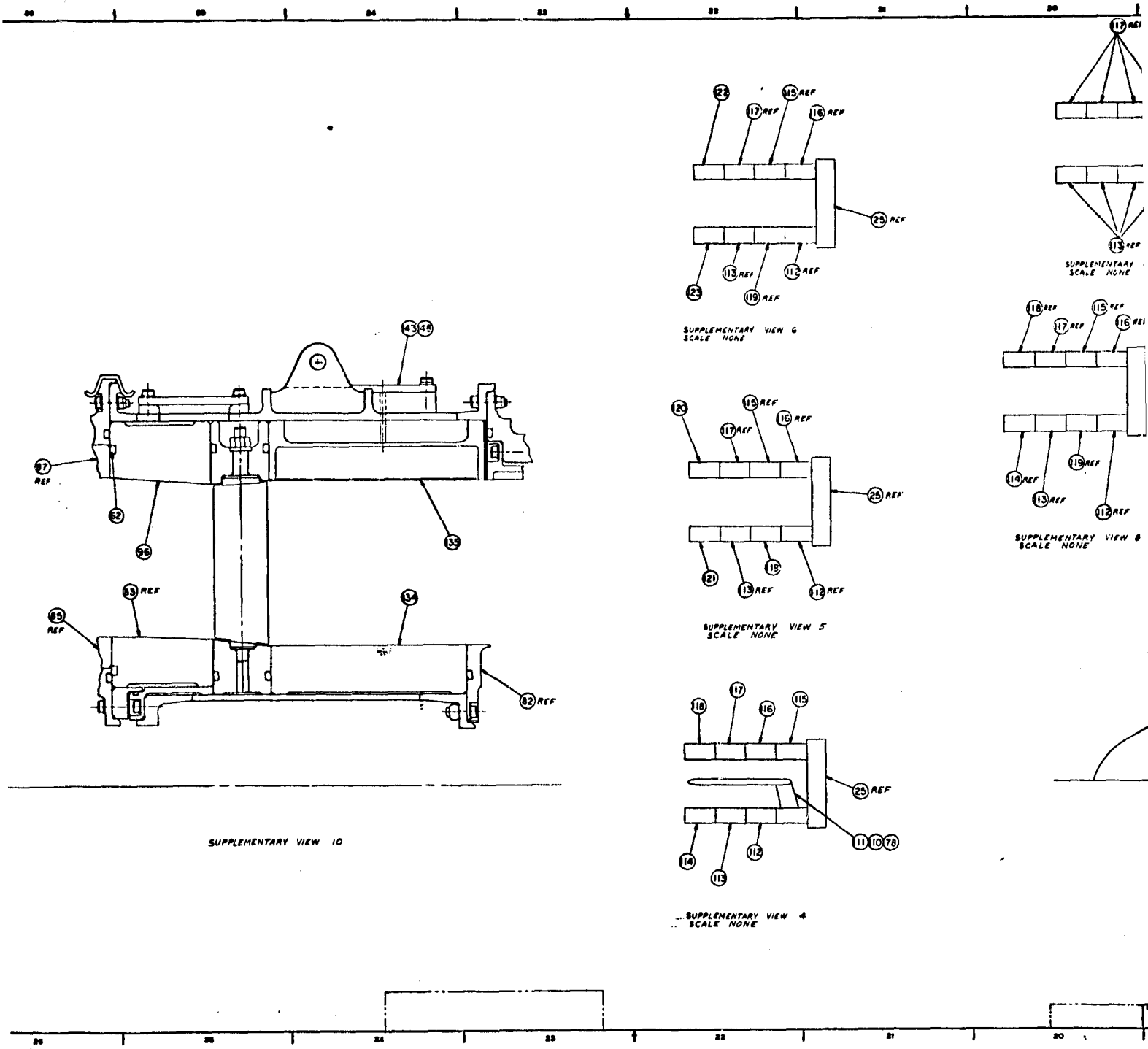

FIGURE 4 SCALE MODEL FAN TEST VEHICLE INSTALLATION DRAWING (SHEET 2 OF 2).

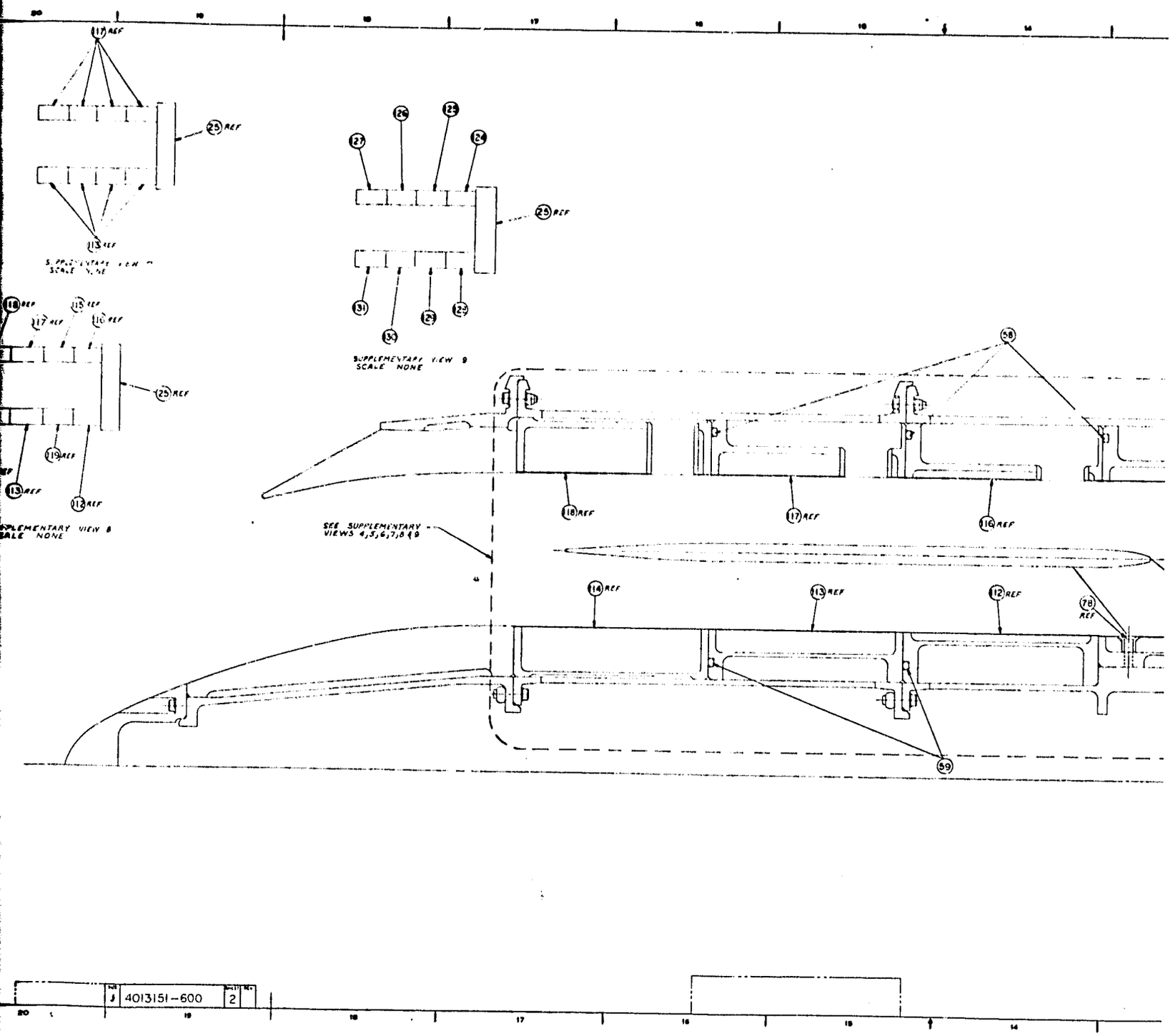

	J	4013151-600	2

OF 2).

FOLDOUT FRAME

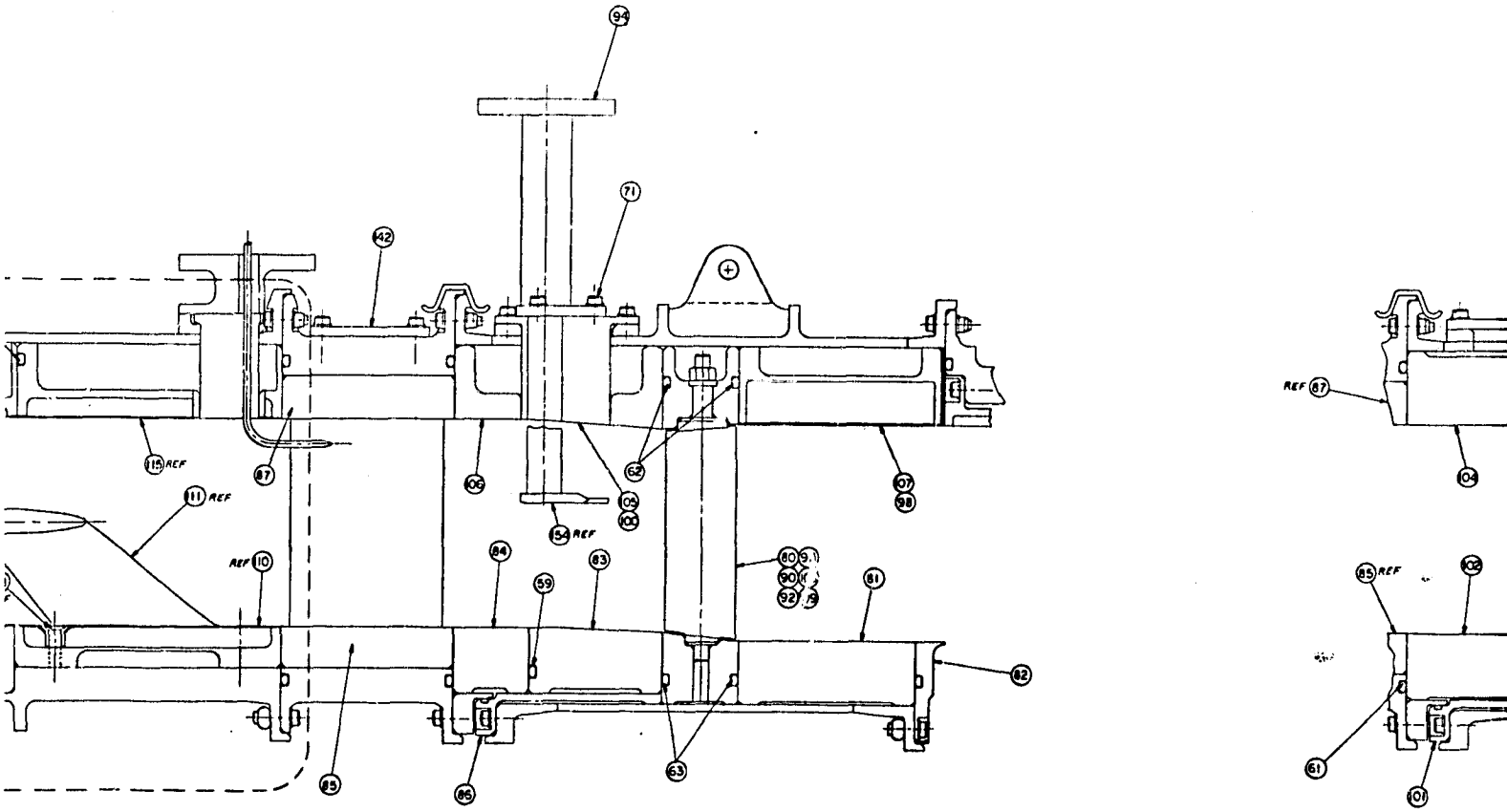

SUPPLEMENTARY VIEW 3

FOLDOUT FRAME 1

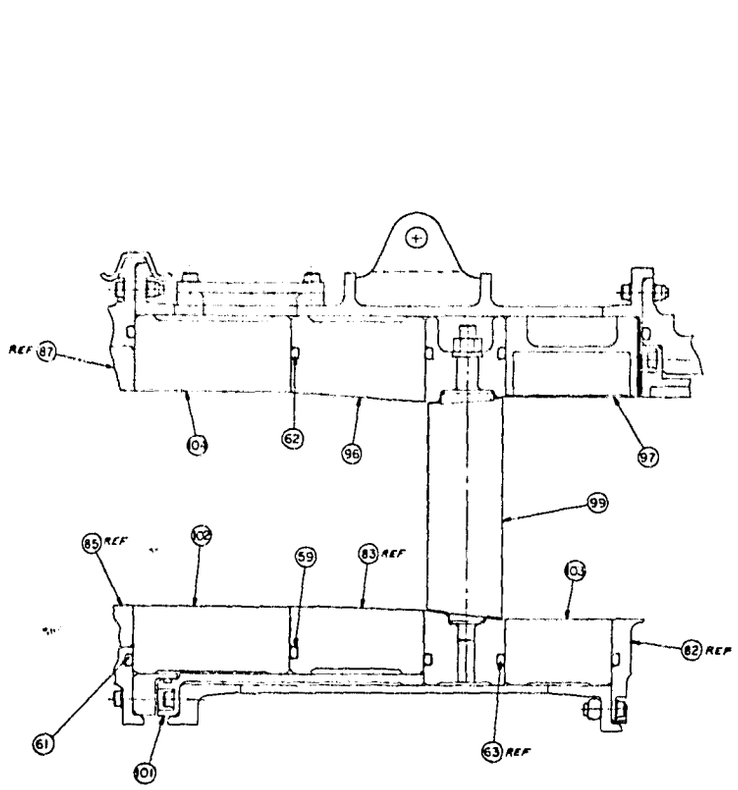

SUPPLEMENTARY VIEW 2

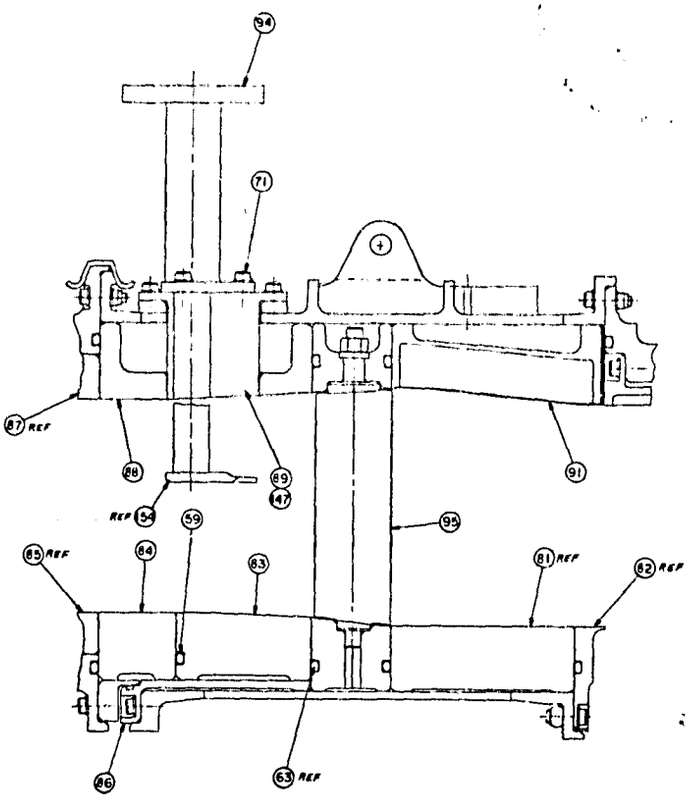

SUPPLEMENTARY VIEW 1

SEE SHEET 1 FOR APPLICABLE NOTES

TO BE CHG BY D-CID ONLY

J	4013151-600	2	

ASSEMBLY — SEE SEPARATE PARTS LIST

GENERAL ELECTRIC AIRCRAFT ENGINE GROUP CINCINNATI, OHIO U.S.A.

QCSEE
20 INCH SCALE MODEL

J	07482	4013151-600

FOLDOUT FRAME

TABLE II - FAN PARAMETERS

• Inlet Guide Vanes		None
• Fan Diameter		20 inches (50.8cm)
• Stage Pressure Ratio (100% N/ $\sqrt{\theta}$)		1.16
• Tip Speed (100% N/ $\sqrt{\theta}$)		700 fps (213 m/sec)
• Fan Speed (100% N/ $\sqrt{\theta}$)		8021 rpm
• Pitch Angle (Degrees Closed from Nominal)		+6°
• Weight Flow		59.5 lbm/sec (27.0 kgm/sec)
• Number of Stators	(Stage 55)	11
	(Baseline Vanes)	25,26,27,28,29,30,31
	(Low Mach)	31
• Spacing	(Stage 55)	1.5 true rotor tip chords
	(Baseline Vanes)	0.5,1.0,1.5,2.0
	(Low Mach Vanes)	1.5
• Radius Ratio		0.46

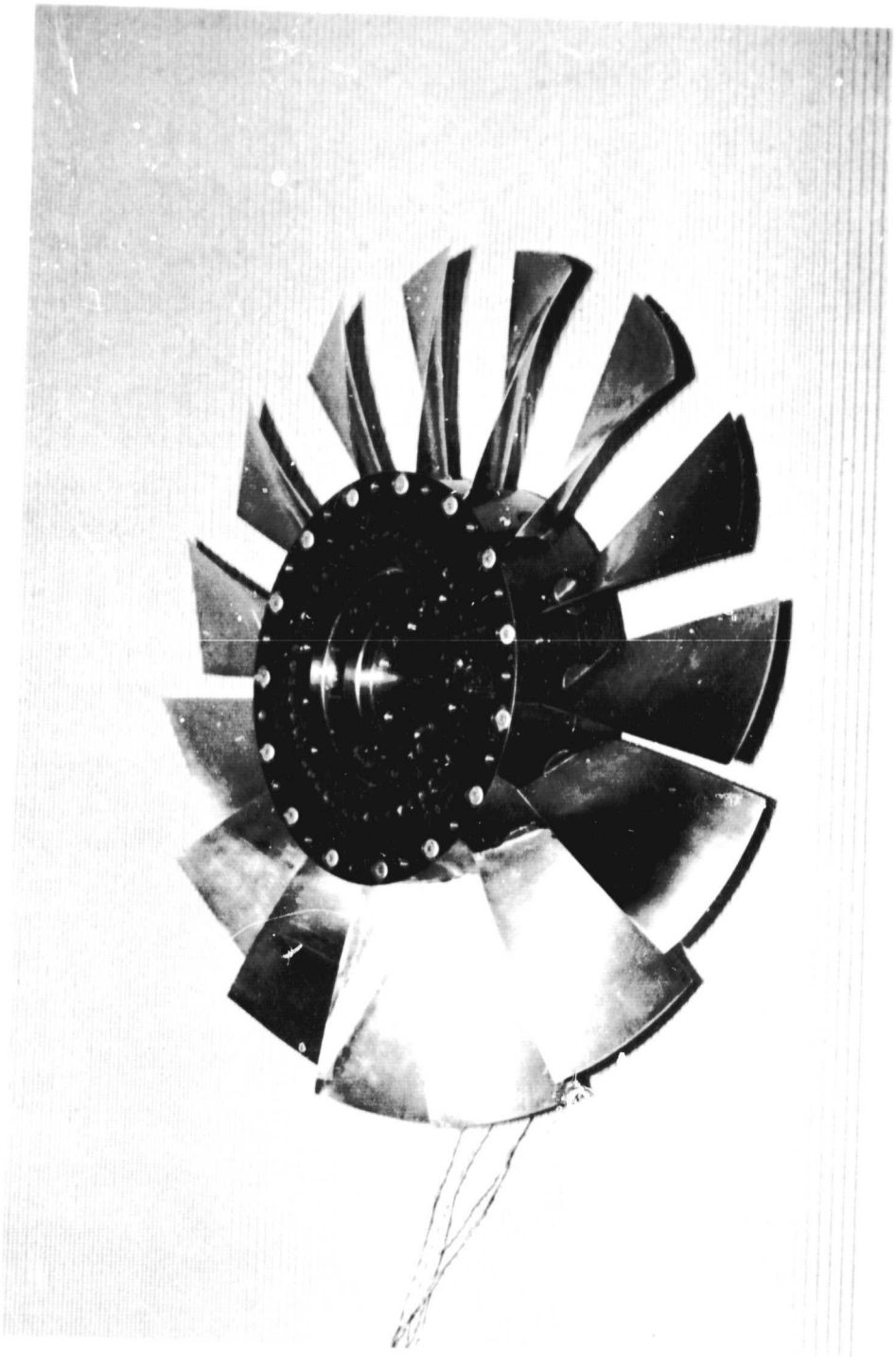

FIGURE 5 NASA LEWIS RESEARCH CENTER ROTOR 55

TABLE III - LOW MACH AND BASELINE VANE DIFFUSION FACTORS

Stream Function	Percent Immersion	Diffusion Factor			
		Low Mach Vanes		Baseline Vanes	
		25	31	25	31
0	0	.3510	.2843	.3073	.2470
0.07	5.1	.3507	.2889	.3134	.2571
0.13	9.5	.3580	.2988	.3198	.2656
0.20	14.8	.3640	.3075	.3264	.2741
0.39	29.7	.3798	.3279	.3455	.2962
0.61	49.0	.3904	.3439	.3560	.3107
0.79	68.1	.3961	.3557	.3533	.3129
0.91	84.4	.4156	.3784	.3511	.3130
0.94	89.2	.4215	.3852	.3461	.3090
0.97	94.4	.4343	.3965	.3469	.3081
1.00	100.0	.4565	.4177	.3572	.3170

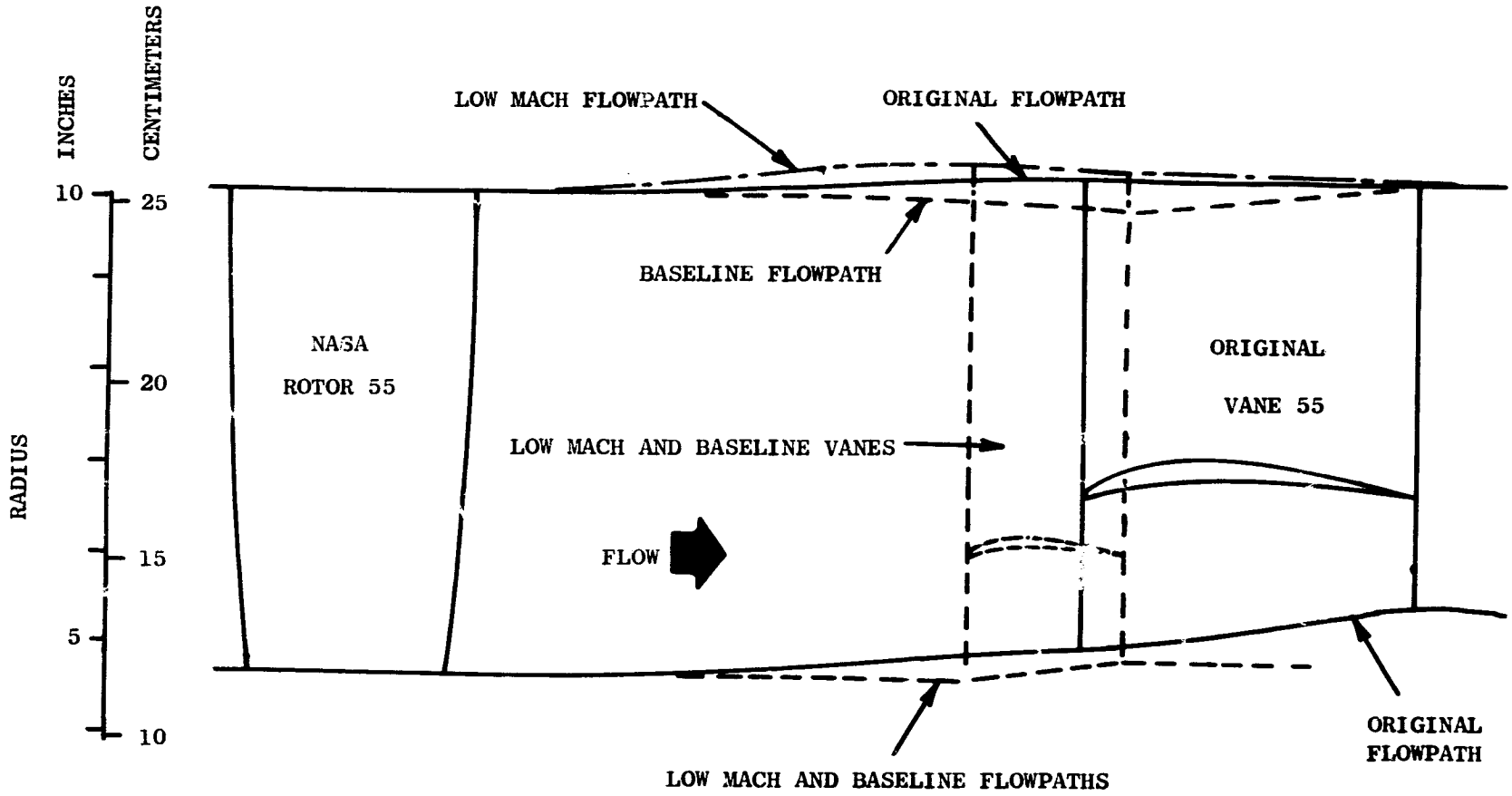

Figure 6 FAN STAGE FLOWPATHS

The t_m/c values were changed to satisfy mechanical design requirements relative to vane frequency characteristics.

Spacing, low Mach vane, and baseline vane-blade ratio tests were conducted with a short hardwall aft duct. Tests with Stage 55 utilized a long hardwall aft duct. These aft ducts are shown schematically in Figure 3.

All aft suppression tests were conducted with the long aft duct version of the test vehicle. A photograph is shown in Figure 7. The long aft duct was designed to hold four pairs (inner and outer) of interchangeable treatment panels. The panels themselves were of various thicknesses and porosities. Also manufactured as part of the aft suppression tests was a 0.6 inch (1.52 cm) thick splitter which had a treatment length L/H of 5.2. Treatment panel parameters are summarized in Table IV.

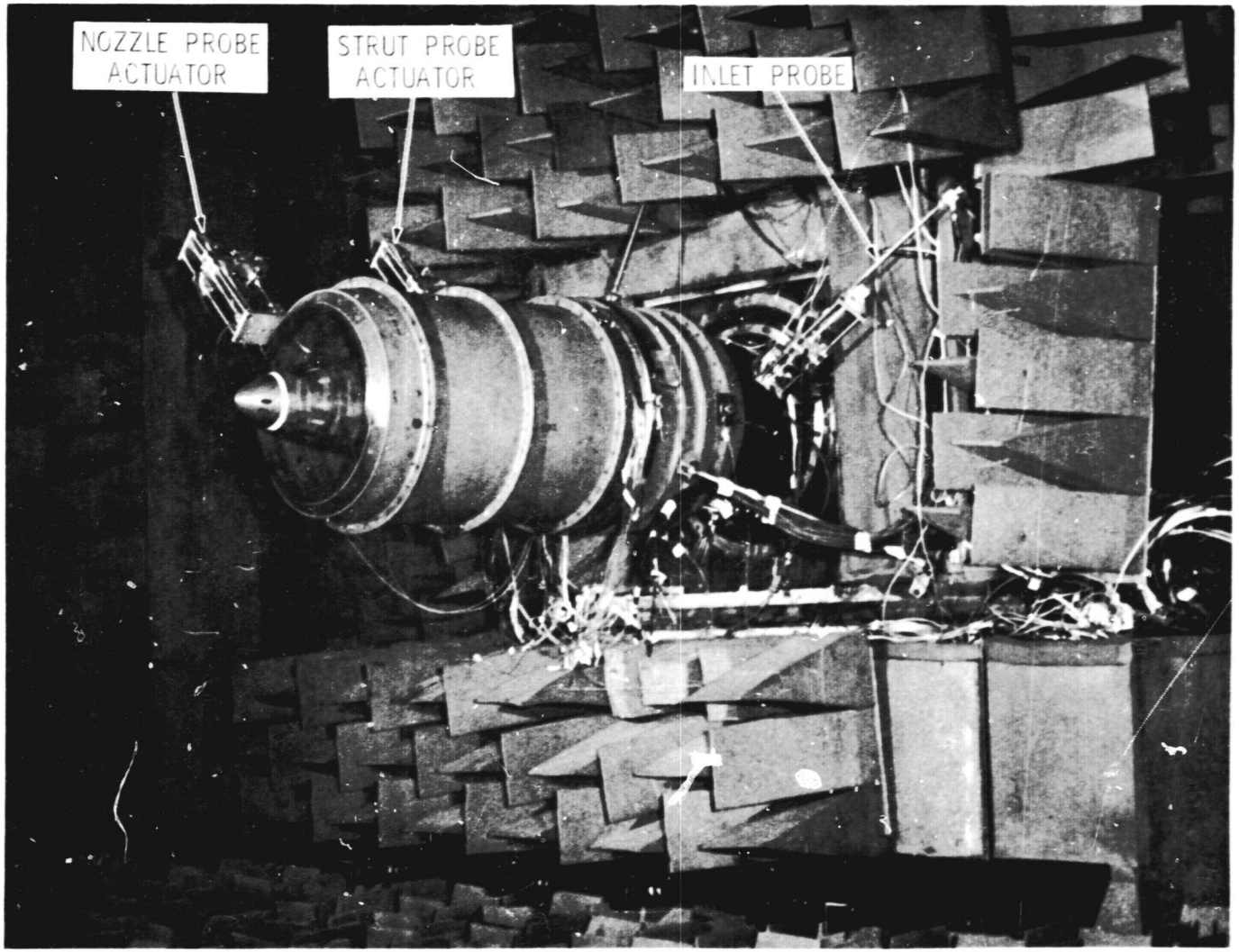

FIGURE 7 SCALE MODEL FAN TEST VEHICLE INSTALLED IN THE GENERAL ELECTRIC COMPANY ANECHOIC CHAMBER

TABLE IV. TREATMENT PANEL PARAMETERS

Treatment Depth in. (cm)	Open-Area Ratio percent	Hole Diameter in. (cm)	Faceplate Thickness in. (cm)	Tuning Frequency Hz
0.25 (0.64)	12	0.050 (0.127)	0.032 (0.081)	5000
0.50 (1.27)	12	0.050 (0.127)	0.032 (0.081)	3150
0.75 (1.91)	12	0.050 (0.127)	0.032 (0.081)	2500
1.50 (3.81)	12	0.050 (0.127)	0.032 (0.081)	1600
0.25 (0.64)	27	0.032 (0.081)	0.018 (0.046)	6300
0.50 (1.27)	27	0.032 (0.081)	0.018 (0.046)	4000
0.75 (1.91)	27	0.032 (0.081)	0.018 (0.046)	3150
1.00 (2.54)	27	0.032 (0.081)	0.018 (0.046)	2500
1.50 (3.81)	27	0.032 (0.081)	0.018 (0.046)	2000
*1.0 (2.54)	27	0.032 (0.081)	0.018 (0.046)	2000

*Slant cell treatment - cavity length 1.5 in. (3.81 cm)

SECTION V

DATA ACQUISITION AND PROCESSING

A. Data Acquisition

1. Aerodynamic

Aerodynamic data were recorded in three modes. Mode 1 included wall static pressure taps, and fixed radial rakes. Mode 2 included wall static pressures, fixed radial rakes, and a traversing arc rake. Mode 3 encompassed only wall static pressures. Basic pressure data were individually sampled through use of two 48 channel scanivalve systems and temperature data were sampled directly through a Hewlett Packard crossbar scanner and digital voltmeter.

During the aft suppression tests, a kiel probe was traversed downstream of the splitter to determine splitter losses. This pressure information was plotted on-line on an X-Y plotter.

Location and types of aerodynamic instrumentation are shown in Figure 8.

2. Acoustic

Farfield microphones were calibrated with a pistonphone with the calibration recorded on magnetic tape. Sound from farfield microphones and wall kulites was recorded simultaneously for at least one minute at each data point using a 28 track Sangamo recorder which has a 40 kHz capability in the FM mode at 60 inches per second (152 cm per second) tape speed. All acoustic probes were retracted to the wall during farfield noise measurements. Repeat data points (with few exceptions) were taken at fan speeds of 70 and 100 percent for all configurations.

Kulite phase shift relation calibrations were determined by applying a pressure on each kulite simultaneously and observing the direction of the DC shift and by inserting a clipped sine wave signal into the amplifier of all kulites simultaneously with the results recorded on tape.

B. Data Reduction

1. Aerodynamic

Data was recorded and reduced in three modes. Mode 1 was used when the fixed inlet and discharge rakes were installed. Pressures and temperatures sensed by the rakes were averaged circumferentially, and radial mass-

- Circumferential Locations Indicated are Clockwise, Aft Looking Forward

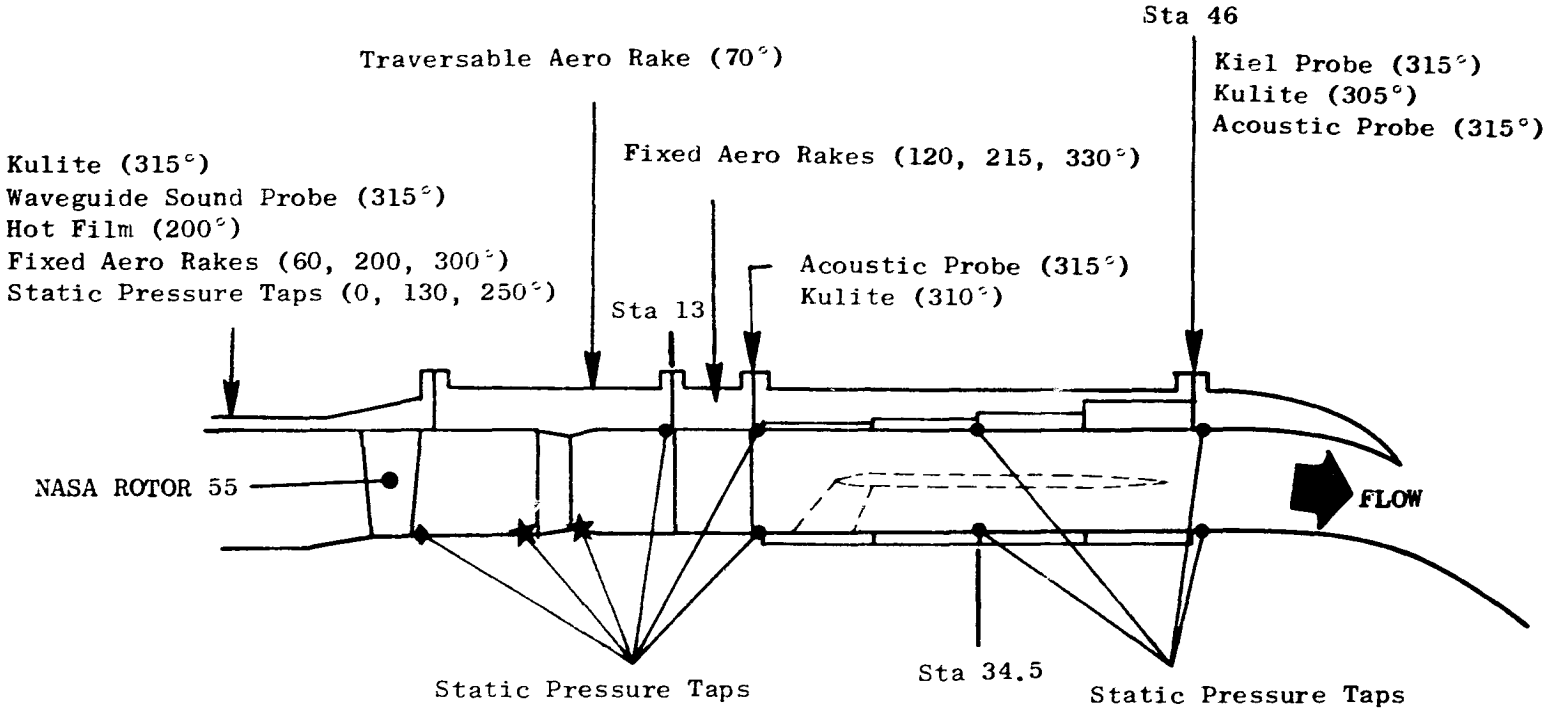

FIGURE 8 LOCATION OF ACOUSTIC AND AERODYNAMIC INSTRUMENTATION

averaging was used to obtain overall stage discharge conditions. The basic performance parameters of airflow, pressure ratio and efficiency were computed in this mode.

Mode 2 was designed for use with the traversing arc rake. Arc rake pressure/temperature elements spanning an integral number of vane passages were used to obtain an average total pressure and temperature downstream of the OGV. The three highest reading elements were used to determine the OGV inlet pressure for the OGV recovery calculation. The traverse data were radially mass-averaged to determine overall OGV discharge conditions.

Mode 3 was designed to provide wall static information for acoustic testing with the fixed rakes removed.

Equations in the data reduction programs conformed to perfect gas relationships. Real gas effects were accounted for through specific heat variation with temperature and humidity and gas constant variation with humidity. These variations were defined for consistency with in-house programs that utilize enthalpy tables.

2. Acoustic

One-third octave band data were processed using a General Radio 1927 real time analyzer whose digital output was put on magnetic tape and run through a Full-Scale Data Reduction Program. A schematic of the acoustic data system is given in Figure 9. In general the data repeatability was excellent to ± 1 dB. Where it is not confusing both the original and the repeat data points are shown on the comparison plots. However, where showing both would lead to too many symbols, only the average of the data points is plotted.

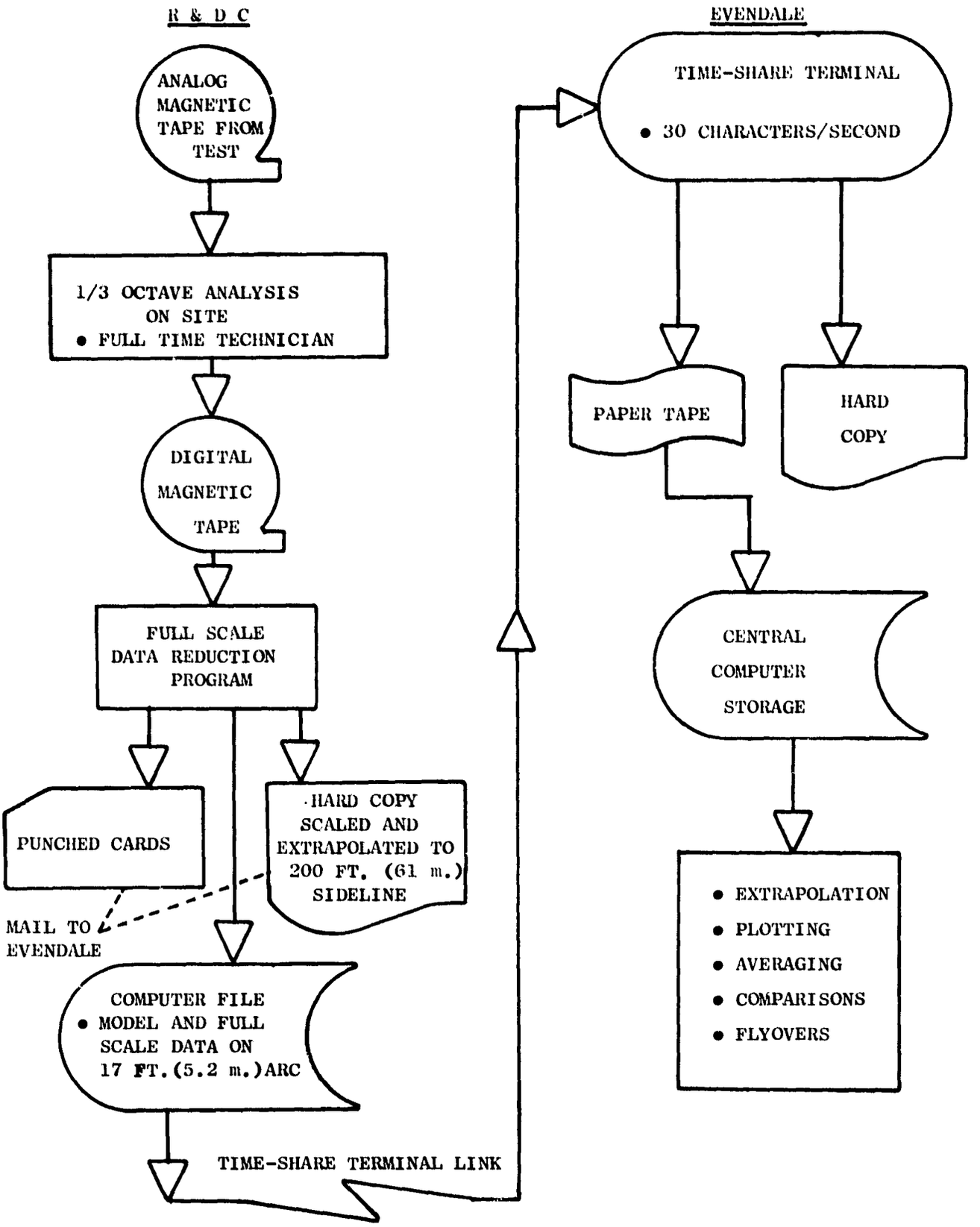

FIGURE 9 DATA REDUCTION SYSTEM

SECTION VI

AERODYNAMIC PERFORMANCE

A. Fan Stage Performance

Fan stage performance was measured to satisfy two basic objectives:

1. Verify the adequacy of the baseline (25) vane design in achieving stage performance comparable to the original NASA 11 vane configuration.

2. Support the acoustic evaluation of the low Mach versus baseline vane configurations by providing data for noise/performance tradeoffs.

Three types of aero data were obtained:

a. Fixed rake data to provide basic fan map information.

b. Vane wake surveys provided by a circumferential arc rake positioned at several radial locations.

c. Static pressure data to provide additional stage information and to monitor vehicle operation during acoustic testing when aero rakes were removed. Instrumentation locations are depicted in Figure 9.

Because of the 90° turn of the inlet flow from the vertical inlet stack to the horizontal inlet duct, shown in Figure 3, the total pressure profiles at the rotor inlet are of interest. Figure 10 shows the rotor inlet radial profiles at three circumferential locations for the baseline vane configuration at 100% $N/\sqrt{\theta}$. Except at the hub, the total pressure at the 200° location was slightly lower, probably reflecting the additional turning and mixing occurring in the bottom quadrant. The higher hub pressure in this quadrant was possibly due to the boundary layer getting a start on the axial portion of the hub flowpath, whereas, at the other positions the hub boundary layer included the total buildup down the stack. Also shown for reference is the inlet pressure profile for Stage 55, (Reference 1) which was at a comparable inlet airflow. Relative to the NASA profile, a small total pressure defect ($\sim$0.6%) existed in the hub at the 60° and 300° rake positions, but essentially no total pressure distortion was measured in the tip.

Stage discharge radial pressure profiles measured with the downstream fixed rakes are also shown in Figure 10. The maximum measured circumferential variation was slightly above 1% for the 31 vane baseline configuration. With this number of vanes, the circumferential position of the rakes relative to a vane was such that the 215° rake was closest to the vane suction surface, followed by the 330° rake. This relative positioning could account for the measured circumferential pressure variation, since the 215° rake measured the lowest pressure at four out of five radial locations.

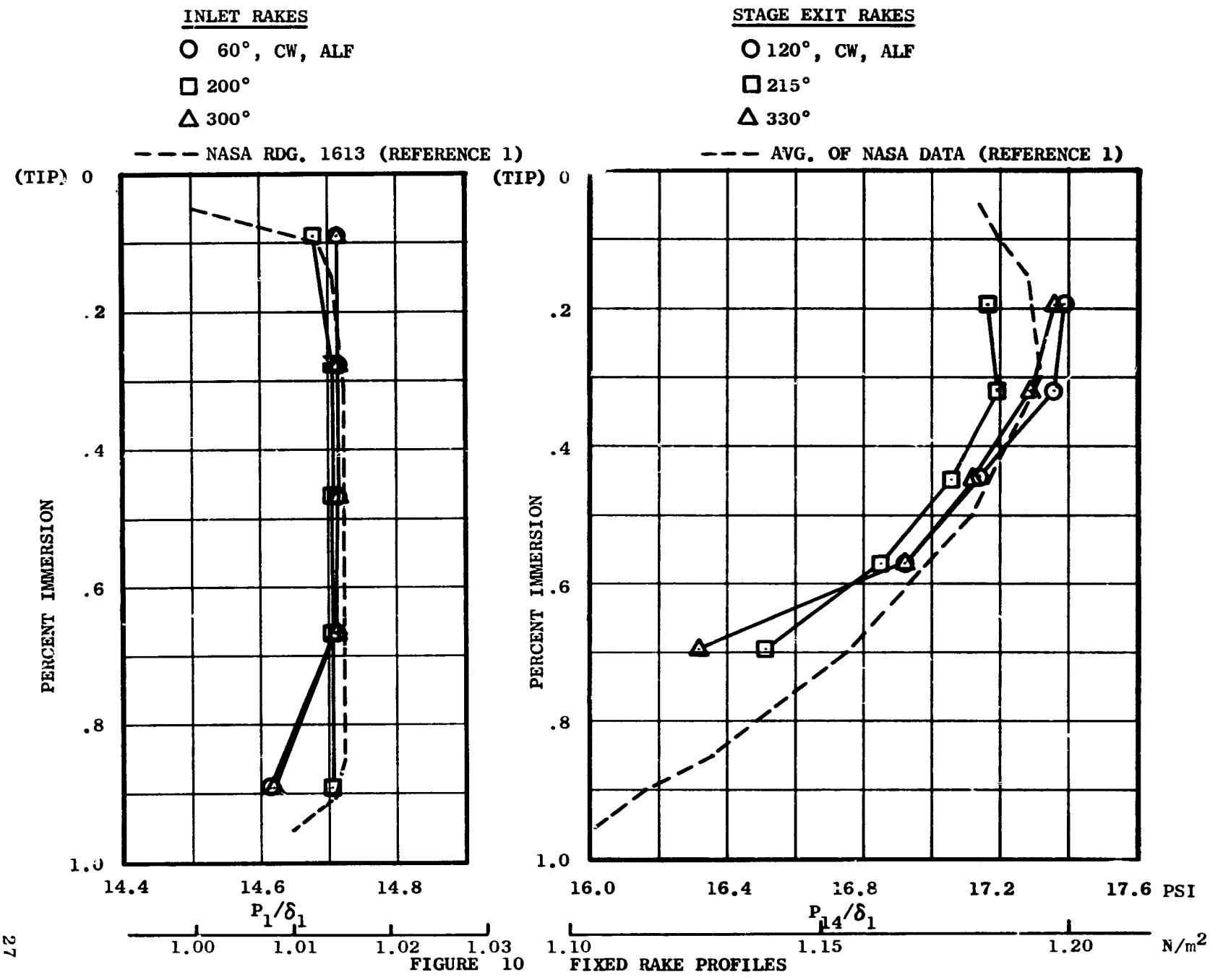

FIGURE 10 FIXED RAKE PROFILES

Aero performance was measured for the baseline and low Mach at a vane-blade ratio of 2.07 (31 vanes) and a rotor-stator spacing of 1.5 true rotor tip chords. Figure 11 shows overall performance data for these vane types against a background map obtained by interpolating the NASA test results (Reference 1) to a rotor pitch angle of 6°. Also shown are the two data points taken with the eleven-vane NASA configuration. The pressure ratios for these configurations were obtained by a radial mass-averaging of the fixed rake immersion averages. The tests were conducted with a common, fixed area exhaust nozzle, so the data should ideally fall on a common operating line. Conclusions regarding the relative pressure losses of the vane configurations were thus based on the airflow-speed relationship, shown in Figure 12. On that basis, airflow at speed is slightly higher for the 31 baseline vanes, indicative of 0.1-0.2% less pressure loss. Fixed rake efficiency data is not shown due to discharge temperatures reading too low, resulting in efficiencies greater than 1.0.

Traverse pressure data at selected immersions are shown for the baseline and low Mach vanes in Figures 13 and 14. The arc rake spanned slightly more than one vane passage in the tip and more than two passages at the hub. The data measured by each arc rake element are thus depicted in a circumferential position relative to a vane trailing edge in order to illustrate the circumferential profile in a single passage. Except at the tip and hub, circumferential profiles of the two vane types are similar. In the tip, high suction surface losses are evident for the baseline vanes at both 90% and 100% $N/\sqrt{\theta}$. The low Mach vanes appear to have higher suction surface losses in the hub.

Temperature profiles at 100% $N/\sqrt{\theta}$ for selected immersions are shown in Figure 15. The relatively larger variation at the end walls, particularly in the hub, are evidence of streamline warping/secondary flow phenomena.

Radial profiles of OGV recovery, stage pressure and temperature rise and stage efficiency derived from the traverse data are presented in Figures 16 and 17. The upstream total pressure used in the OGV recovery computation was the average of the three highest reading are rake pressures. Reference profiles at 100% $N/\sqrt{\theta}$ derived from averaged Stage 55 NASA data are shown in Figure 17.

The recovery levels of the baseline and low Mach vanes were about the same except near the end walls, where the low Mach vanes were better in the tip and worse in the hub, as discussed previously. Both vane types indicated improvement relative to the eleven vane NASA configuration data from Reference 1. No comparison between the NASA configuration and the 25 baseline vane configuration was available since the latter was not traversed. The stage pressure and temperature rise profiles are similar to the NASA results but a temperature level discrepancy of 1° to 2° R (0.6 to 1.1° K) was evident. It could not be determined whether the inlet rake or arc rake temperatures were at fault, but the arc rake was suspect due to the use of a connector rather than continuous leads. Because of the relatively low rotor temperature rise, the 1° to 2° R (0.6 to 1.1° K) temperature discrepancy resulted in a large efficiency error. However, one would not expect the 25 baseline vane performance to vary significantly from the 31 baseline vanes.

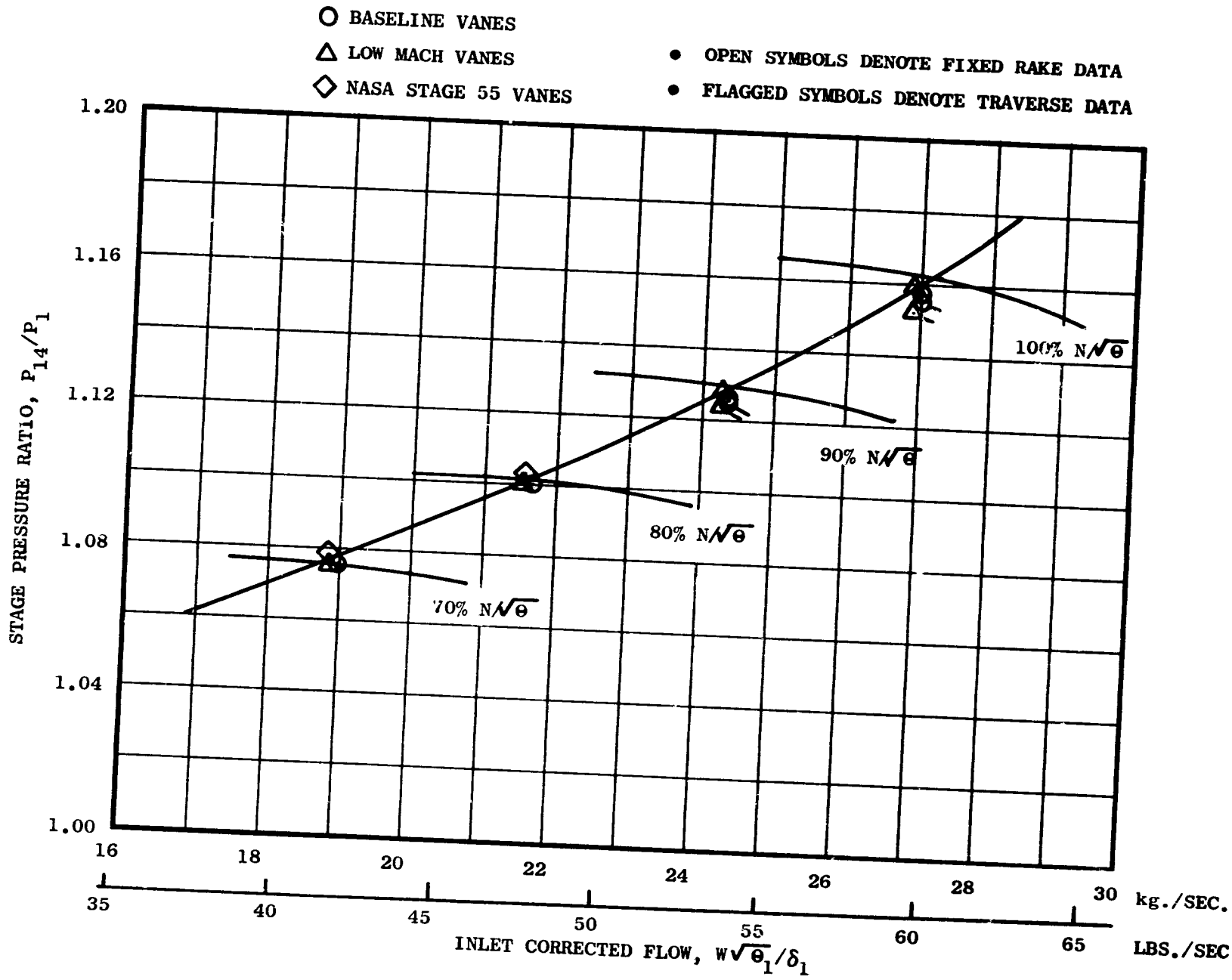

FIGURE 11 PERFORMANCE MAP

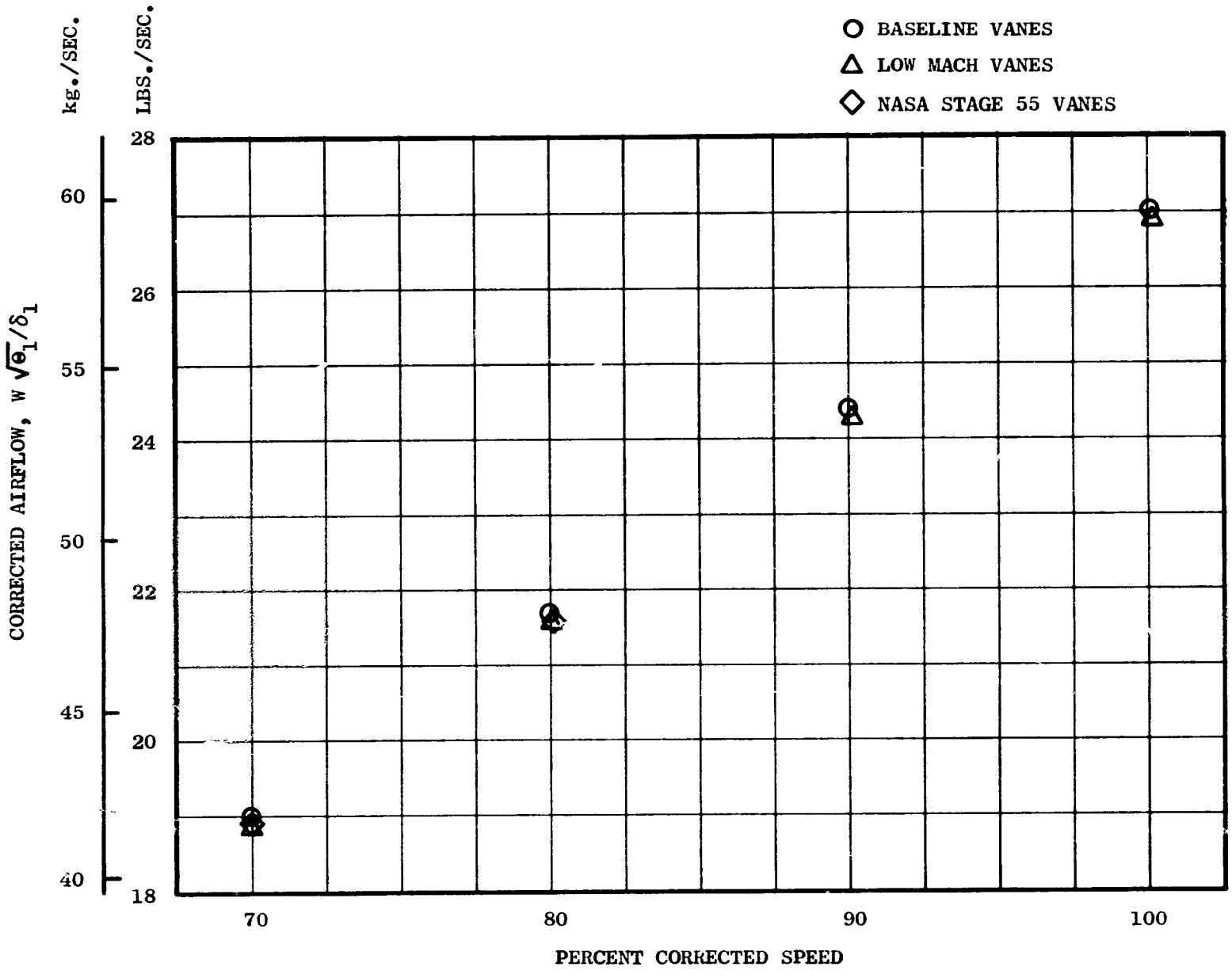

FIGURE 12 AIRFLOW - SPEED RELATIONSHIP

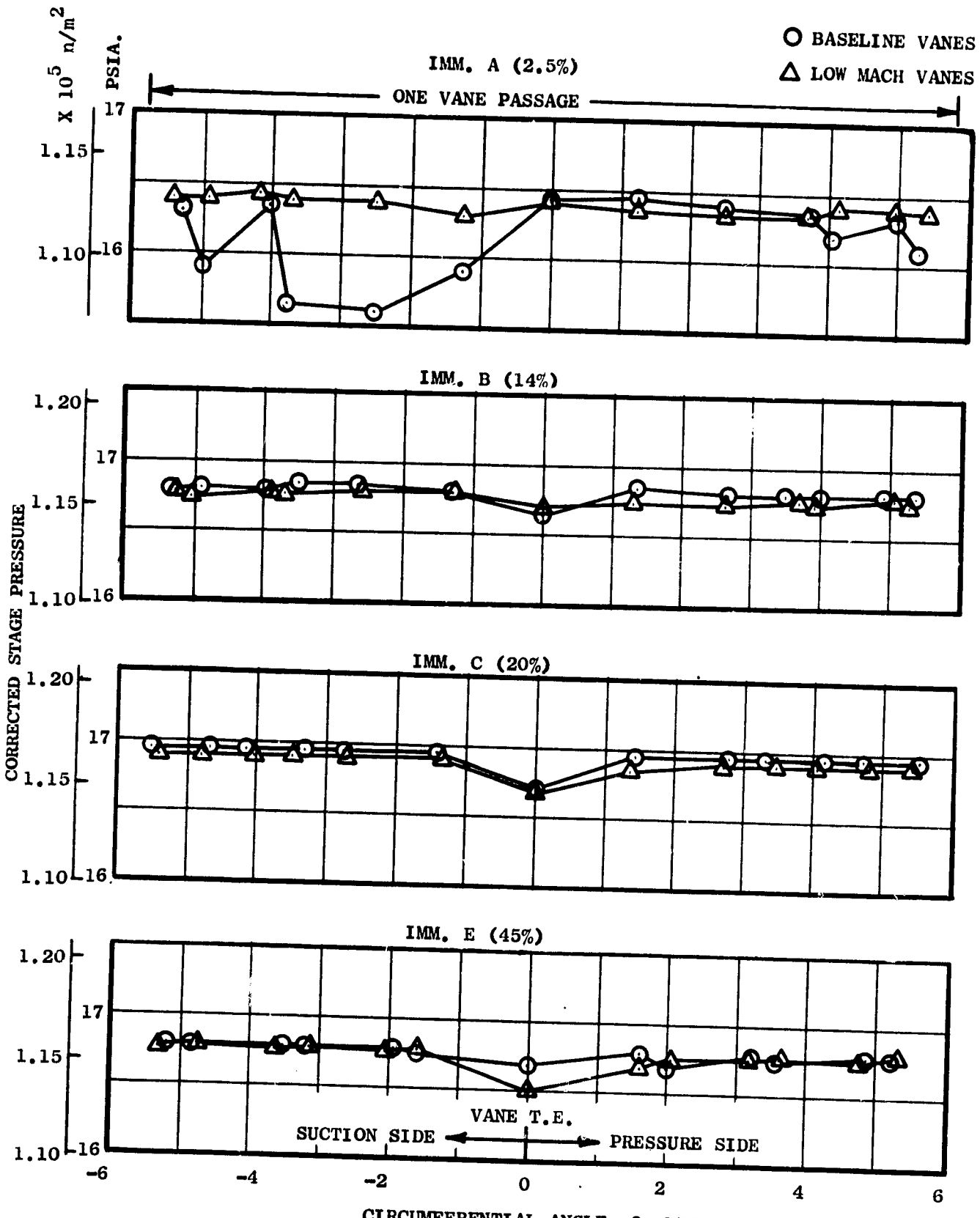

FIGURE 13 VANE WAKE PROFILES AT 90% $N/\sqrt{\theta}$

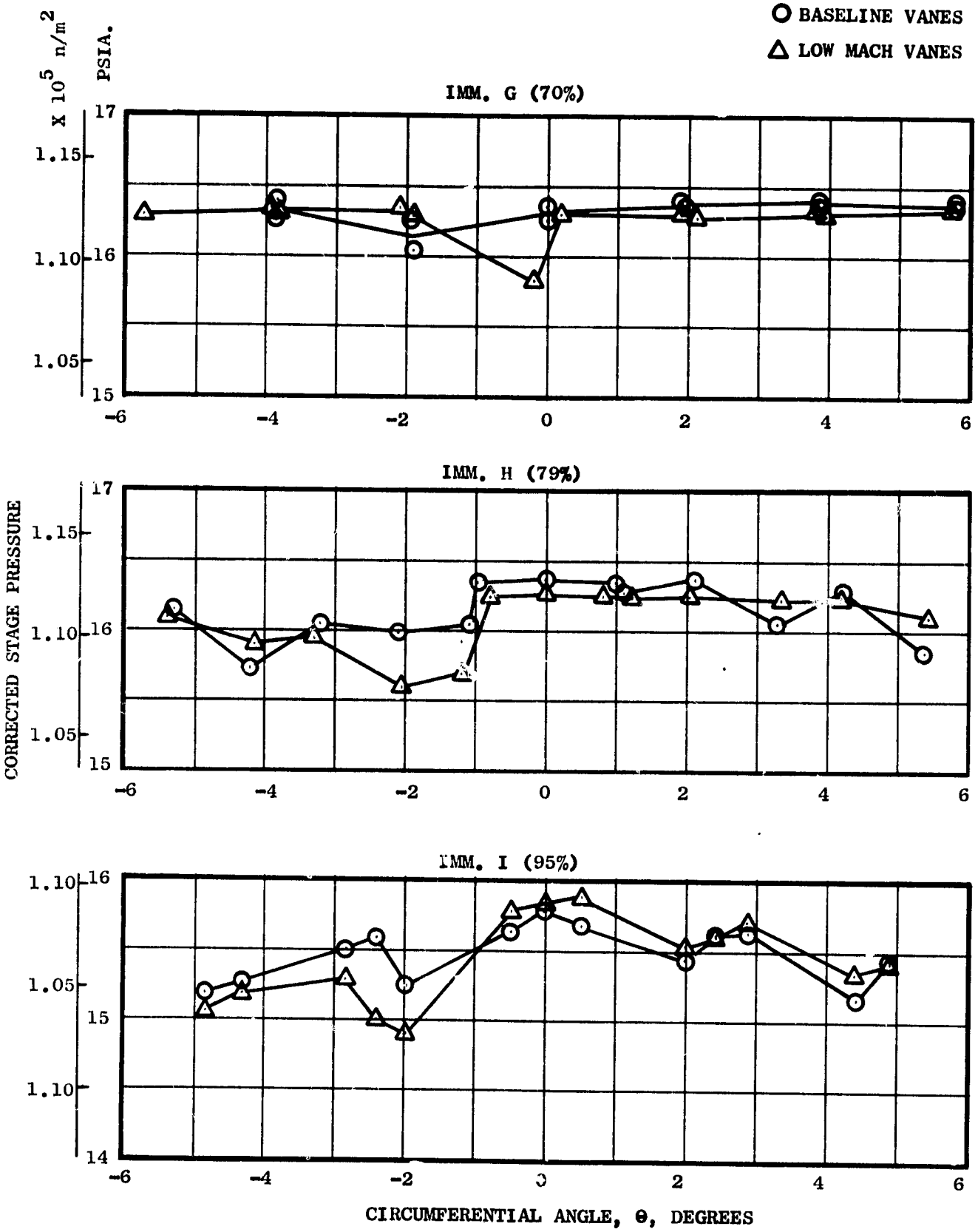

FIGURE 13(CONCLUDED) VANE WAKE PROFILES AT 90% $N/\sqrt{\theta}$

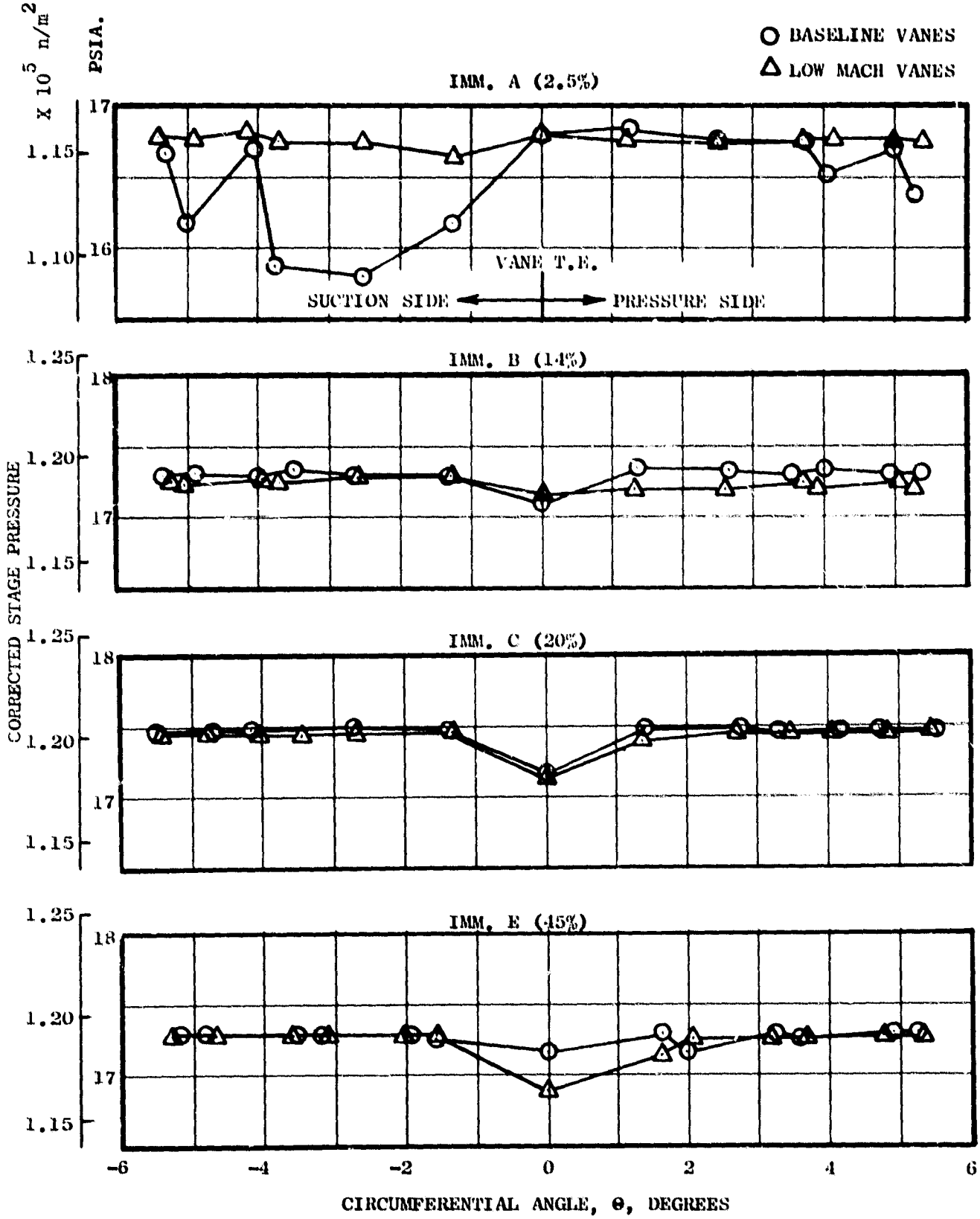

FIGURE 14 VANE WAKE PROFILES AT 100% $N/\sqrt{\theta}$

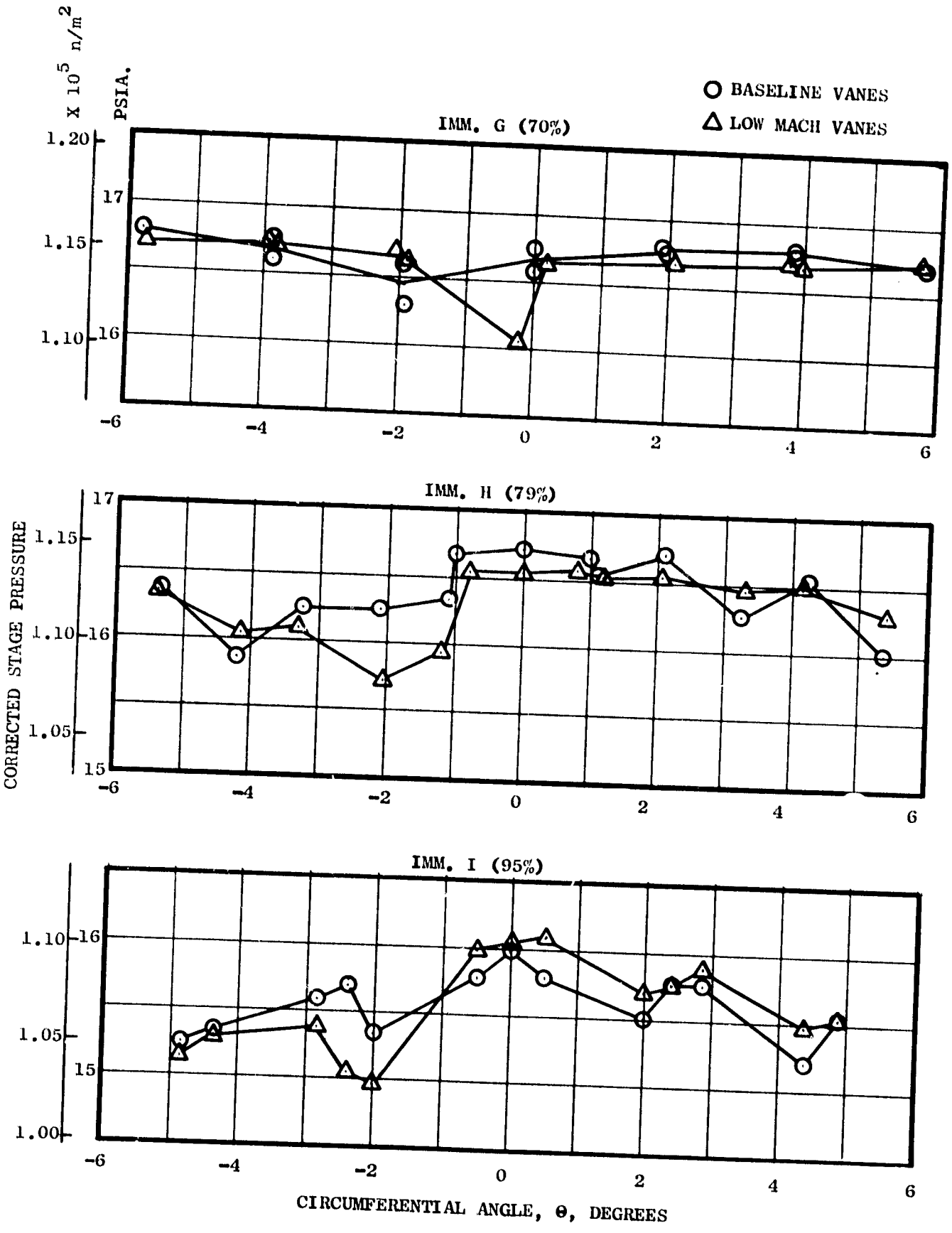

FIGURE 14 (CONCLUDED) VANE WAKE PROFILES AT 100% N/$\sqrt{\theta}$

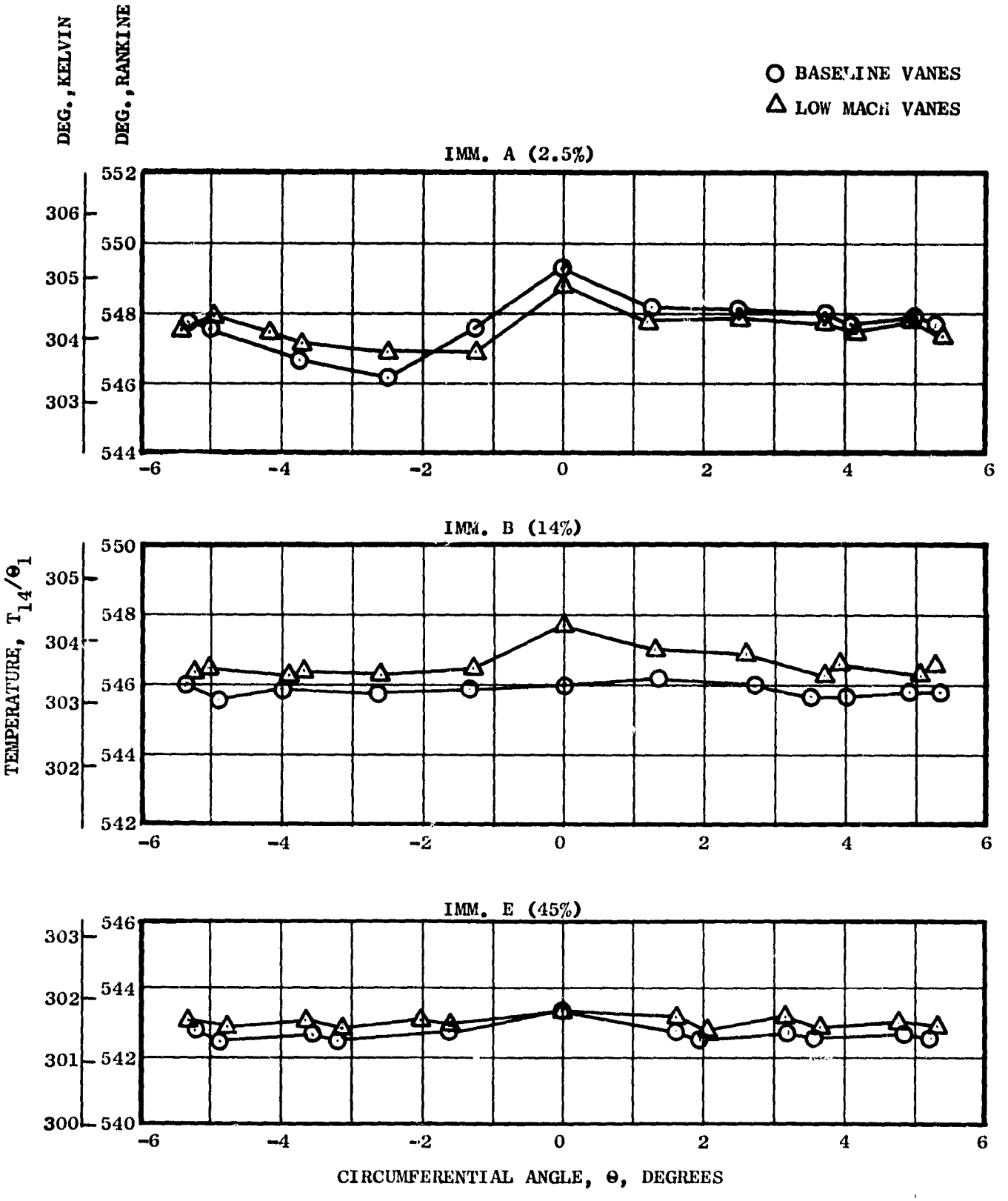

FIGURE 15 TEMPERATURE PROFILE ACROSS VANE PASSAGE

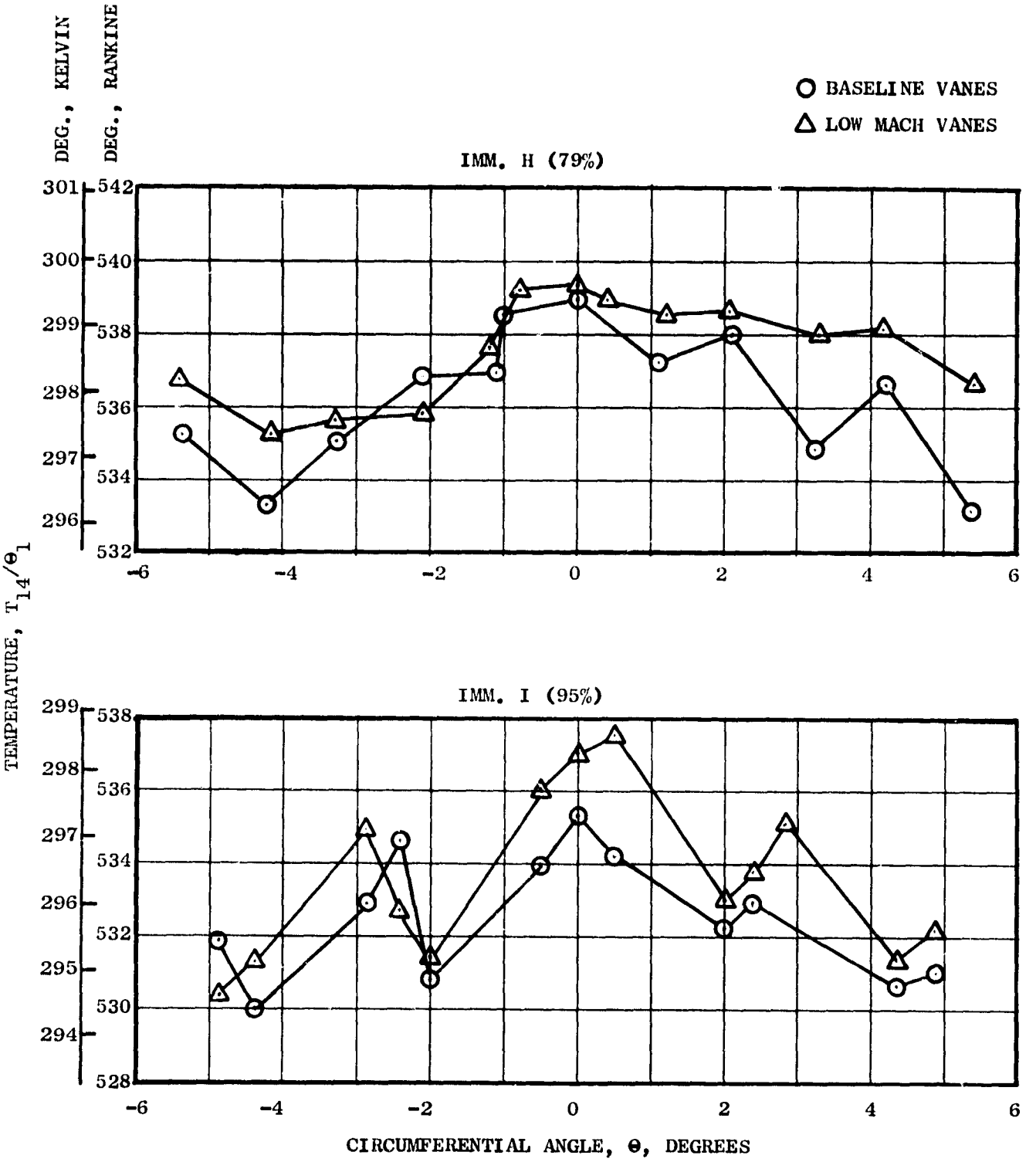

FIGURE 15 (CONCLUDED) TEMPERATURE PROFILE ACROSS VANE PASSAGE

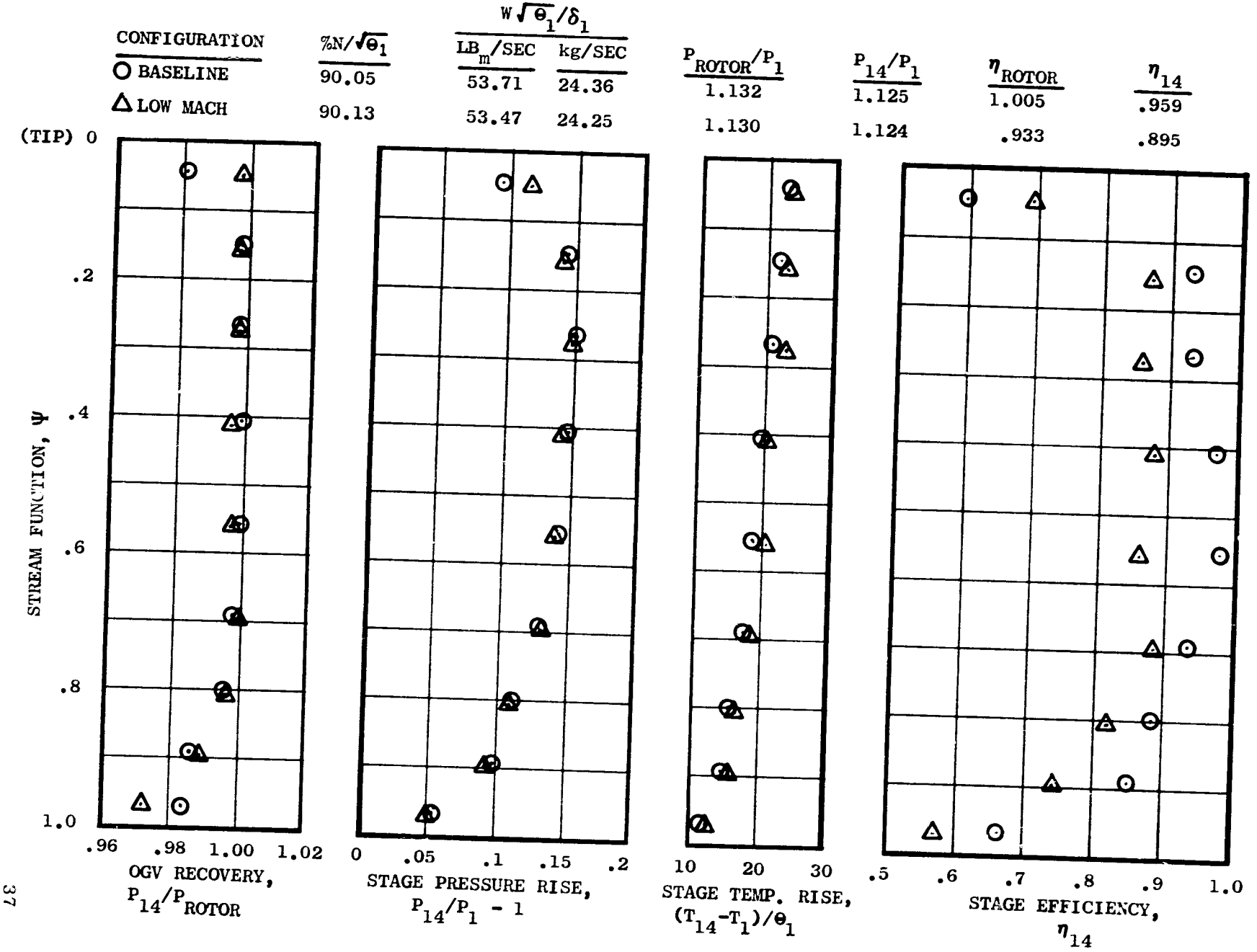

FIGURE 16 STAGE EXIT PROFILES AT 90% $N/\sqrt{\theta}$

CONFIGURATION	$\%N/\sqrt{\theta_1}$	$W\sqrt{\theta_1}/\delta_1$ LB$_m$/SEC	kg/SEC	P_{ROTOR}/P_1	P_{14}/P_1	η_{ROTOR}	η_{14}
○ BASELINE	100.03	59.49	26.98	1.162	1.155	.979	.934
△ LOW MACH	100.12	59.34	26.91	1.160	1.152	.931	.893
– – – AVG. OF NASA DATA (REFERENCE 1)							

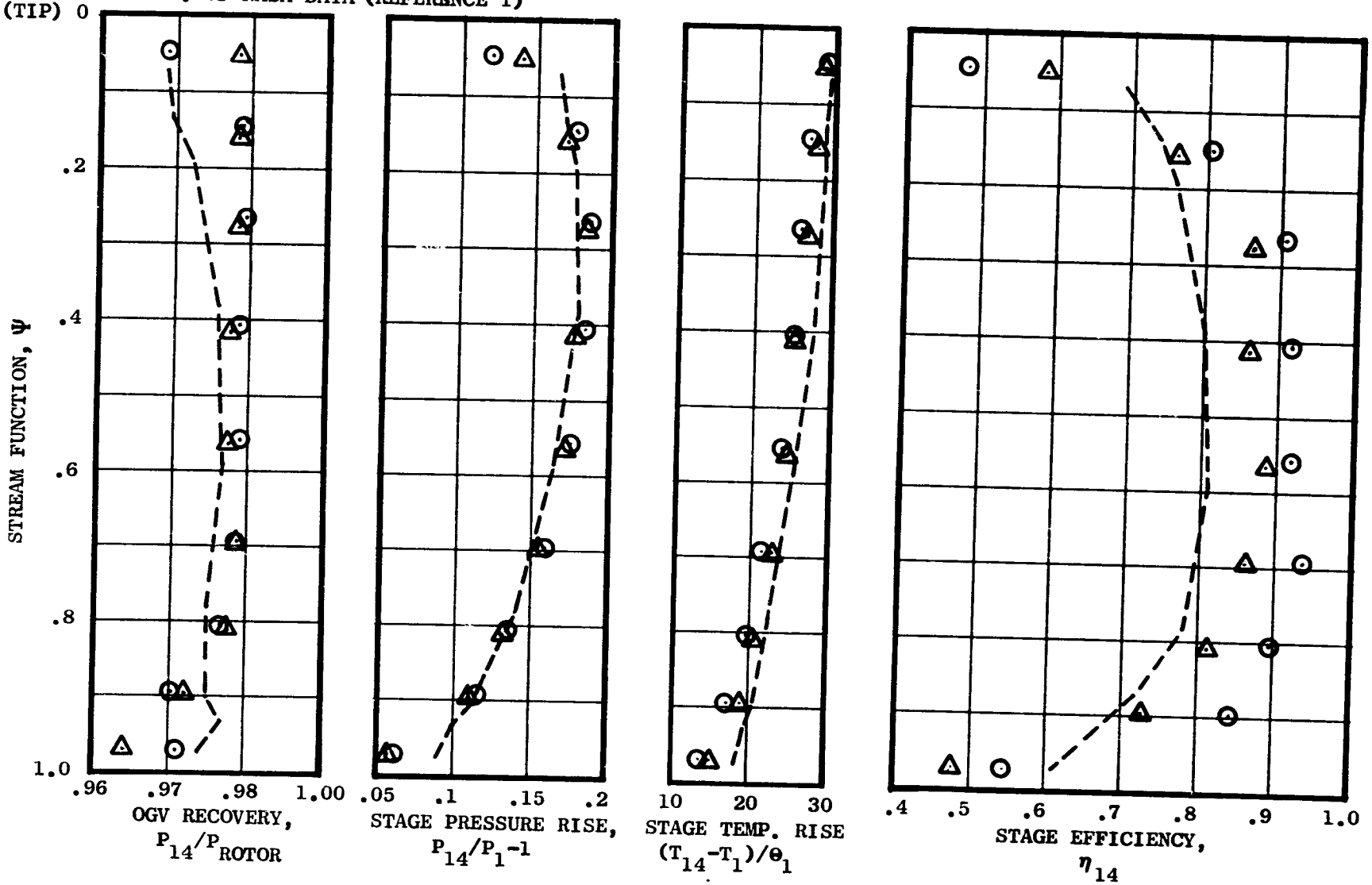

FIGURE 17 STAGE EXIT PROFILES AT 100% $N/\sqrt{\theta}$

A limited amount of static pressure data within the fan stage was obtained. Of most interest was a comparison of the baseline vane and low Mach vane hub static pressures at the rotor exit and OGV inlet which is summarized below:

P_s/δ_1	Baseline	Low Mach
Rotor Exit	13.77 psia ($9.494 \times 10^4/m^2$)	13.85 ($9.549 \times 10^4/m^2$)
OGV Inlet	14.01 ($9.650 \times 10^4/m^2$)	14.21 ($9.797 \times 10^4/m^2$)

The low Mach vane configuration exhibited both a higher rotor exit hub static pressure and a greater hub static pressure rise between rotor and stator. Defining a static pressure coefficient as:

$$C_p = \frac{\Delta P_s}{\overline{P_t} - P_s}$$

where ΔP_s - hub static pressure rise between rotor and stator.

P_s - rotor exit hub static pressure.

$\overline{P_t}$ - mass-weighted discharge pressure

Design and measure values are tabulated below:

	Design	Measured
Baseline	0.053	0.073
Low Mach	0.110	0.112

It is noted that the difference in measured pressure coefficient between the baseline and low Mach configurations is roughly 70% of the pressure coefficient difference predicted by the design point axisymmetric flow solutions. Because the design point solutions corresponded to a 0° rotor pitch, 110% $N/\sqrt{\theta}$ conditions, the design rotor discharge Mach numbers ($\sim$0.6) were considerably higher than actual test conditions ($\sim$0.49). It is estimated that the Mach number difference and the difference in hub swirl between the 0° and 6° rotor pitch angles could account for roughly half the difference in delta pressure coefficient. Other effects, such as the additional wall boundary layer growth of the low Mach configuration which was not accounted for in the axisymmetric solution, could account for the remaining difference. Thus, it is concluded that opening the annulus area at the OGV inlet was largely effective in achieving the intended prediffusion.

In summary, stage performance comparable to the original NASA configuration was achieved. Overall vane losses were in line with expectations. The 4 point efficiency decrement indicated by the arc rake traverse of the low Mach configuration was not believed due to the previously mentioned temperature measurement problems. The reasonable assumption that the rotor performance was unaffected by the OGV configuration implied approximately equivalent stage performance for the low Mach and baseline vanes since the vane losses were about the same for both.

B. Inlet Turbulence

As mentioned in the previous section, the facility inlet geometry was of interest due to the turning involved. Prior to design of the inlet stack and bellmouth, a scale model was built and tested. These model results found that turbulence levels (ratio of root mean square of the fluctuating velocity to the freestream velocity) of less than 1% could be obtained at all circumferential locations except at the lowest point of the model where levels of 1.5 percent were measured. Accordingly, on the first configuration of this test vehicle, turbulence was measured with a single axis hot film probe 6.7 inches (17 cm) forward of the rotor. The resulting levels are presented in Figure 18. For reference hot film data at equal mass flow from tests of NASA Rotor 11 are shown in Figure 18. Rotor 11, a 20 inch (50.8 cm) diameter, 1.57 pressure ratio fan was tested to measure inlet radiated noise and was thus oriented to pull air from the anechoic chamber rather than from the stack as did Rotor 55. Rotor 11 represents typical inlet turbulence levels for static anechoic chamber testing.

The inlet turbulence levels measured on Rotor 55 are comparable to those measured on a typical static test of an inlet in the anechoic chamber.

C. Aft Duct Performance

One of the objectives of the aft suppression tests was to determine the effect of aft duct Mach number on flow regenerated noise. In support of this, aerodynamic measurements were taken in the aft duct. These measurements consisted of static pressure data and a total pressure traverse upstream of the nozzle. These are depicted in Figure 9 and were used to determine aft duct Mach numbers.

Figures 19, 20, and 21 present the 100% $N/\sqrt{\theta}$ duct Mach number profiles which were derived from the aft duct aerodynamic data for the duct without splitter, with splitter, and with splitter plus opened nozzle (12% open from nominal). Mass weighted average Mach numbers and calculated duct total pressure losses (excluding nozzle) are tabulated in Table V for both 90 and 100% $N/\sqrt{\theta}$. The maximum Mach number of 0.556 achieved was over the splitter in the outer channel while 0.516 was achieved in the inner channel. Figure 22 shows the aft duct Mach number variation with fan speed.

● DUCT HEIGHT = 6.0 INCHES (15.24 cm.)

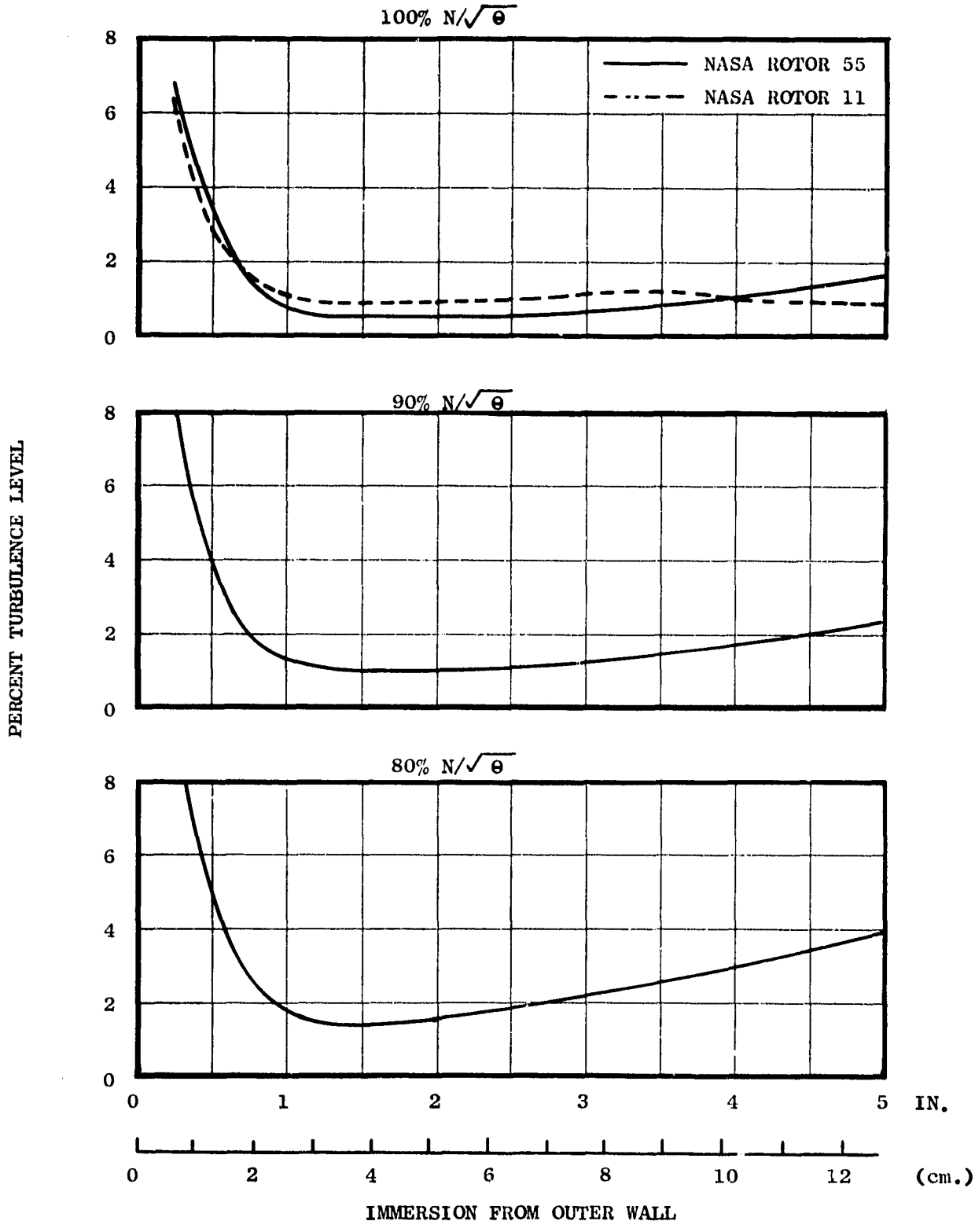

FIGURE 18 INLET TURBULENCE PROFILES

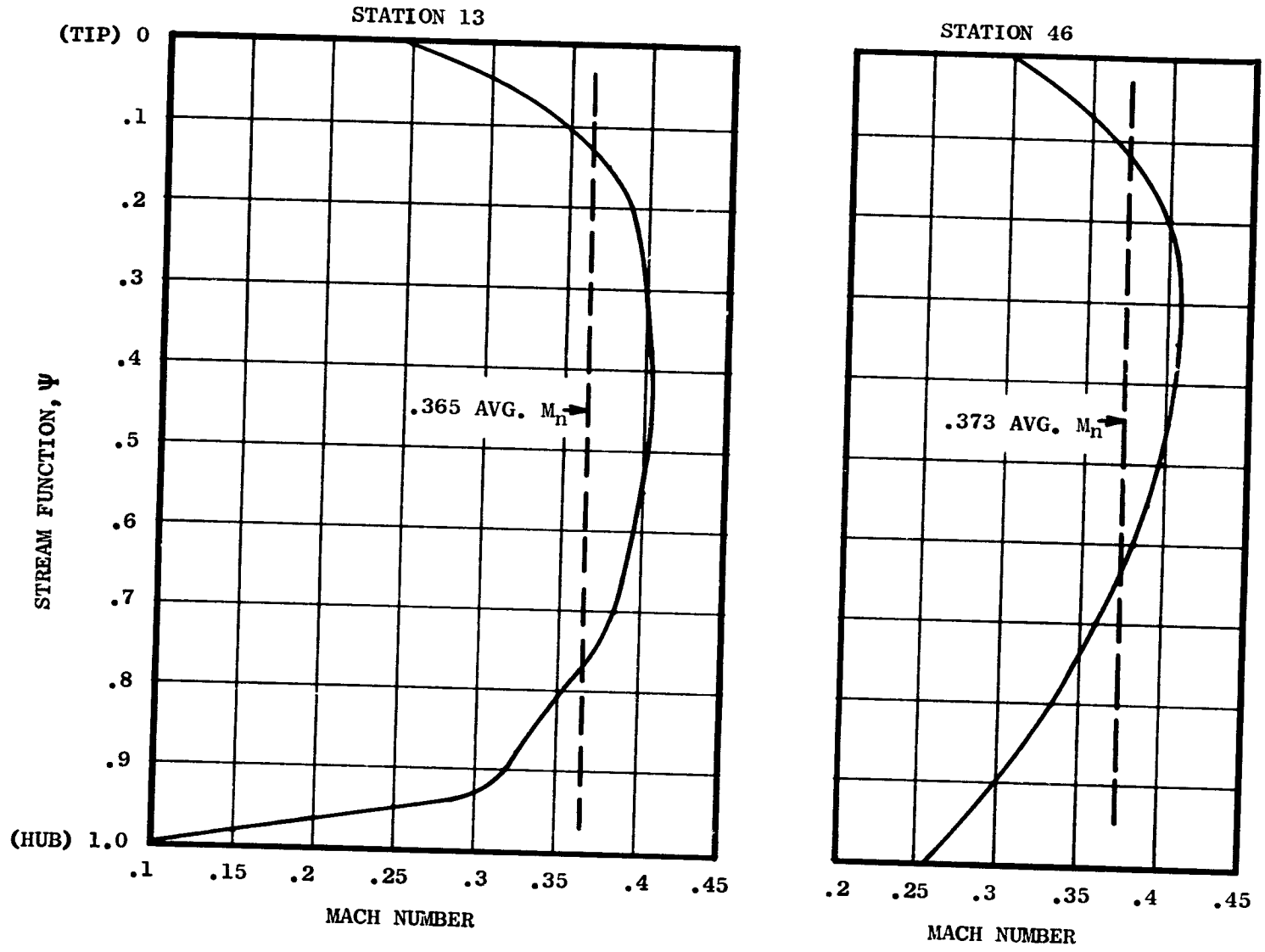

FIGURE 19 LONG HARDWALL AFT DUCT MACH NUMBER DISTRIBUTION

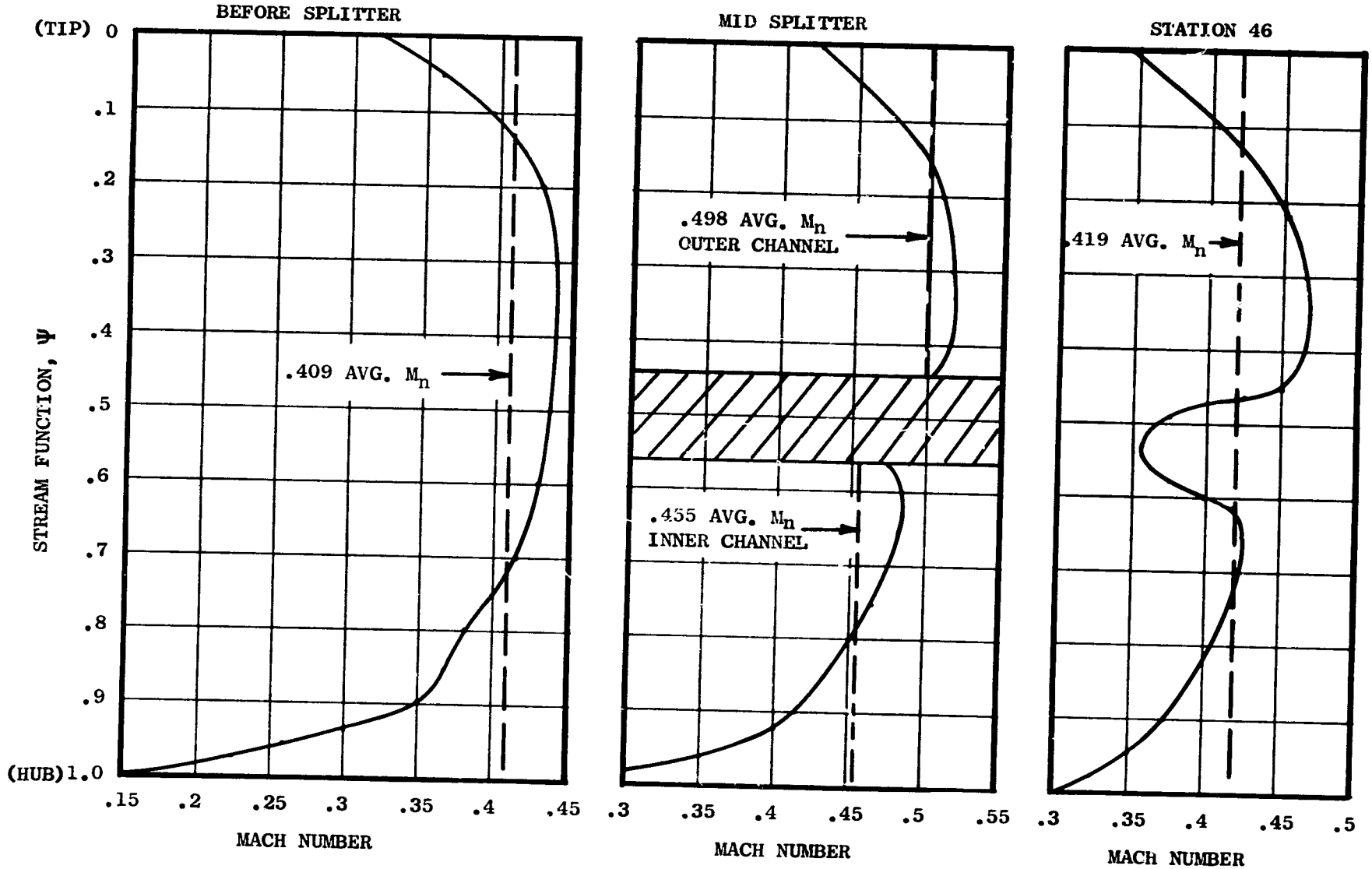

FIGURE 20 AFT DUCT MACH NUMBER DISTRIBUTION WITH SPLITTER AND NOMINAL NOZZLE

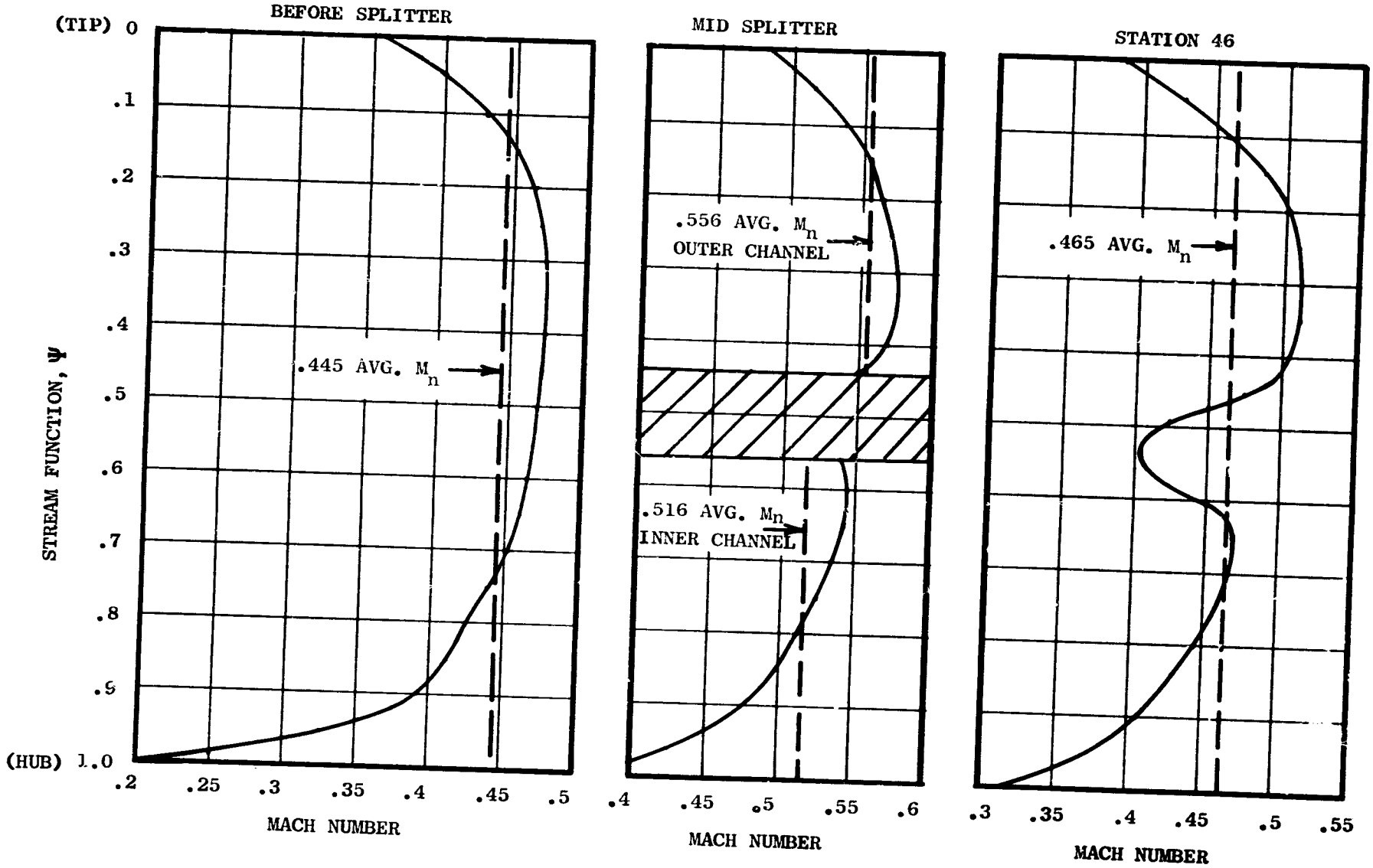

FIGURE 21 AFT DUCT MACH NUMBER DISTRIBUTION WITH SPLITTER AND OPEN NOZZLE

TABLE V - AFT DUCT PERFORMANCE AND MACH NUMBERS

Configuration	% $N/\sqrt{\theta}$	Mass Weighted Mach Number				$\Delta P_T/P_T$
		Sta 13	Sta 34.5		Sta 46	
			Outer Channel	Outer Channel		
6	90	.327	-	-	.334	0.50%
6	100	.365	-	-	.373	0.55%
9	90	.369	.447	.415	.376	1.62%
9	100	.409	.498	.455	.419	1.93%
10	90	.407	.500	.467	.419	2.36%
10	100	.445	.556	.516	.465	2.77%

- 28 BASELINE VANES
- 1.5 CHORD SPACING

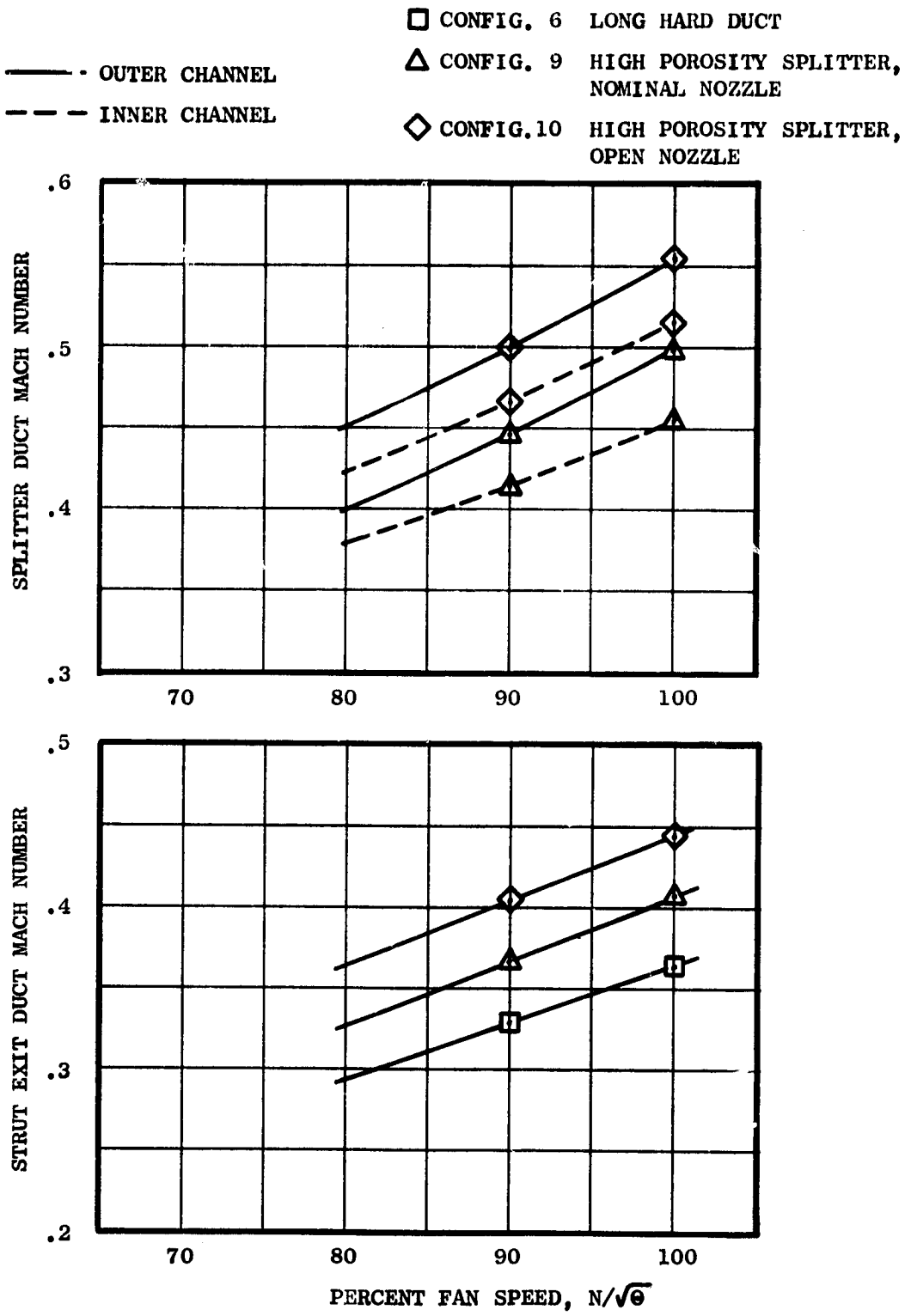

FIGURE 22 AFT DUCT MACH NUMBER VARIATION WITH FAN SPEED

SECTION VII

SOURCE NOISE TEST RESULTS

A. Vane-Blade Ratio Effects

A theoretical analysis developed by Mani (Reference 2) determined that rotor-stator noise can be reduced by the judicious selection of vane/blade ratio. The sources of the rotor-stator noise are the fluctuating forces exerted by the blades on the fluid. These forces - as a first approximation - have an orientation which may be taken as that of the lift vector determined from the steady state fluid velocity diagrams. The noise is propagated as spiraling waves which have an orientation that depends only on the number of stator and rotor blades, the rotor frequency, and the velocity of the moving medium. The efficiency with which a blade row produces discrete frequency noise due to interaction with a neighboring row can be significantly reduced if the orientation of the spiraling wave system is approximately perpendicular to the orientation of the fluctuating forces.

Normally, the analysis would be used to select the vane-blade ratio that would reduce the BPF. However, on the QCSEE under-the-wing engine the BPF is at 1000 Hz and the second harmonic 2000 Hz. Due to the higher noy-weighting of the second harmonic, minimizing it could be more beneficial. Rotor 55 was used to reduce the second harmonic thus verifying the analysis which was used to select the proper vane number on the engine.

Predicted level changes due to minimizing the second harmonic rotor stator interaction noise levels are shown in Figure 23 for various radial locations. The minimum energy transmittal occurs at 28 vanes or 1.87 vane/blade ratio. A series of vane numbers were tested (Table VI) with the 15 blades of Rotor 55. This testing was done at two spacings - 1.5 and 0.5 rotor tip chords. Each vane number from 25 to 31 was tested which resulted in vane/blade ratios from 1.67 to 2.07. In addition, testing of the 11 vane configuration which originally made up Stage 55 provided data at a vane/blade ratio of 0.73 at 1.5 chord spacing only. The configurations are summarized in Table IV. Test results are presented in Figures 24 and 25 at 100 and 70% $N/\sqrt{\theta}$ respectively. Both 1.5 and 0.5 chord spacing results are shown at three aft angles. Examining the 1.5 chord spacing results indicates that there was no significant change in the second harmonic SPL as vane/blade ratio was varied. However, with the 0.5 chord spacing data, there is a definite trend to minimum SPL's at 28 vanes or a vane/blade ratio of 1.87. There are two conclusions to be observed from these results. First, the close spacing (0.5 chord) static test results substantiate Mani's analysis and justify its use as a tool to choose the proper vane/blade ratios on the UTW engine. Second, at a wide spacing (1.5 chord) the static test results imply that some source other than rotor-stator interaction is controlling. This may be rotor-turbulence interaction noise and the effect of vane-blade ratio at wide spacing could be beneficial in-flight if rotor-turbulence noise is reduced. Therefore, the QCSEE design intent is justified if rotor turbulence noise is not controlling during flight.

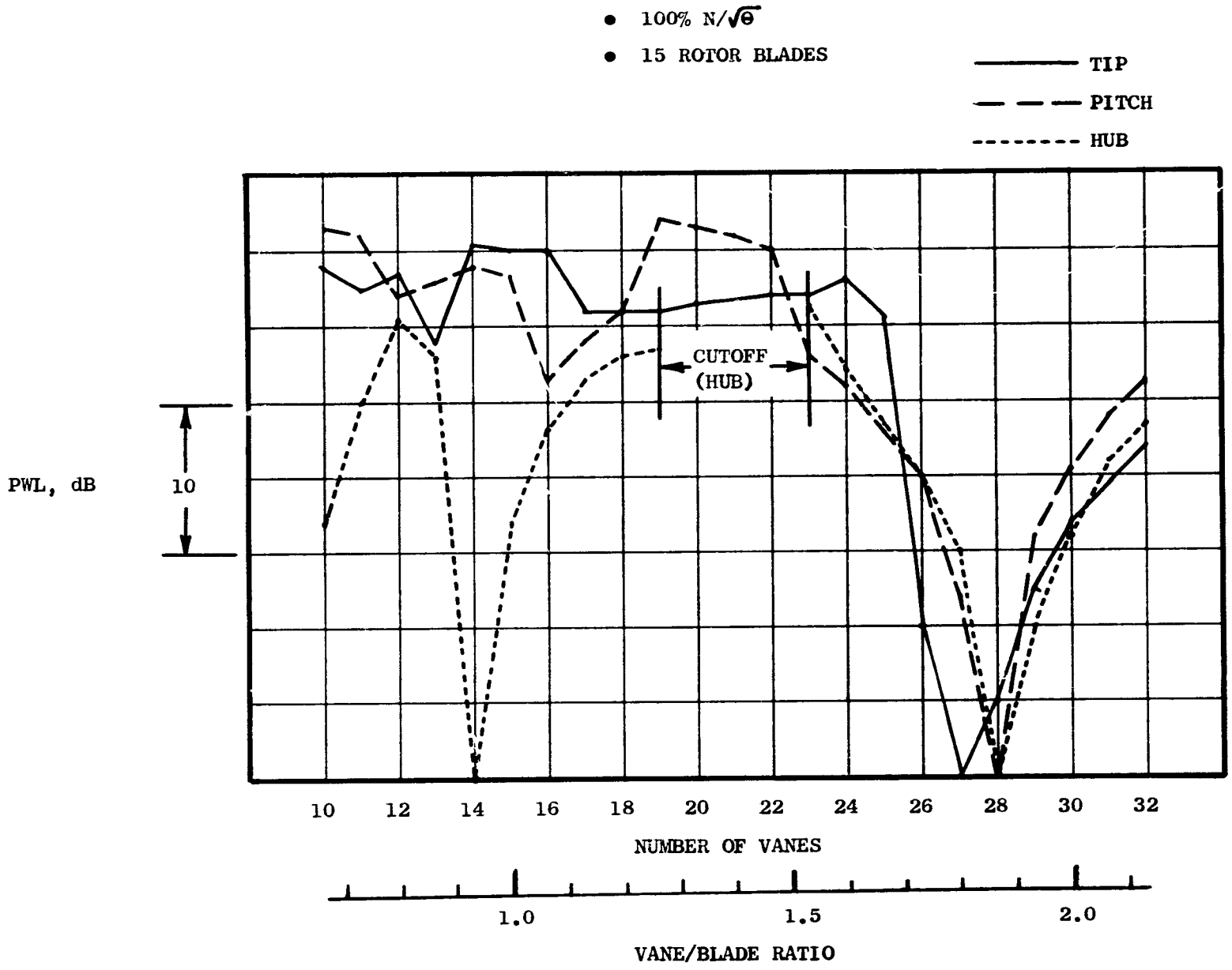

FIGURE 23 PREDICTED PWL DECREASE AS A FUNCTION OF VANE NUMBER

TABLE VI SOURCE NOISE TEST CONFIGURATIONS

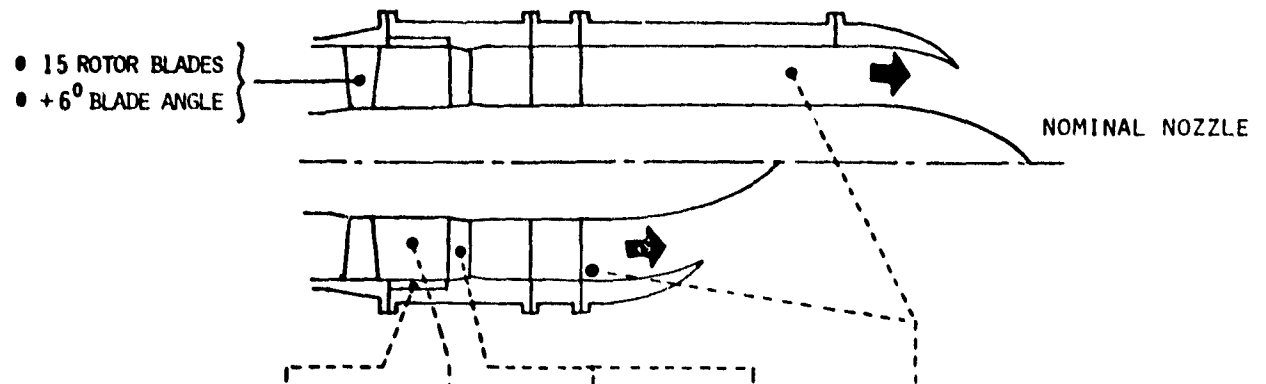

CONFIGURATION	ROTOR-OGV TREATMENT	SPACING	VANE NUMBER	VANE/BLADE RATIO	DUCT LENGTH	COMMENTS
1B	NO	1.5	11	0.73	LONG	STAGE 55 VANES
2	YES	1.5	28	1.87	SHORT	BASELINE VANES
3A	↓	1.5	31	2.07	↓	BASELINE VANES
4B	↓	1.5	31	2.07	↓	LOW MACH VANES
5	↓	1.0	28	1.87	↓	BASELINE VANES
6	↓	1.5	28	1.87	LONG	↓
12	↓	1.5	26	1.73	SHORT	↓
13	↓	1.5	27	1.80	↓	↓
14A	↓	2.0	28	1.87	↓	↓
18	NO	1.5	28	1.87	LONG	↓
19	YES	1.5	25	1.67	SHORT	↓
20	↓	1.5	29	1.93	↓	↓
21	↓	1.5	30	2.00	↓	↓
22	↓	1.5	28	1.87	↓	(REPEAT OF CONFIG. 2)
27	NO	0.5	31	2.07	↓	↓
28	↓	↓	30	2.00	↓	↓
29	↓	↓	29	1.93	↓	↓
30	↓	↓	28	1.87	↓	↓
31	↓	↓	27	1.80	↓	↓
32	↓	↓	26	1.73	↓	↓
33	↓	↓	25	1.67	↓	↓

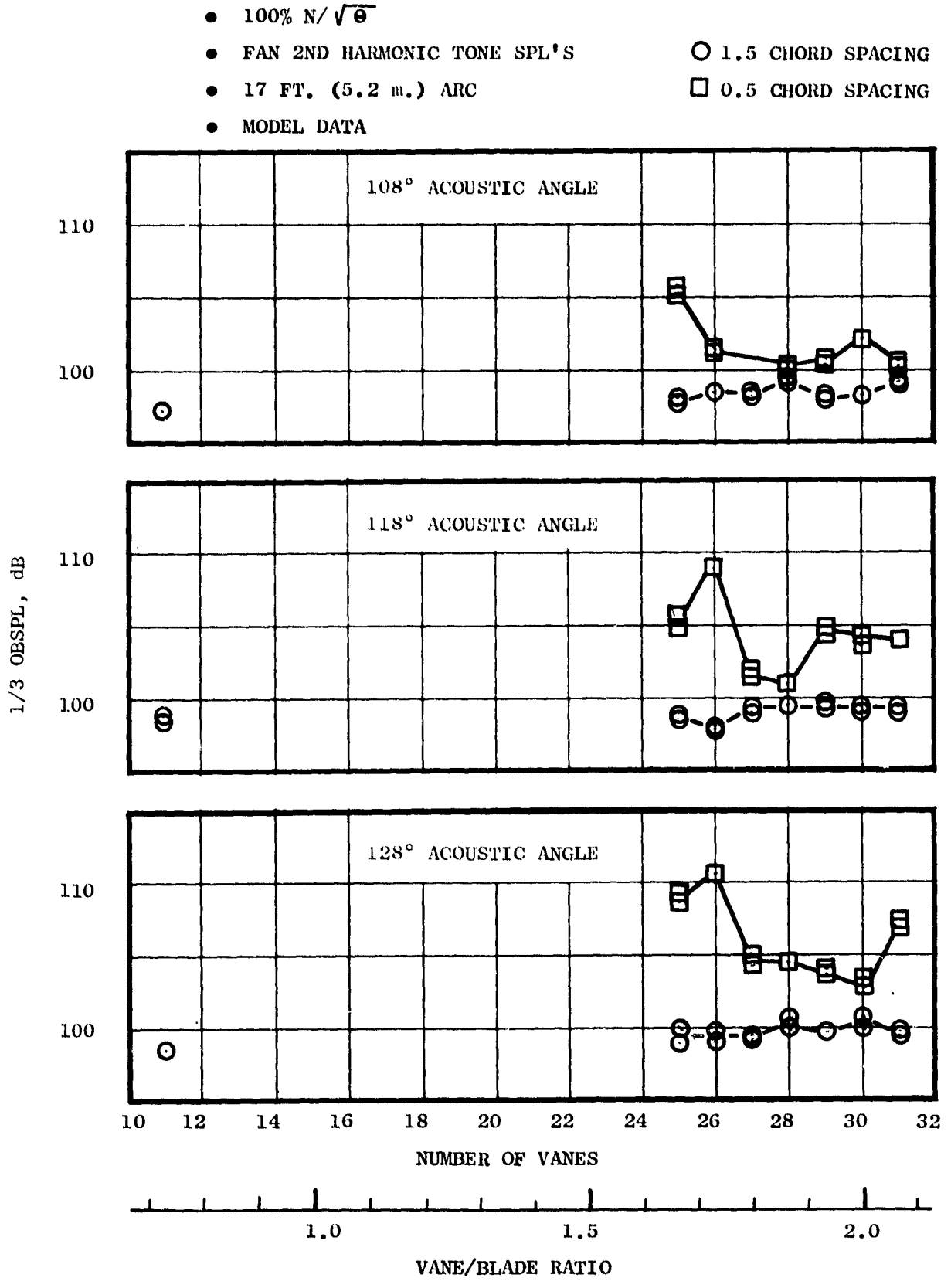

FIGURE 24 EFFECT OF VANE NUMBER ON SECOND HARMONIC SPL'S AT 100% N/√θ

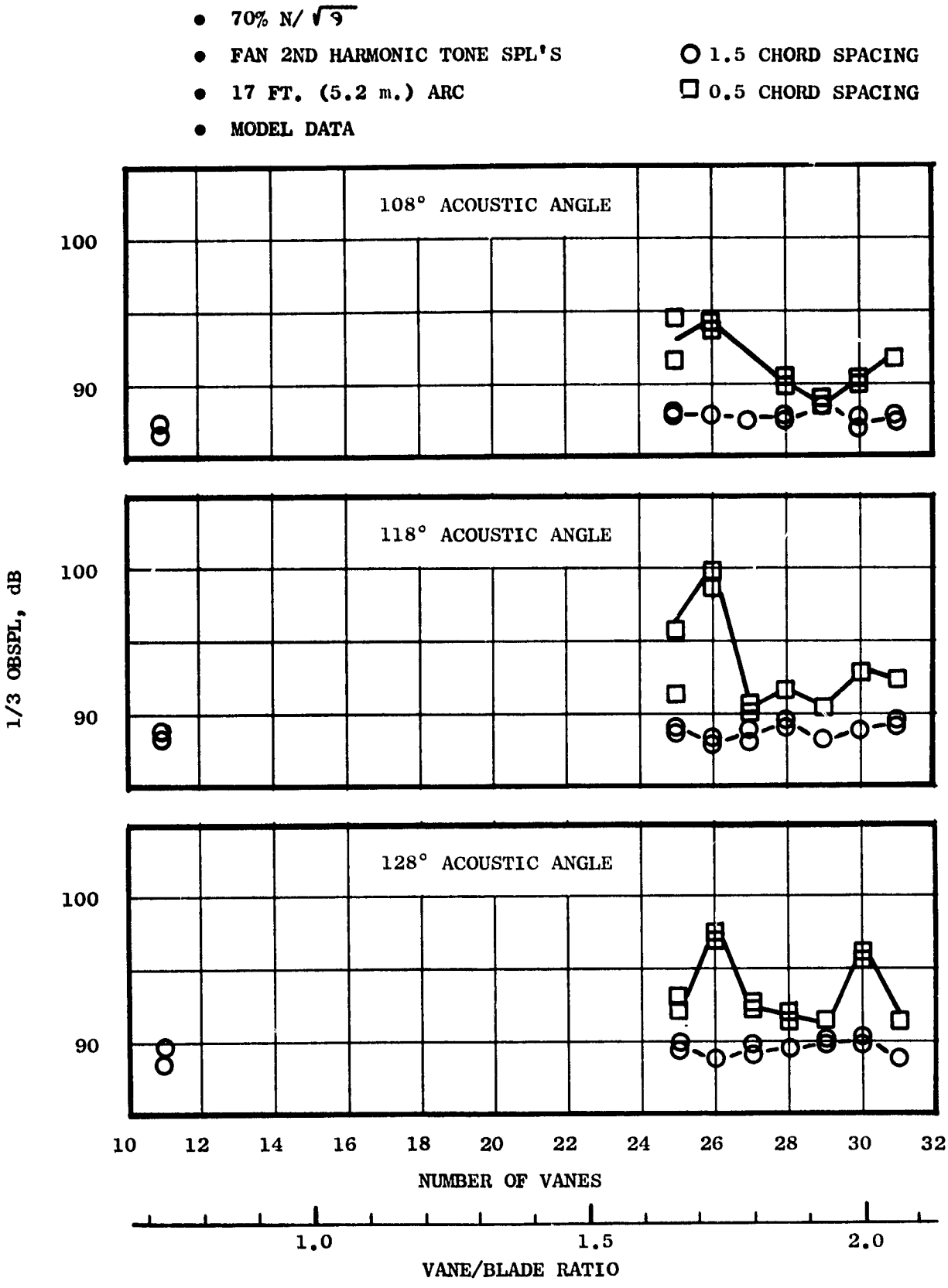

FIGURE 25 EFFECT OF VANE NUMBER ON SECOND HARMONIC SPL'S AT 70% N/√θ

B. Rotor-Stator Spacing Effects

An investigation of rotor-stator spacing effect was conducted at the optimum vane-blade ratio (28 baseline vanes) for minimizing second harmonic tone propagation in the exhaust. The four values of spacing - ratioed to true rotor tip chords were 0.5, 1.0, 1.5, and 2.0.

At all test speeds for this vane/blade ratio the viscous wake discrete frequency noise is cut off for the BPF and cut on for the second and third harmonics. Hence, if ideal inlet conditions prevailed, the BPF would not be discernible in farfield spectra. However, it has been shown that inlet conditions are far from ideal in static tests. Nonideal conditions may result from any or all of the following:

- turbulence eddies
- ground vortices
- wall boundary layer fluctuations
- thermal gradients

Various investigators, References 2 and 3, have shown how interaction of these inlet disturbances results in noise generation by the rotor alone. Generally, the turbulence eddies form the dominant noise generation mechanisms, Reference 4, and since the incoming turbulence is normally aggravated by static test conditions, an apparent noise reduction is seen going from static to inflight tests. The noise spectrum generated by rotor turbulence interaction is controlled by the incoming turbulence spectrum; however, both discrete frequency and broadband noise may result (References 2 and 4). It has been found that the turbulence spectrum normally peaks at the low frequencies and falls off rapidly at the higher frequencies. Correspondingly, the noise spectrum was also found to decay with frequency.

The 100% $N/\sqrt{0}$ 1/3-octave band PWL spectra presented in Figure 26 indicate no significant change with spacing at the BPF. This is more clearly seen in Figure 27 where the effect of spacing is shown on the 1/3-octave frequencies of 2000 Hz (BPF) to 6300 Hz. However, there is another effect which must be considered when looking at these curves, and that is the effect of the rotor-OGV treatment. The 0.5 chord spacing was hardwall while the 1.0, 1.5, and 2.0 chord spacings had R-OGV treatment with L/H's of 0.26, 0.43, and 0.60, respectively. As will be shown in a later section, the PWL suppression achieved by R-OGV treatment at 1.5 chord spacing was 4.0, .5, .5, 1.0, 1.0 and 2 dB for the 1/3-octave bands from 2000 to 6300 Hz.

The effect of rotor-OGV treatment has not been completely analyzed and therefore needs additional analysis. However, some definite trends are present in the 4000, 5000, and 6300 Hz bands. If we examine the curve at 4000 Hz or the second harmonic more closely, a definite decrease in PWL with spacing can be seen. Our current prediction of viscous wake spacing effect on the second harmonic using the Silverstein wake model from Reference 5 is shown in Figure 28. If we observe that R-OGV treatment has a negligible effect

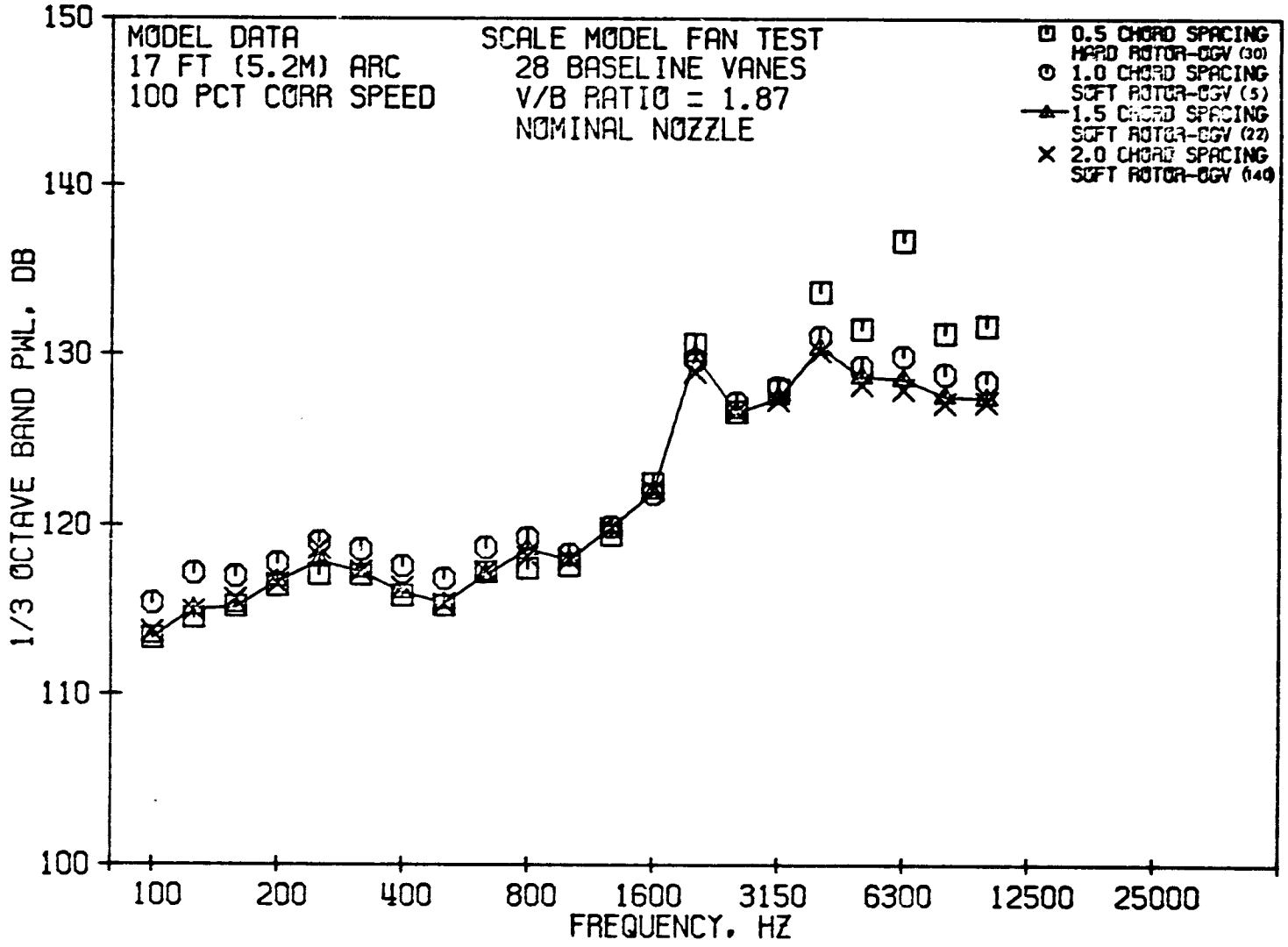

FIGURE 26 EFFECT OF ROTOR-STATOR SPACING ON PWL SPECTRA AT 100% $N/\sqrt{\theta}$

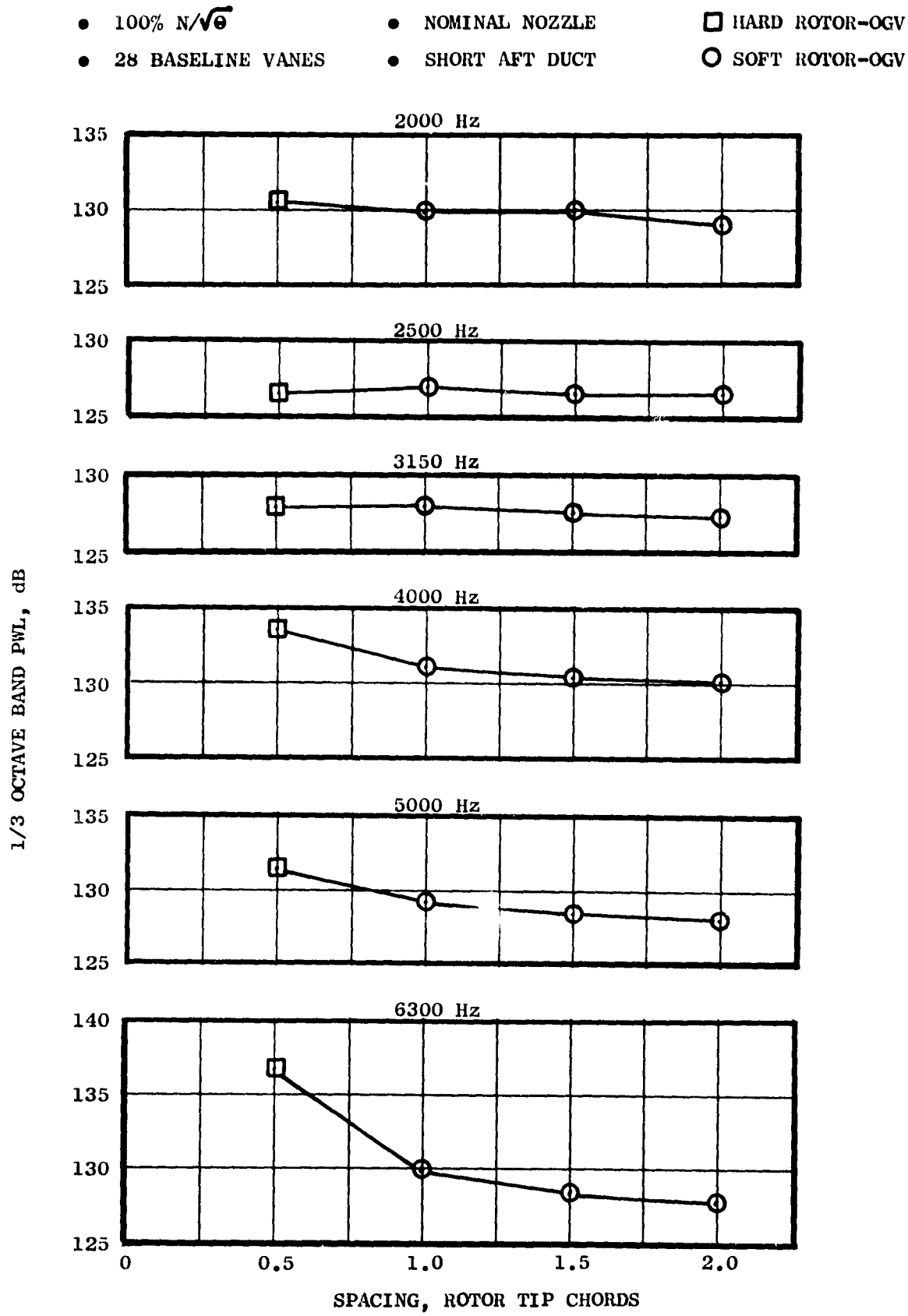

FIGURE 27 PWL CHANGE AT 2000 TO 6300 Hz AS A FUNCTION OF ROTOR – STATOR SPACING

- 28 BASELINE VANES
- 2ND HARMONIC
- SILVERSTEIN WAKE MODEL (Reference 5)

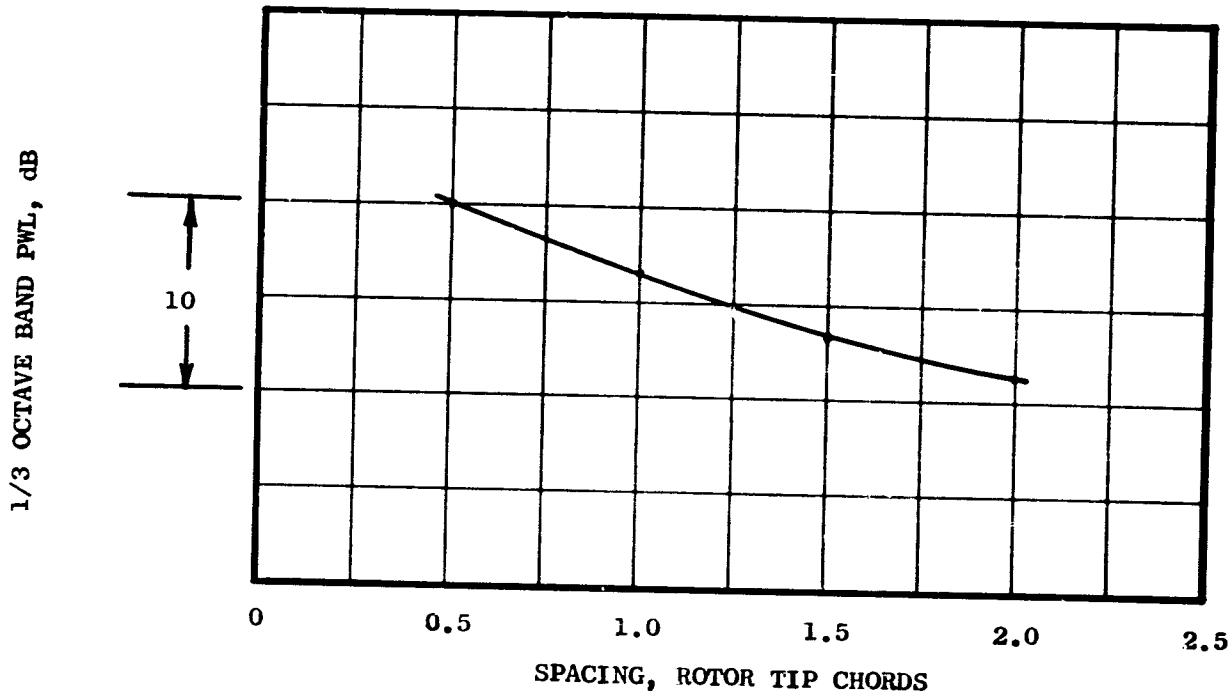

FIGURE 28 PREDICTED PWL CHANGE WITH SPACING

at 4000 Hz (less than 1 dB) and further assume that the PWL of 130 dB at 2 chord spacing is the level of the inlet turbulence noise, which would not be expected to vary with spacing then the level at 0.5 chord spacing is made up of two sources. The first is inlet turbulence at 130 dB which is relatively unchanged with spacing and the second is rotor-stator noise which is 130.8 dB because together these two must add to give the 0.5 chord value of 133.5. Figure 29 shows the relative levels of rotor-turbulence and rotor-stator noise at each spacing under the assumption outlined above with the Silverstein model applied to the rotor-stator noise. The sum of the components is in good agreement with the measured PWL results. Similarly, at 1.0 chord the viscous wake PWL using the GE prediction is at 127.4 dB which when combined with the inlet turbulence level of 130 dB gives 131.9 dB. This is in good agreement with the measured PWL data.

At 6300 Hz, the decay in PWL is highly indicative of viscous wake noise. Several investigators, e.g. Reference 6, suggest that the intensity of higher harmonics generated by rotor-inlet distortion interaction falls off rather rapidly with harmonic number. This effect would appear to be reflected by the 6300 Hz 1/3-octave band PWL's.

Clearly, the subject of spacing has not been examined in this report in enough detail to answer all questions. However, the discussion here points out the need for more investigation into this test data in an attempt to better define the relative contributions of rotor-turbulence interaction and viscous wake interaction.

C. Low Mach Vanes

A potential fan source noise reduction technique, low Mach vanes, was investigated during this test program. This technique consists primarily of a flow diffusion between the rotor and OGV's to lower the axial flow Mach numbers entering and through the vane row. An annular area increase of 11% resulted in approximately an 11% decrease in the axial Mach number. Analysis indicates that this axial Mach number decrease should result in a 1.0 to 1.5 dB decrease in the stator generated noise (30 log axial velocity ratio).

Test results however, indicate no significant change in farfield SPL's. Figure 30 shows a typical aft angle which indicates that the low Mach vanes increased the BPF by 1.5 dB and also increased the broadband levels near the BPF by less than 1 dB. Similar results are evident with the 1/3-octave band PWL's at 100% $N/\sqrt{\theta}$ in Figure 31.

There are two possible reasons for the apparent lack of noise reduction with the low Mach vanes. The first is that aerodynamic performance had changed enough to make a direct comparison between the low Mach and baseline vanes unrealistic. Aerodynamic data indicates only a slight decrease in the low Mach vane total pressure recovery and airflow when compared to the baseline vanes. This indicates that the low Mach vanes were operating well aerodynamically and thus, it is unlikely that there is a performance basis for the lack of noise reduction.

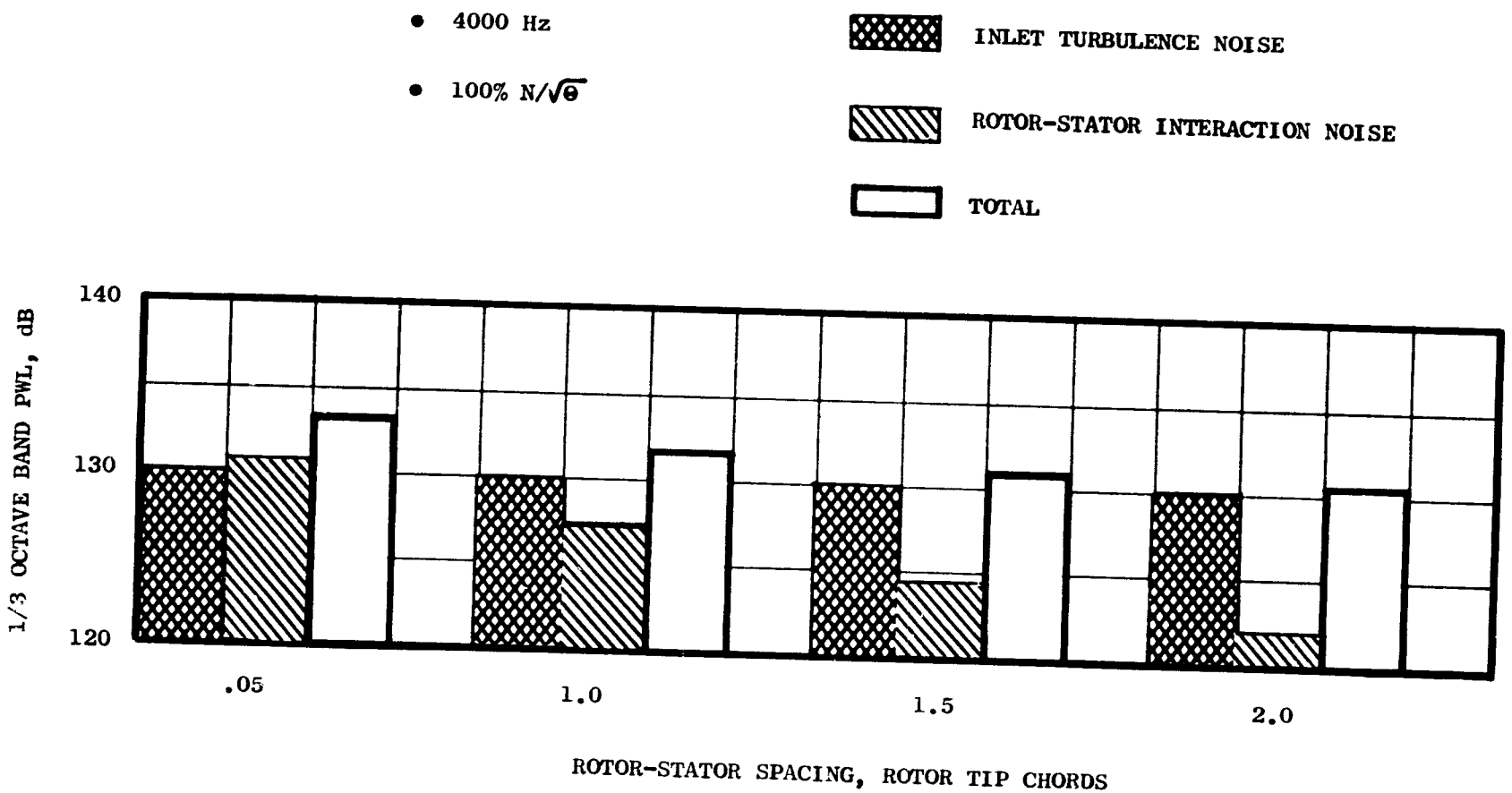

FIGURE 29 RELATIVE CONTRIBUTION OF ROTOR-TURBULENCE AND ROTOR-STATOR NOISE AS A FUNCTION OF SPACING

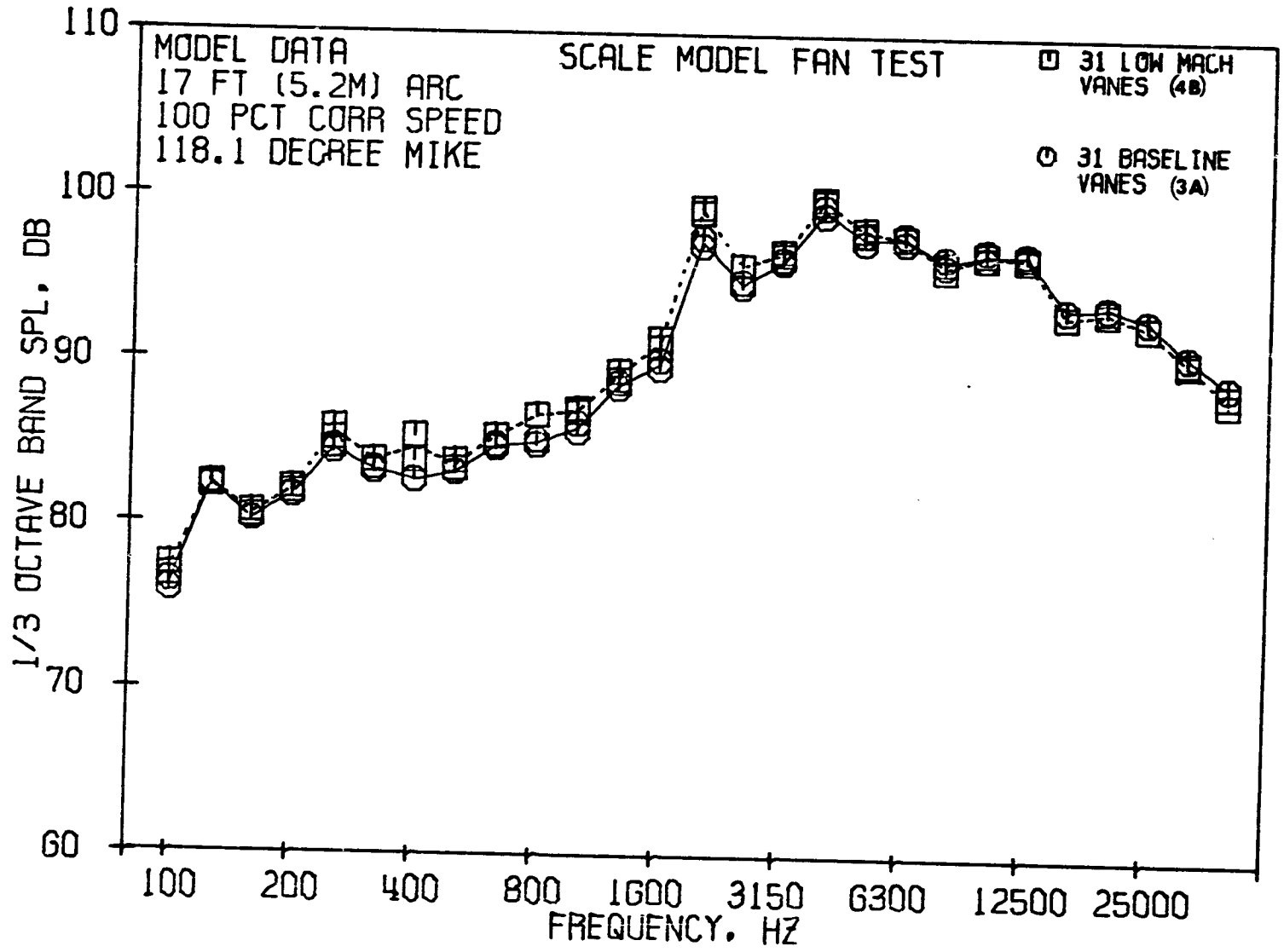

FIGURE 30 SPL COMPARISON OF LOW MACH AND BASELINE VANES AT 100% N/$\sqrt{\theta}$

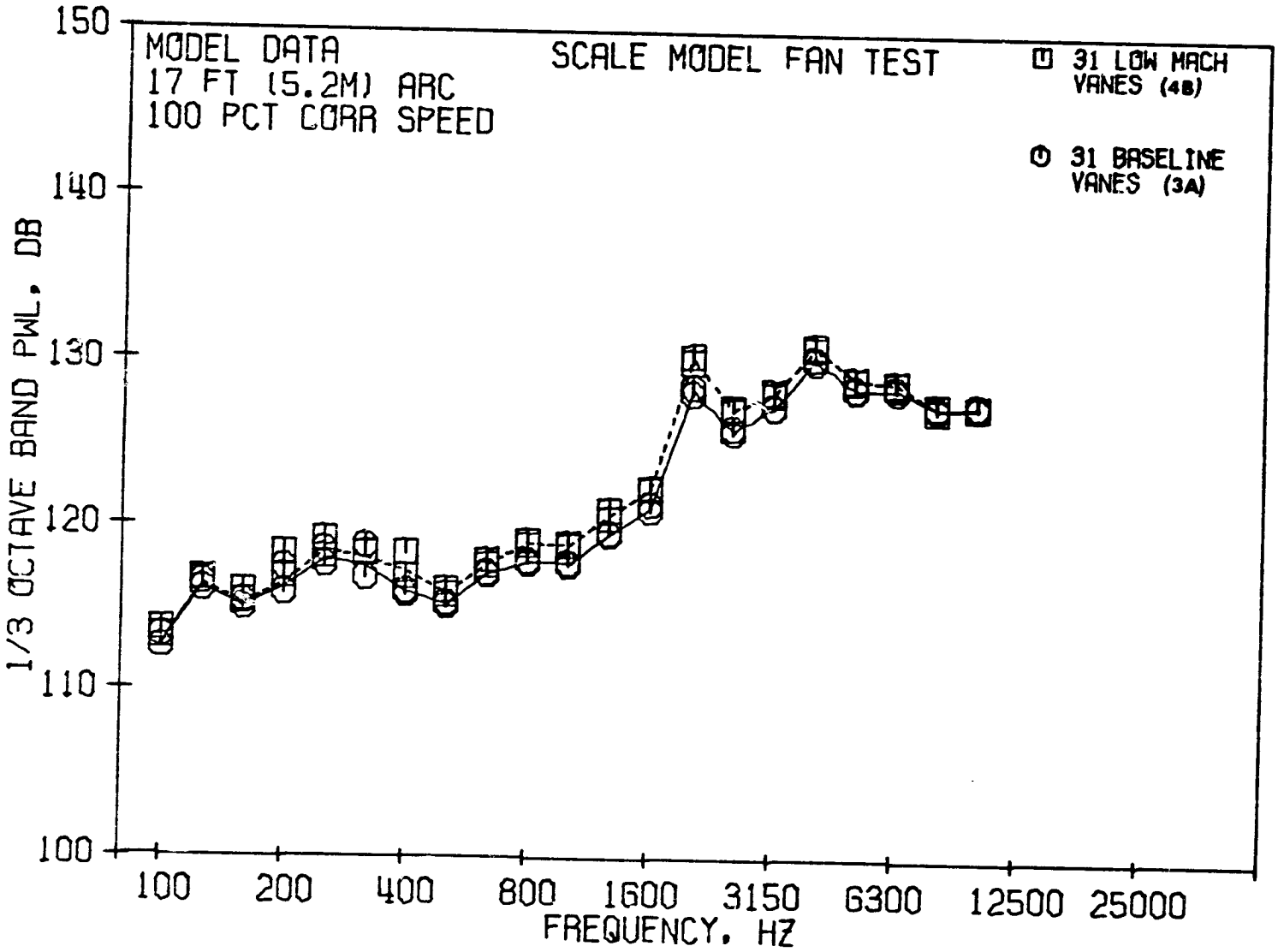

FIGURE 31 PWL COMPARISON OF LOW MACH AND BASELINE VANES AT 100% $N/\sqrt{\theta}$

The second possibility is that at 1.5 chord spacing the aft fan noise is controlled by some other source and this is consistent with the results obtained on the vane/blade ratio study which observed a rotor-stator interaction effect at close chord spacing but none at 1.5 chord spacing. It appears that even though low turbulence levels were measured on-line upstream of the fan, this did not give enough information to provide detailed insight into the spectrum of the turbulence, the eddy sizes seen by the rotor and therefore the turbulence - rotor interaction noise levels.

D. Long Duct Versus Short Duct

As noted in earlier discussions, the test vehicle was designed to be tested with either a long aft duct or a short aft duct where the nozzle was mounted directly aft of the support struts. This was shown in Figure 3.

A comparison of the PWL at 100% $N/\sqrt{\theta}$ is presented in Figure 32. It is evident that the long hardwall aft duct (L/H = 5) attenuated the sound by 1 to 2 dB at frequencies at or above the BPF. PWL's at lower fan speeds exhibited similar results. Not surprisingly there was a difference in directivity pattern between the two configurations. Model PNL directivity is shown in Figure 33 and shows the short duct to be about 1 to 2 PNdB higher in the region of 70° to 130°. In Figure 34 the 1/3-octave band which contains the BPF, 2000 Hz, shows a marked change in directivity on the 17 foot (5.2 m) arc.

The key item here is that aft suppression tests should use the long duct as their baseline when comparing suppression levels. The source noise comparisons where a long duct was involved, specifically Configuration 1B, should be used with the awarness of the effect of the duct length in any such comparison.

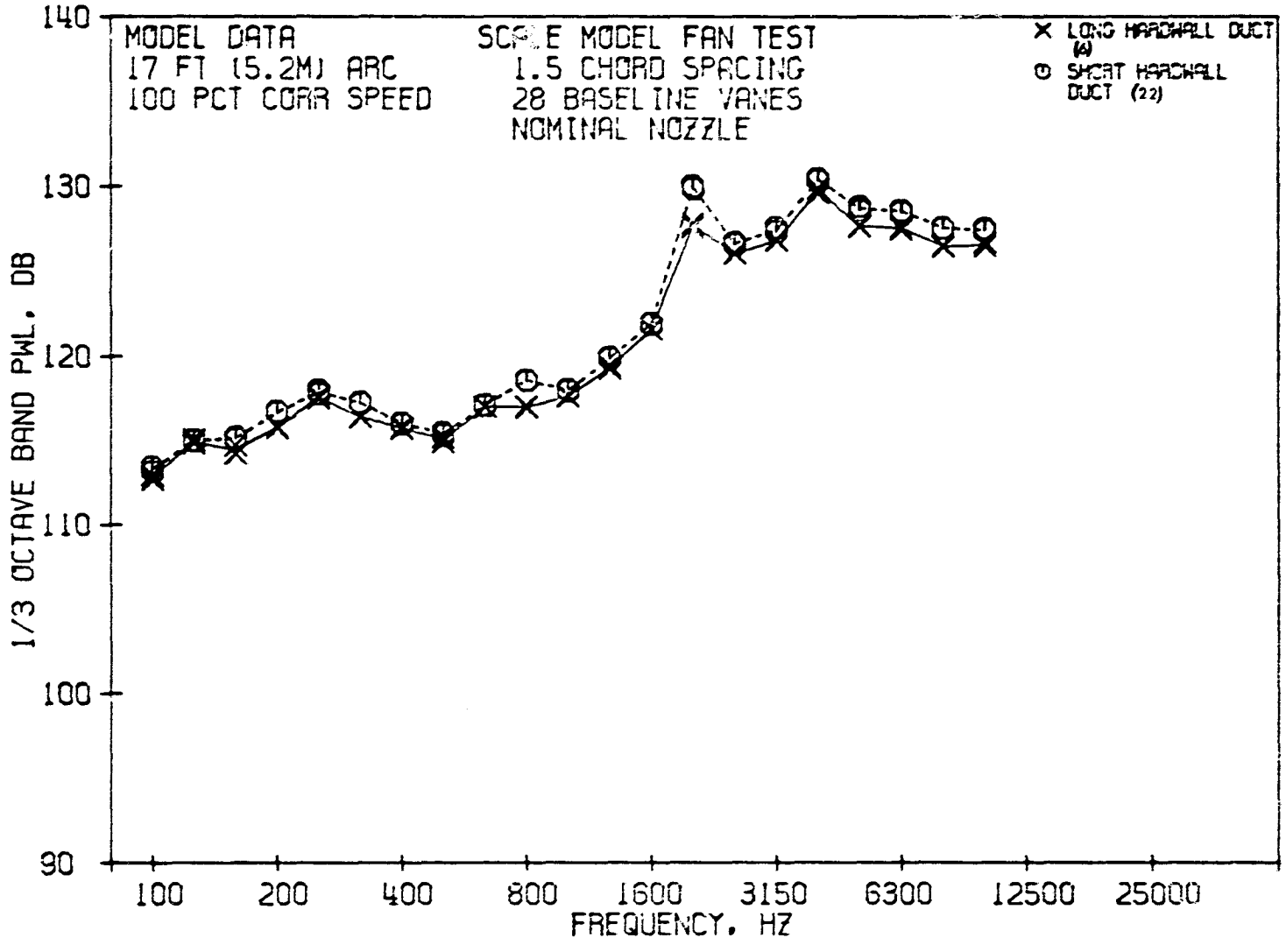

FIGURE 32 COMPARISON OF LONG AND SHORT AFT DUCT PWL SPECTRA AT 100% $N/\sqrt{\theta}$

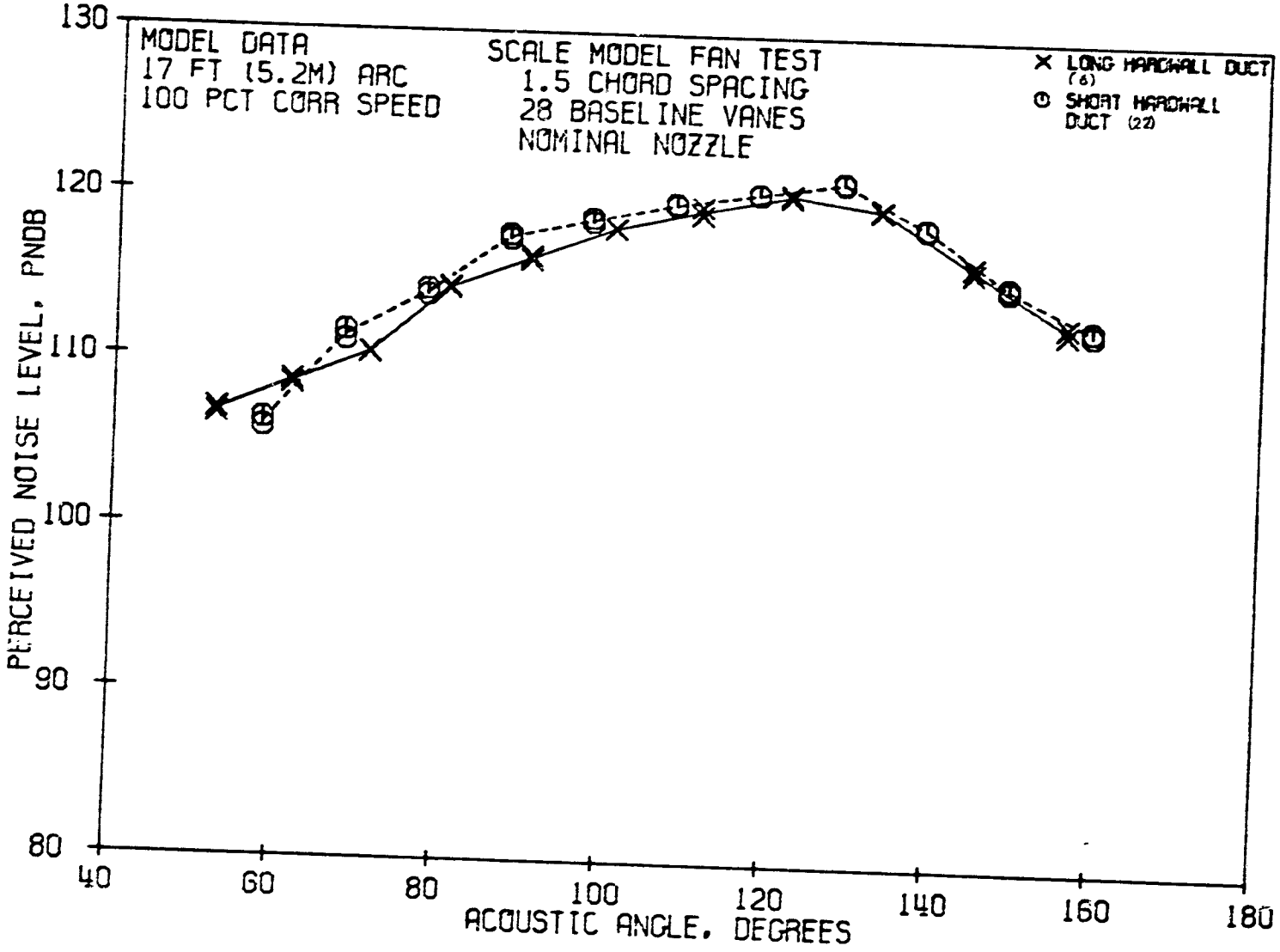

FIGURE 33 COMPARISON OF LONG AND SHORT AFT DUCT PNL DIRECTIVITY AT 100% $N/\sqrt{\theta}$

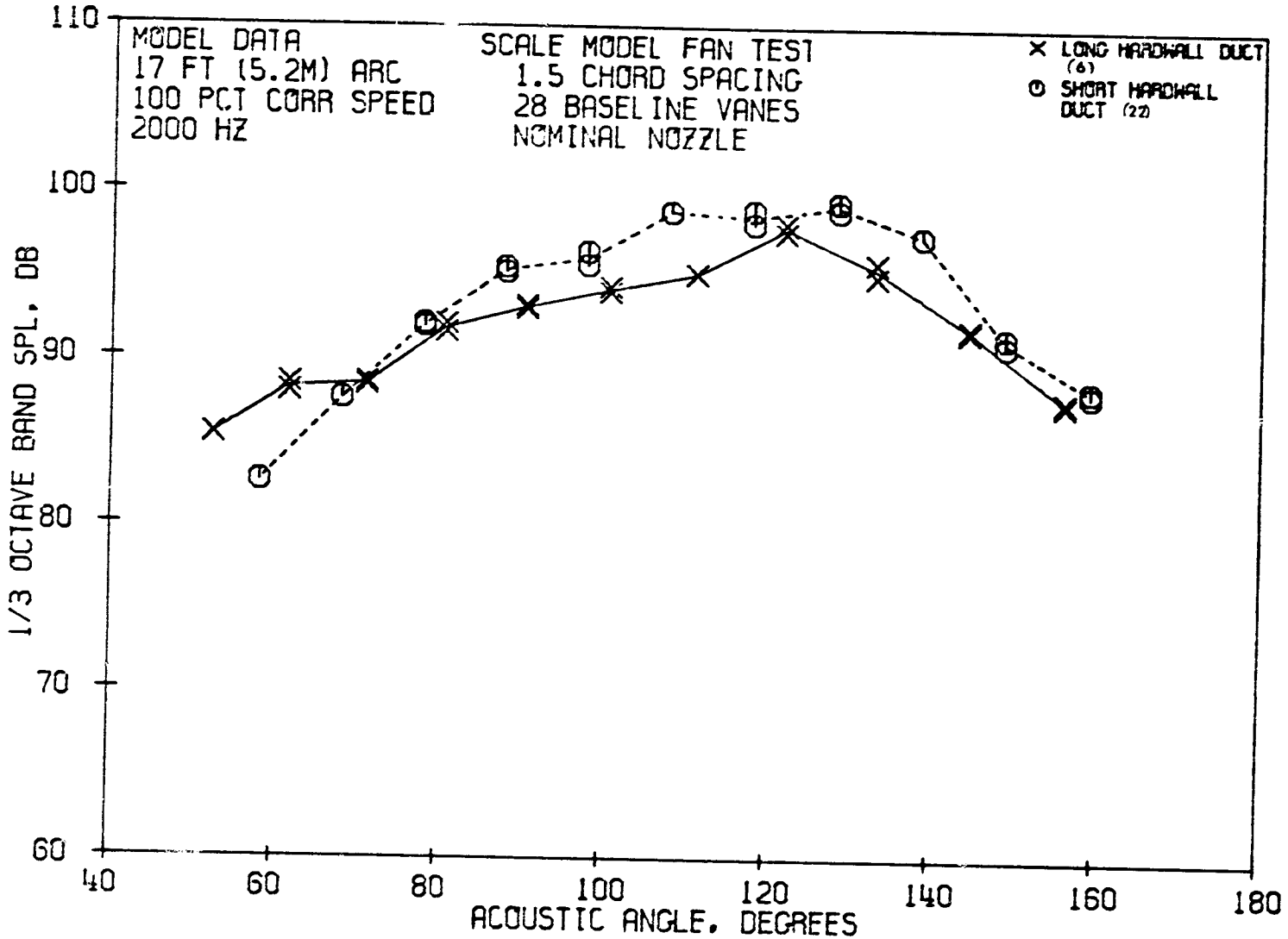

FIGURE 34 COMPARISON OF LONG AND SHORT AFT DUCT BPF SPL DIRECTIVITY AT 100% N/ $\sqrt{\theta}$

SECTION VIII

AFT SUPPRESSION TEST RESULTS

The aft suppression tests evaluated wall treatment, splitter suppression, and the effect of aft duct Mach number. Table VII summarizes the various configurations that were tested. The results are analyzed as model data which can be evaluated directly or representative of full scale results since the treatment for both model and full scale are tuned to 3000 Hz, the maximum noy-weighted region of the spectrum.

With the number of aft suppression configurations tested there are many comparisons that can be made. The following discussions will cover only the more obvious. For looking at all the configurations (L/H = 4.6), Table VIII summarizes the aft angle PNL suppression achieved for each configuration plus the PWL suppression achieved at 2000 Hz (BPF 1/3-octave band).

A. Porosity Effects

The aft suppression configurations that were tested included test to determine the effectiveness of high (27 percent open area) and low (12 percent open area) porosity designs. Cold flow duct test results were used to choose these two porosities. Porosity effects are available from two aft duct configurations one with variable depth, thin-to-thick treatment and one with constant thickness treatment. These are sketched in Figure 35.

1. Constant Thickness Treatment

Comparison of the 12 and 27 percent porosity designs with constant thickness single-degree-of-freedom treatment indicates that the 12 percent porosity has a higher peak suppression and wider suppression bandwidth. Figure 36 shows this result for the PWL's at 100% $N/\sqrt{\theta}$ while similar SPL results are observed at 122 degrees in Figure 37.

2. Variable Thickness Treatment

Figures 38 and 39 present PWL and 122 degree SPL comparisons at 100% $N/\sqrt{\theta}$ with variable thickness, thin-to-thick treatment, 12 and 27 percent porosities. As with the constant thickness designs, the low porosity achieved better suppression. However, as Figure 40 indicates the suppression bandwidth is increased only at frequencies above the peak frequency. Similar trends are observed at lower fan speeds.

TABLE VII AFT SUPPPESSION TEST CONFIGURATIONS

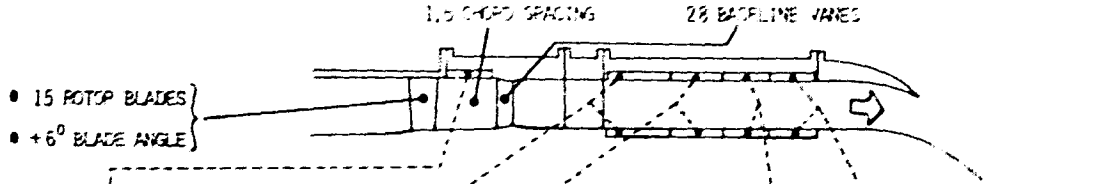

*INNER AND OUTER PANELS ARE THE SAME DEPTH AND POROSITY UNLESS OTHERWISE NOTED BY (I) AND (O).

**P DENOTES AERODYNAMIC RAKES IN FRONT OF THE ROTOR.

CONFIGURATION	ROTOR-OGV TREATMENT	DEPTH IN.(CM.)	POROSITY %	DEPTH IN.(CM.)	POROSITY %	DEPTH IN.(CM.)	POROSITY %	DEPTH IN.(CM.)	POROSITY %	NOZZLE	COMMENTS
6	YES	0	0	0	0	0	0	0	0	NOMINAL	
7,7R	NO	.25(.64)	12	.5(1.27)	12	.75(1.91)	12	1.5(3.81)	12		
8,8R		.25(.64)	27	.5(1.27)	27	.75(1.91)	27	1.5(3.81)	27		
9,9R		.5(1.27)	27	.25(.64)	27	.75(1.91)	27	1.5(3.81)	27		WITH 0.6 IN.(1.52CM) SPLITTER, L/H= 2.30
10,10R		.5(1.27)	27	.25(.64)	27	.75(1.91)	27	1.5(3.81)	27	OPEN	
15,16R		.25(.64)	27	.5(1.27)	27	.75(1.91)	27	1.0(2.54)	27	NOMINAL	
17		.75(1.91)	27	.75(1.91)	27	.75(1.91)	27	.75(1.91)	27		
18,18R		0	0	0	0	0	0	0	0		
23		0	0	0	0	0	0	0	0	OPEN	
24		(O).25(.64)	27	.5(1.27)	27	.75(1.91)	27	1.5(3.81)	27	NOMINAL	
		(I).75(1.91)	27	.75(1.91)	27	.75(1.91)	27	.75(1.91)	27		
25		(O).25(.64)	27	.5(1.27)	27	.75(1.91)	27	1.0(2.54)	27		SLANT CELL - LAST OUTER PANEL
		(I).25(.64)	27	.5(1.27)	27	.75(1.91)	27	1.5(3.81)	27		
26		1.5(3.81)	12	.75(1.91)	12	.5(1.27)	12	.25(.64)	12		
75-1A		0	0	0	0	0	0	.25(.64)	12		
75-1B								.5(1.27)	12		
75-1C								.75(1.91)	12		
75-1D								1.5(3.81)	12		
75-1E								1.0(2.54)	27		SLANT CELL
75-1F								0	0		

TABLE VII AFT SUPPRESSION TEST CONFIGURATIONS (CONCLUDED)

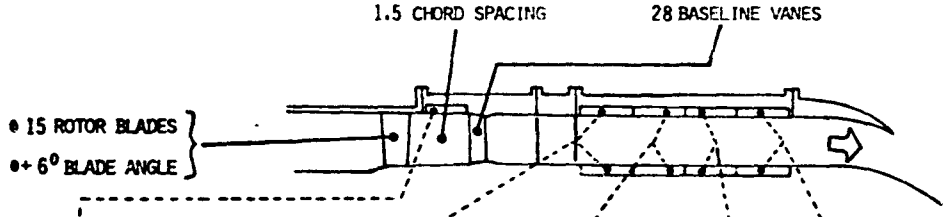

• INNER AND OUTER PANELS ARE THE SAME DEPTH AND POROSITY UNLESS OTHERWISE NOTED BY (I) AND (O).

CONFIGURATION	ROTOR-OGV TREATMENT	DEPTH IN.(CM.)	POROSITY %	DEPTH IN.(CM.)	POROSITY %	DEPTH IN.(CM.)	POROSITY %	DEPTH IN.(CM.)	POROSITY %	NOZZLE	COMMENTS
75-1G	NO	0	0	0	0	0	0	.25(.64)	27	NOMINAL	
75-1H								.50(1.27)	27		
75-1I								.75(1.91)	27		
75-1J								1.0(2.54)	27		
75-1K								1.5(3.81)	27		
75-2	YES	.25(.64)	12	.50(1.27)	12	.75(1.91)	12	1.5(3.81)	12		
75-3	NO	.75(1.91)	12	.75(1.91)	12	.75(1.91)	12	.75(1.91)	12		
75-4		(O) .25(.64)	12	.50(1.27)	12	.75(1.91)	12	1.5(3.81)	12		
		(I) .75(1.91)	12	.75(1.91)	12	.75(1.91)	12	.75(1.91)	12		
75-5		1.5(3.81)	27	.75(1.91)	27	.50(1.27)	27	.25(.64)	27		
75-6A		.75(1.91)	12	.75(1.91)	12	.75(1.91)	12	.75(1.91)	12		STAGE 55 VANES
75-6B		0	0	0	0	0	0	0	0		
75-6C		1.5(3.81)	27	0	0	0	0	0	0		
75-6D		0	0	0	0	0	0	1.5(3.81)	27		
75-7		.25(.64)	12	.75(1.91)	27	.50(1.27)	12	1.5(3.81)	27		
75-8		.50(1.27)	12	.75(1.91)	12	.25(.64)	12	1.5(3.81)	27		
75-9		.25(.64)	12	.50(1.27)	12	.75(1.91)	12	1.5(3.81)	12		TREATMENT L/H = 3.68

TABLE VIII MEASURED PNL AND BPF PWL SUPPRESSION

- 100% $N/\sqrt{5}$
- 17 ft arc (5.2 m)

Config.	ΔPNL 111°	ΔPNL 122°	ΔPNL 133°	ΔPWL 2000 Hz BPF	Porosity Distribution	Panel Thickness Orientation inches	Panel Thickness Orientation (cm)
7	13.2	11.0	8.4	15.2	12-12-12-12	.25-.50-.75-1.5	(.64-1.27-1.91-3.81)
8	10.4	9.2	6.9	16.6	27-27-27-27	.25-.50-.75-1.5	(.64-1.27-1.91-3.81)
9	11.1	10.9	10.1	16.1	27-27-27-27	.50-.25-.75-1.5	(1.27-.64-1.91-3.81)
10	9.8	9.6	9.4	14.2	27-27-27-27	.50-.25-.75-1.5	(1.27-.64-1.91-3.81)
16	10.6	8.1	7.0	14.0	27-27-27-27	.25-.50-.75-1.0	(.64-1.27-1.91-2.54)
17	8.8	7.6	6.2	13.6	27-27-27-27	.75-.75-.75-.75	(1.91-1.91-1.91-1.91)
24	9.3	8.0	6.3	13.5	27-27-27-27	.25-.50-.75-1.5 .75-.75-.75-.75	(.64-1.27-1.91-3.81) (1.91-1.91-1.91-1.91)
25	10.6	9.3	7.6	17.1	27-27-27-27	.25-.50-.75-1.0 .25-.50-.75-1.5	(.64-1.27-1.91-2.54) (.64-1.27-1.91-3.81)
26	12.5	10.7	9.8	16.8	12-12-12-12	1.5-.75-.50-.75	(3.81-1.91-1.27-.64)
75-2	14.0	11.9	9.8	18.5	12-12-12-12	.25-.50-.75-1.5	(.64-1.27-1.91-3.81)
75-3	10.1	8.8	6.8	18.7	12-12-12-12	.75-.75-.75-.75	(1.91-1.91-1.91-1.91)
75-4	12.5	10.4	7.5	16.8	12-12-12-12	.25-.50-.75-1.5 .75-.75-.75-.75	(.64-1.27-1.91-3.81) (1.91-1.91-1.91-1.91)
75-5	8.9	8.5	8.8	17.17.8	27-27-27-27	1.5-.75-.50-.75	(3.81-1.91-1.27-.64)
75-6A	10.7	9.8	7.1	22.5	12-12-12-12	.75-.75-.75-.75	(1.91-1.91-1.91-1.91)
75-7	12.3	10.9	9.4	17.8	12-27-12-27	.25-.75-.50-1.5	(.64-1.91-1.27-3.81)
75-8	12.6	10.8	9.6	18.0	12-12-12-12	.50-.75-.25-1.5	(1.27-1.91-.64-3.81)
75-9	11.9	10.9	8.4	15.2	12-12-12-12	.25-.50-.75-1.5	(.64-1.27-1.91-3.81)

- HARD ROTOR-OGV
- NOMINAL NOZZLE
- TREATMENT L/H = 4.6

CONFIGURATION 18, HARDWALL

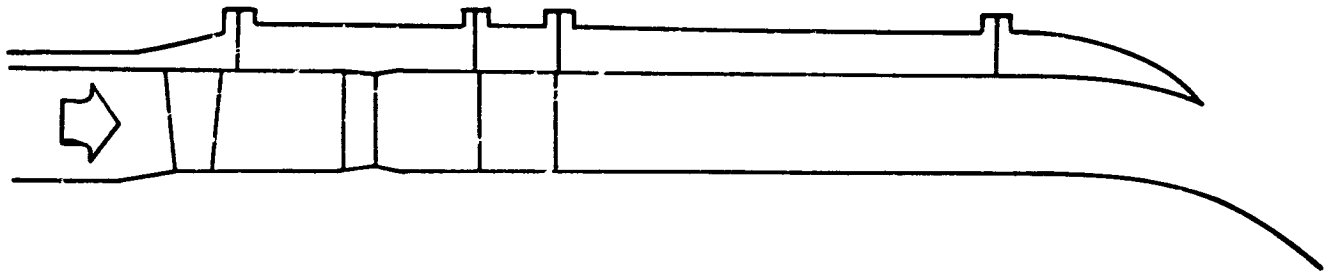

CONFIGURATION 75-3A, POROSITY = 12%
CONFIGURATION 17, POROSITY = 27%

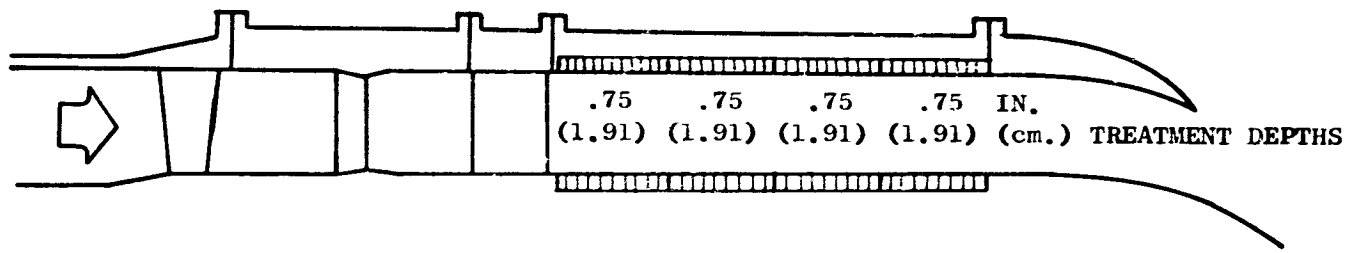

CONFIGURATION 7, POROSITY = 12%
CONFIGURATION 8, POROSITY = 27%

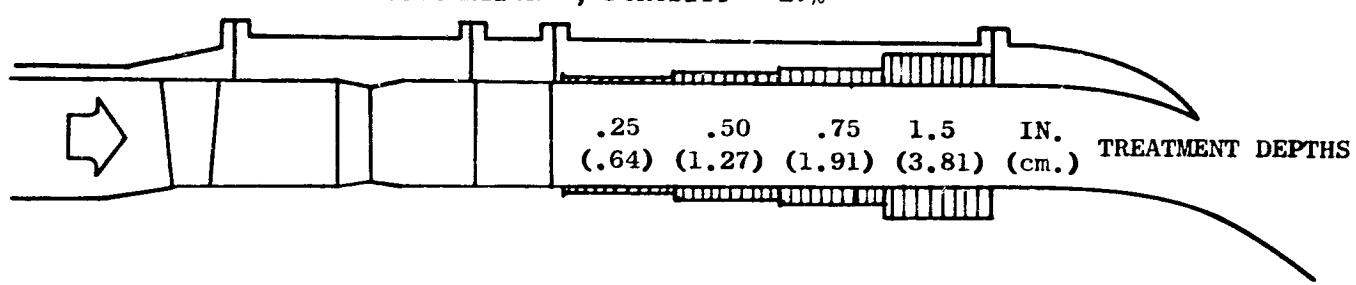

FIGURE 35 POROSITY EFFECT CONFIGURATIONS

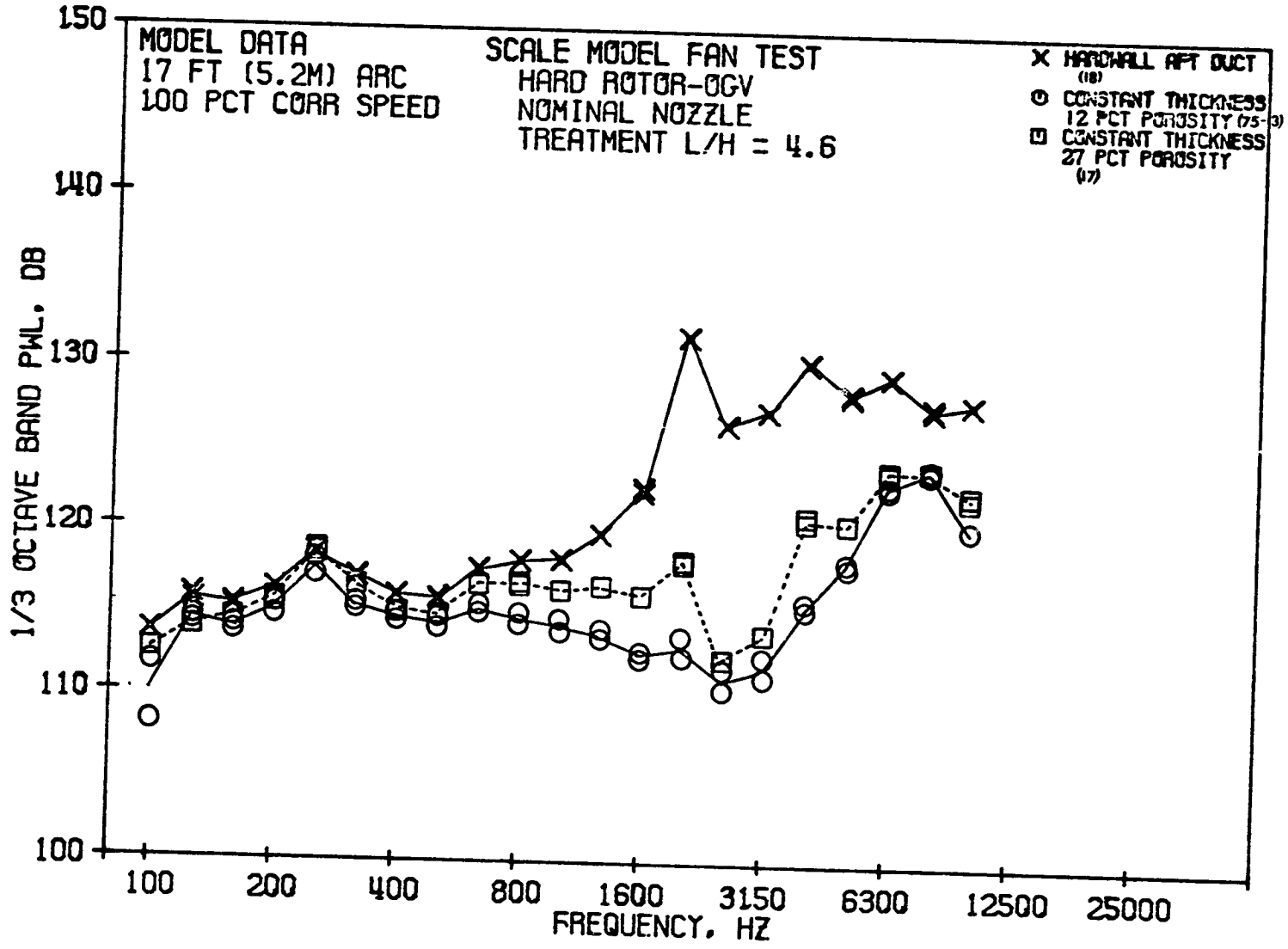

FIGURE 36 COMPARISON OF 12 AND 27 PERCENT POROSITY CONSTANT DEPTH PWL SPECTRA AT 100% $N/\sqrt{\theta}$

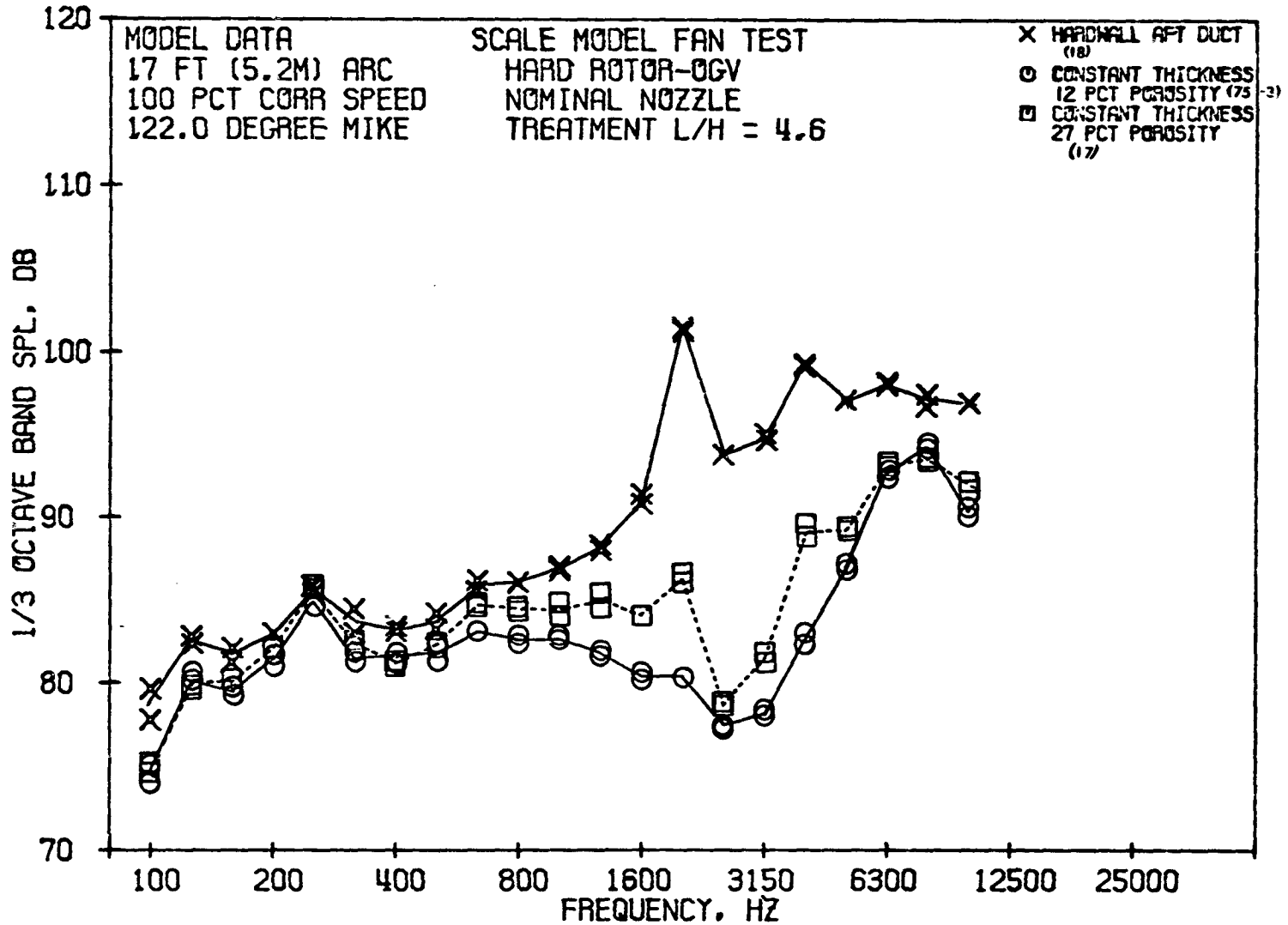

FIGURE 37 COMPARISON OF 12 AND 27 PERCENT POROSITY CONSTANT DEPTH SPL'S AT 100% $N/\sqrt{\theta}$

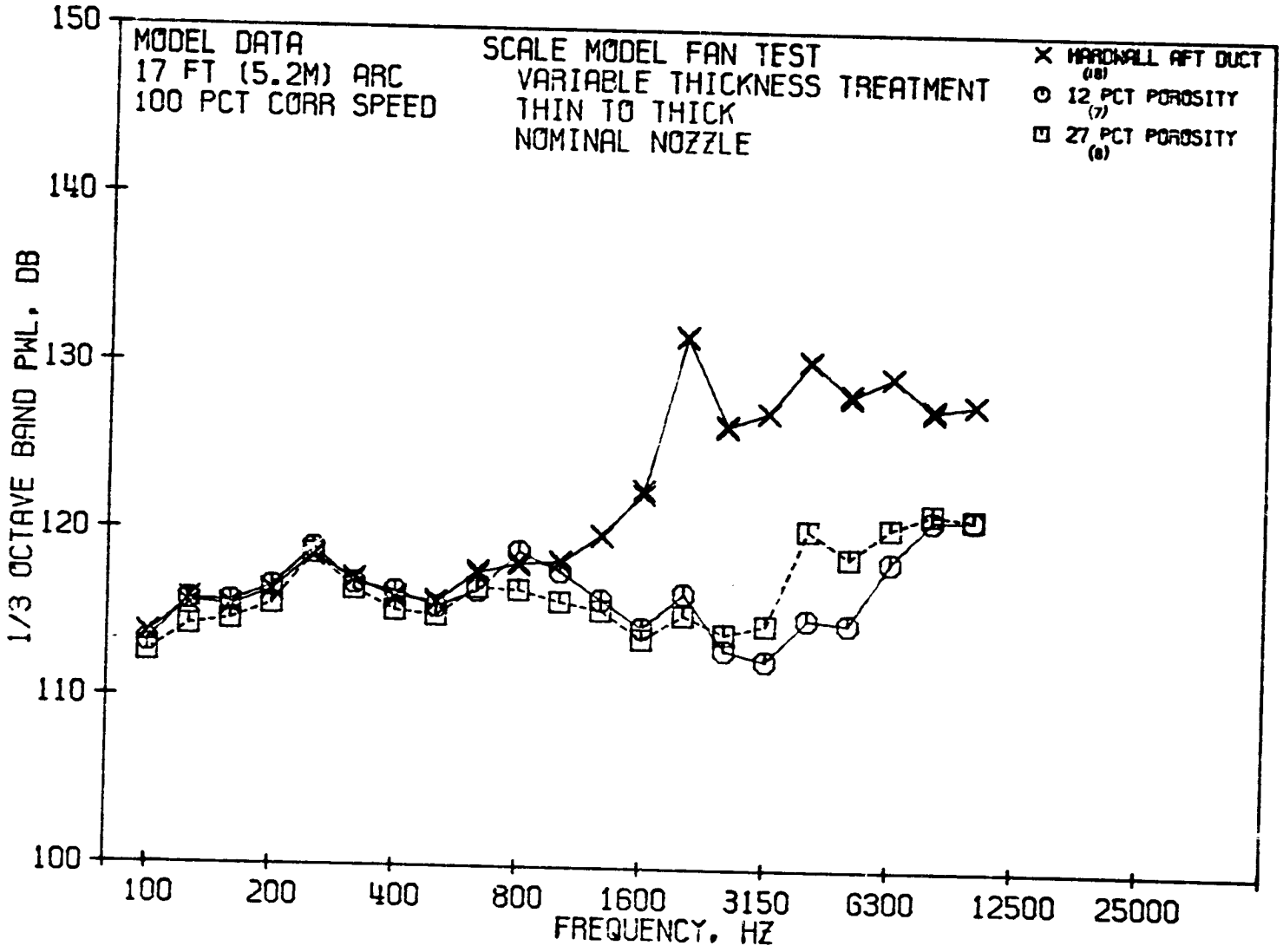

FIGURE 38 COMPARISON OF 12 AND 27 PERCENT POROSITY VARIABLE DEPTH PWL SPECTRA AT 100% $N/\sqrt{\theta}$

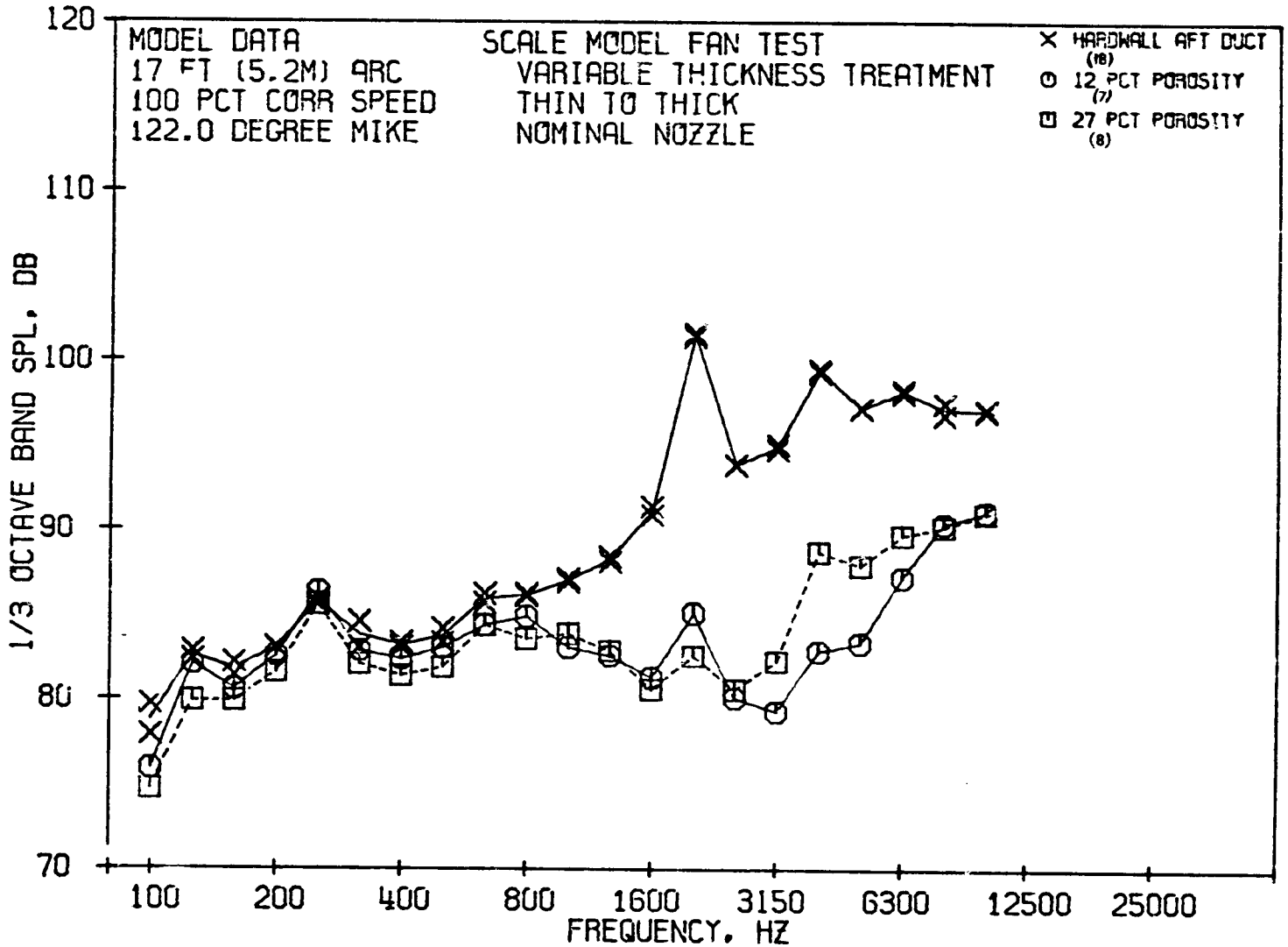

FIGURE 39 COMPARISON OF 12 AND 27 PERCENT POROSITY VARIABLE DEPTH SPL'S AT 100% $N/\sqrt{\theta}$

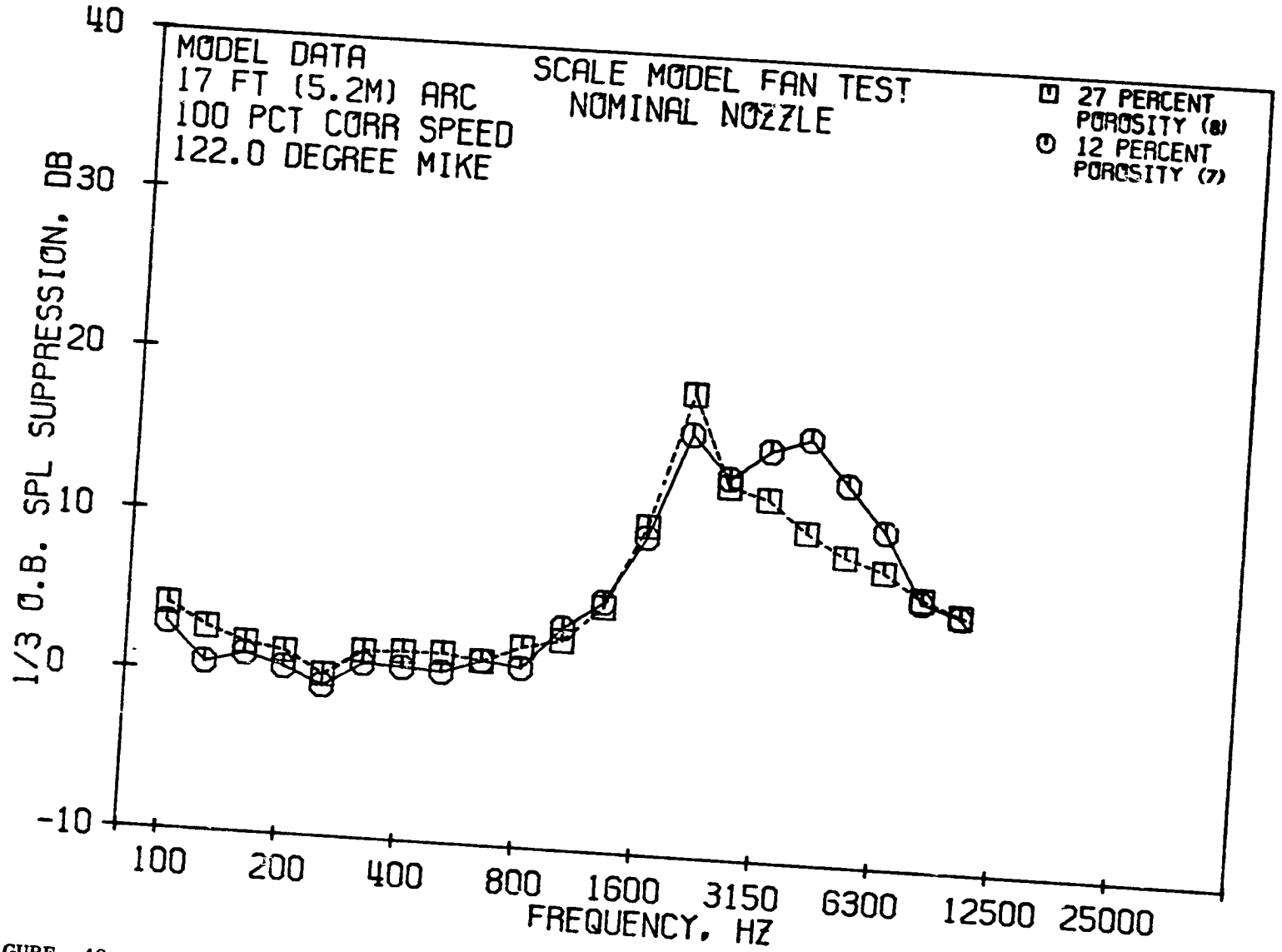

FIGURE 40 COMPARISON OF 12 AND 27 PERCENT POROSITY VARIABLE DEPTH SPL SUPPRESSION AT 100% $N/\sqrt{\theta}$

B. Phasing Effect

A series of tests were conducted to investigate phasing effects with aft suppression variable depth treatment. By placing treatment whose impedance characteristics are quite different in successive lengths, an "interaction or phasing effect" is obtained which produces greater attenuation than just the sum of the individual treatment elements with equal L/H values. Based upon analytical experience, it is felt that the most likely explanation of the effect is that energy is redistributed into higher order modes which are more readily suppressed. Figure 41 shows the sets of configurations which were tested.

Cold flow duct test data showed that the arrangement of treatment thicknesses had a significant effect on phasing at high porosity and that high porosity faceplate was more effective than low porosity. Thus, two porosities -12 and 27 percent- were tested with variable depth treatment oriented both thin-to-thick and thick-to-thin in the direction of sound propagation.

In addition to comparisons on the arrangement of the treatment, the variable depth designs at both porosities are compared to constant thickness designs which were tuned to the high noy-weighted frequency and which represents a conventional nonphasing type of design.

1. 12 Percent Porosity Faceplate

Acoustic data taken in the General Electric Company rectangular duct indicated no change in suppression levels of the variable thickness treatment with 12 percent porosity faceplate when tested in a thin-to-thick or a thick-to-thin configuration. At low fan speeds, there was more suppression indicated for the 111 degree, 12 percent porosity, thin-to-thick combination at frequencies of 2500 to 8000 Hz as shown in Figure 42 at 70% $N/\sqrt{\theta}$.

At 80% $N/\sqrt{\theta}$ in Figure 43, there is less difference between the two suppression configurations. At 100% $N/\sqrt{\theta}$ (not shown) there is no significant difference between the two configurations at any aft angle. This implies that any phasing effect present is sensitive to fan speed or perhaps fan duct Mach number.

PWL suppression spectra achieved for the 12 percent variable depth and the constant thickness treatments are compared in Figures 44 and 45 for 70 and 100% $N/\sqrt{\theta}$, respectively. The constant thickness gives increased peak suppression, however, the variable depth has a wider bandwidth at the higher frequencies. The suppression differences at frequencies below the peak attenuation frequency do not correlate with fan speed. At 70 and 100% $N/\sqrt{\theta}$ shown above, the constant thickness achieved more suppression. At 80 and 90% $N/\sqrt{\theta}$ (not shown); however, little difference in suppression was evident.

A comparison of the model PNL directivities in Figure 46, shows that the increased bandwidth above the peak attenuation frequency makes the variable depth treatment more effective in suppressing the high noy-weighted frequencies. This trend continues with fan speed as shown in Figure 47 which indicates the PNL suppressions at 111, 122, and 133 degrees are consistently higher with the 12 percent variable depth, thin-to-thick treatment.

- NOMINAL NOZZLE
- HARD ROTOR-OGV
- TREATMENT L/H = 4.6

CONFIGURATION 18, HARDWALL

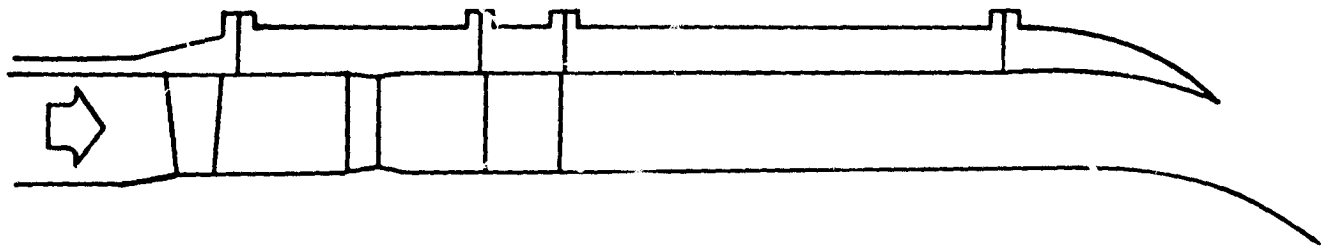

CONFIGURATION 7, POROSITY = 12%

CONFIGURATION 8, POROSITY = 27%

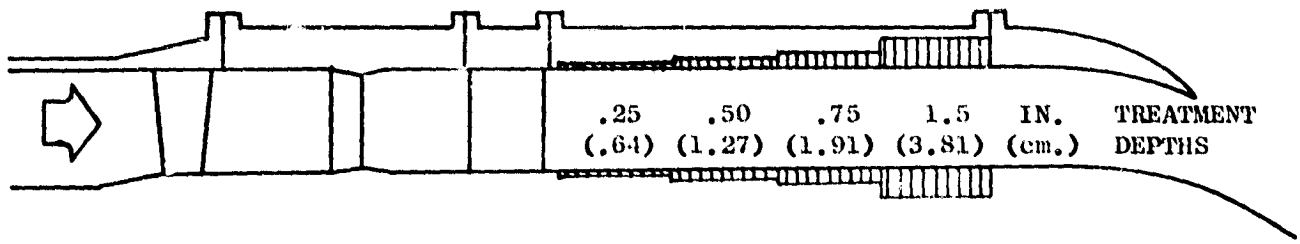

CONFIGURATION 26, POROSITY = 12%

CONFIGURATION 75-5, POROSITY = 27%

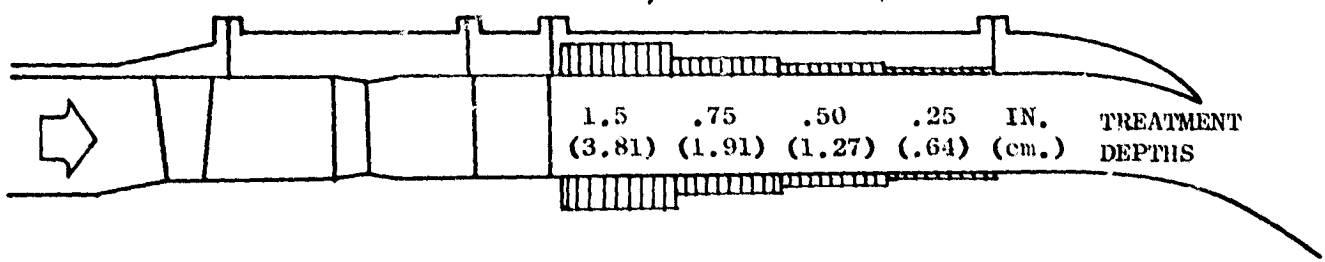

CONFIGURATION 75-3, POROSITY = 12%

CONFIGURATION 17, POROSITY = 27%

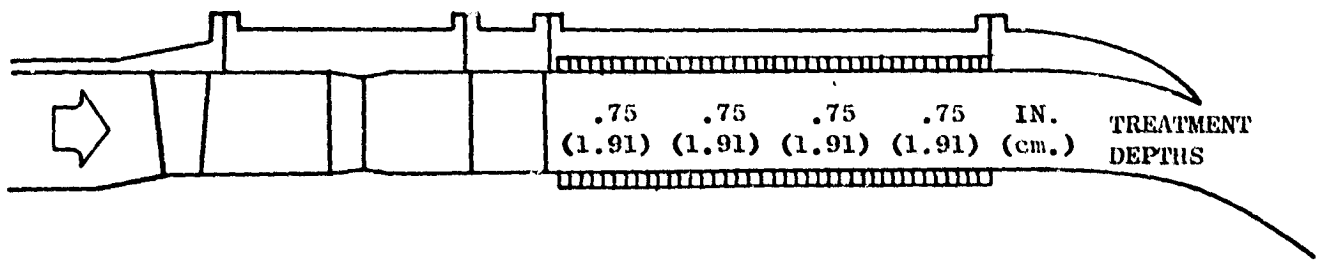

FIGURE 41 PHASING EFFECT CONFIGURATIONS

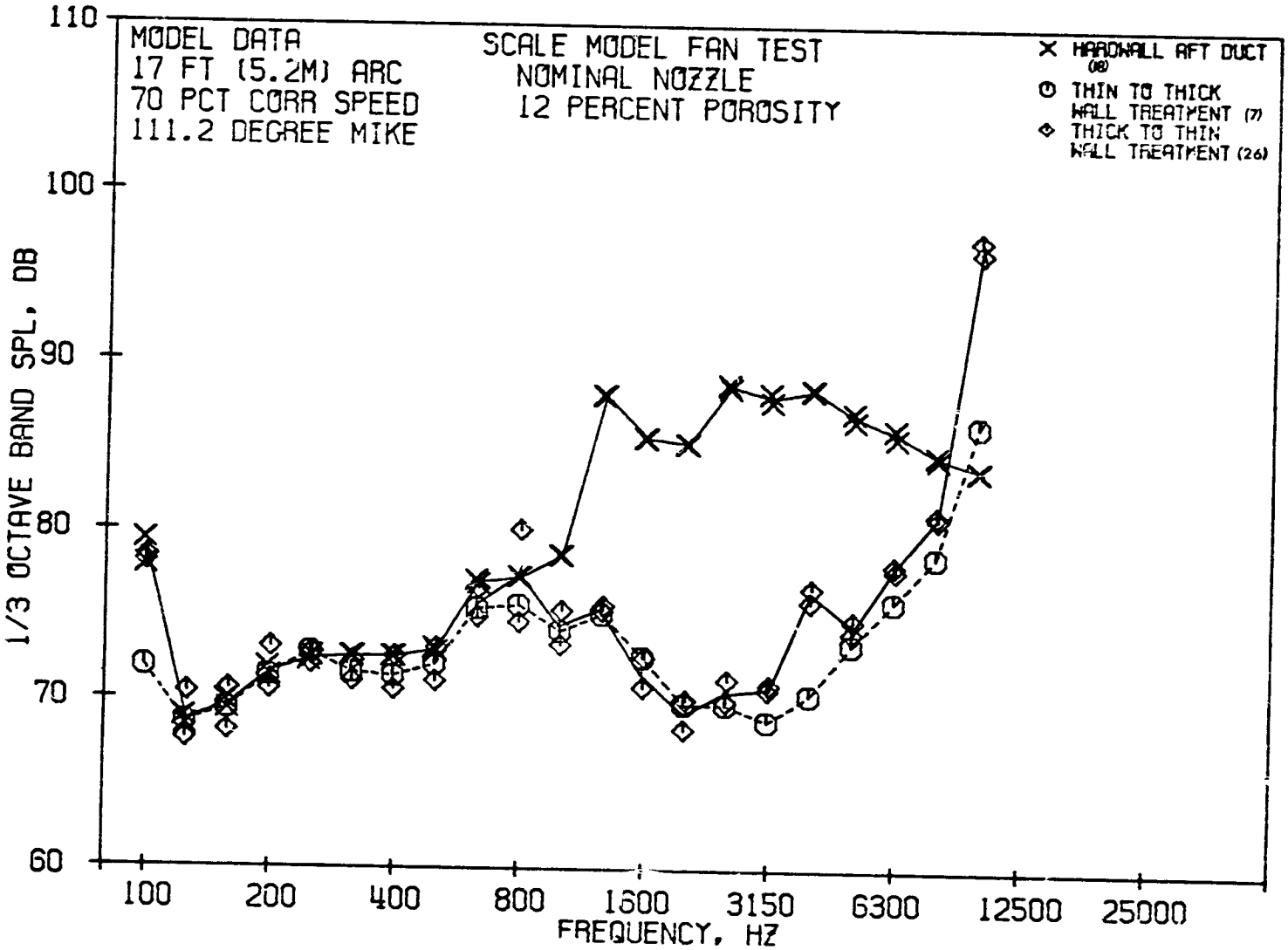

FIGURE 42 12 PERCENT POROSITY VARIABLE DEPTH TREATMENT SPL'S AT 70% $N/\sqrt{\theta}$

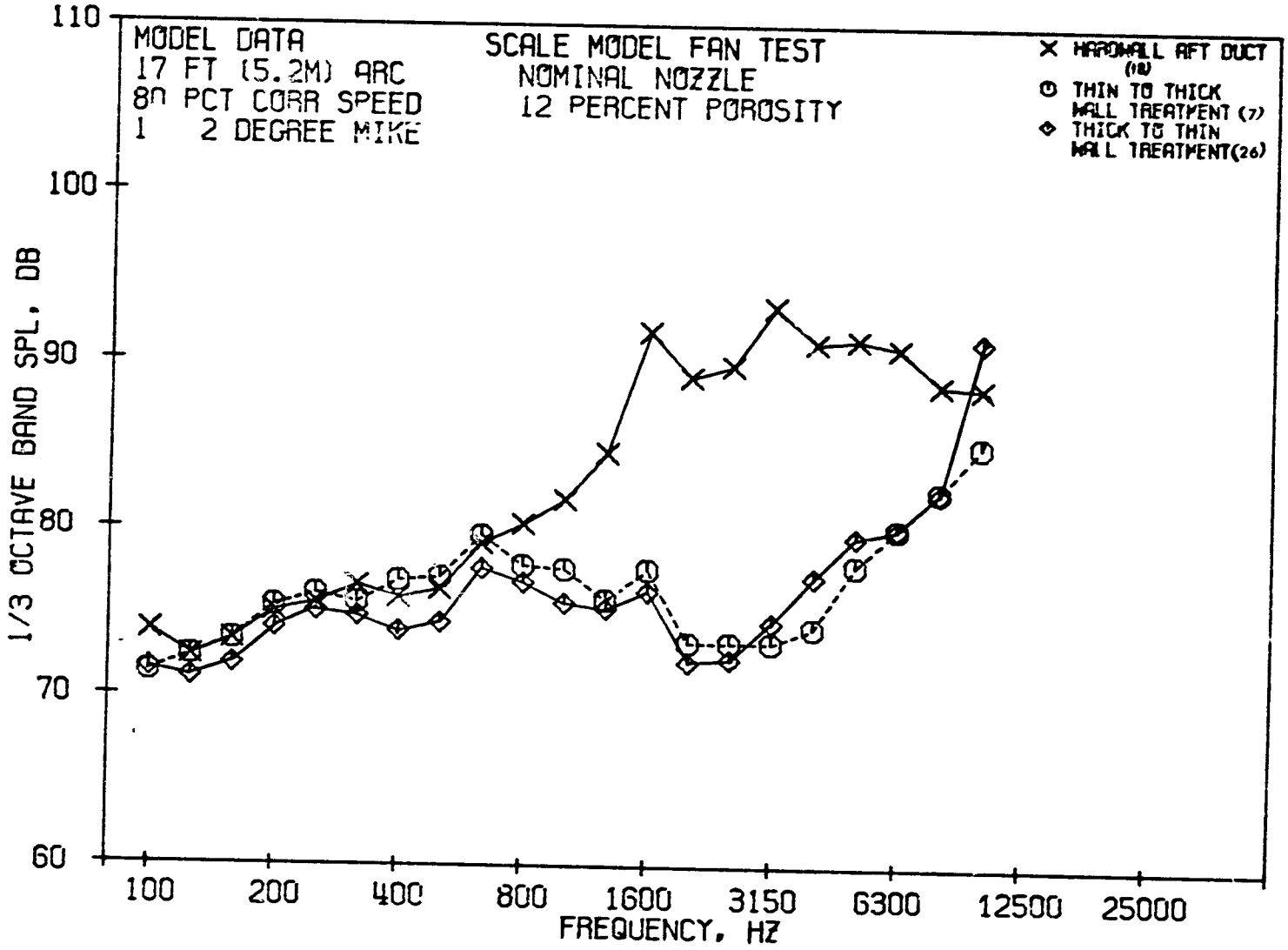

FIGURE 43 12 PERCENT POROSITY VARIABLE DEPTH TREATMENT SPL'S AT 80% $N/\sqrt{\theta}$

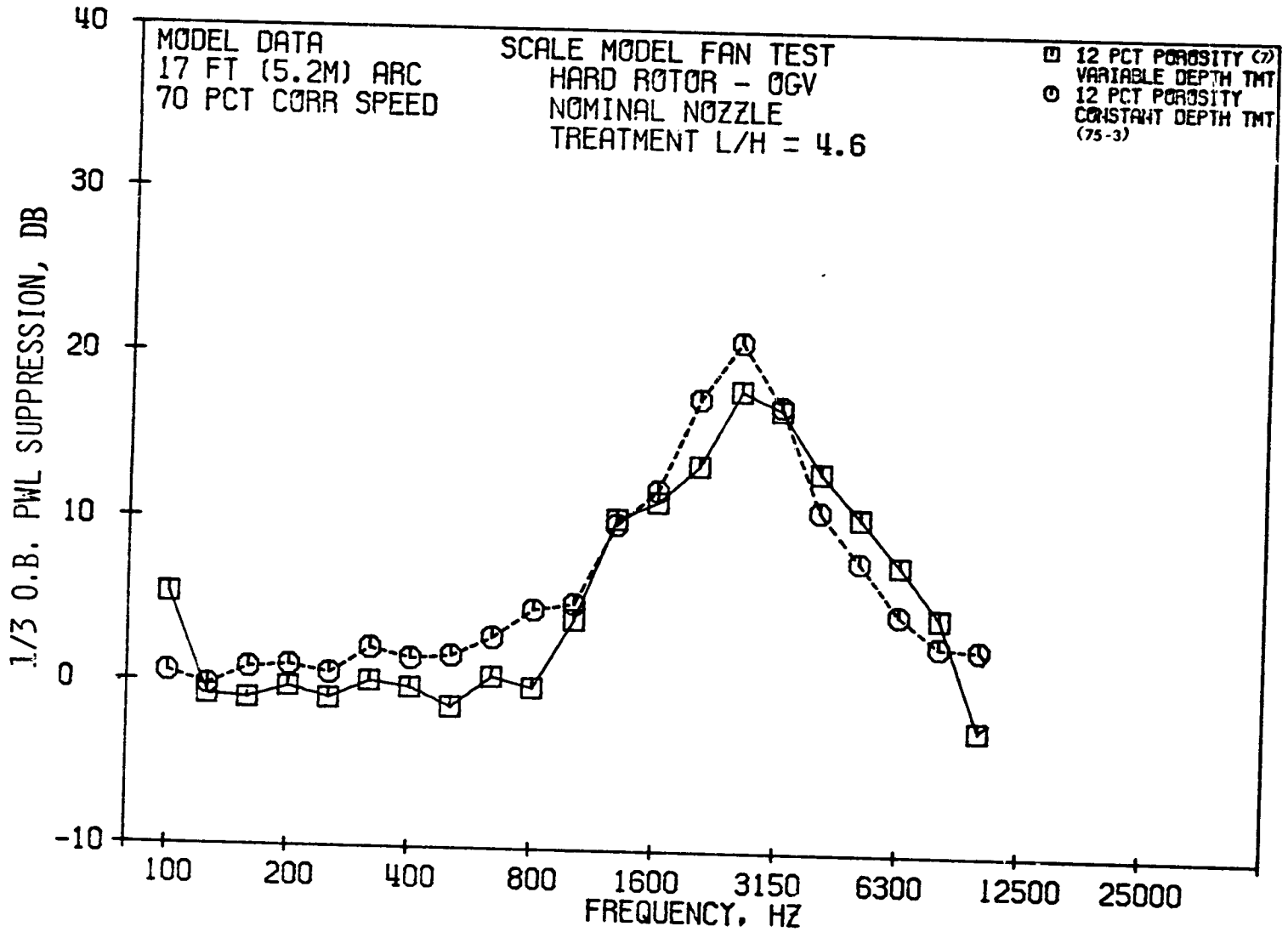

FIGURE 44 12 PERCENT POROSITY VARIABLE AND CONSTANT DEPTH TREATMENT PWL SUPPRESSION AT 70% $N/\sqrt{\theta}$

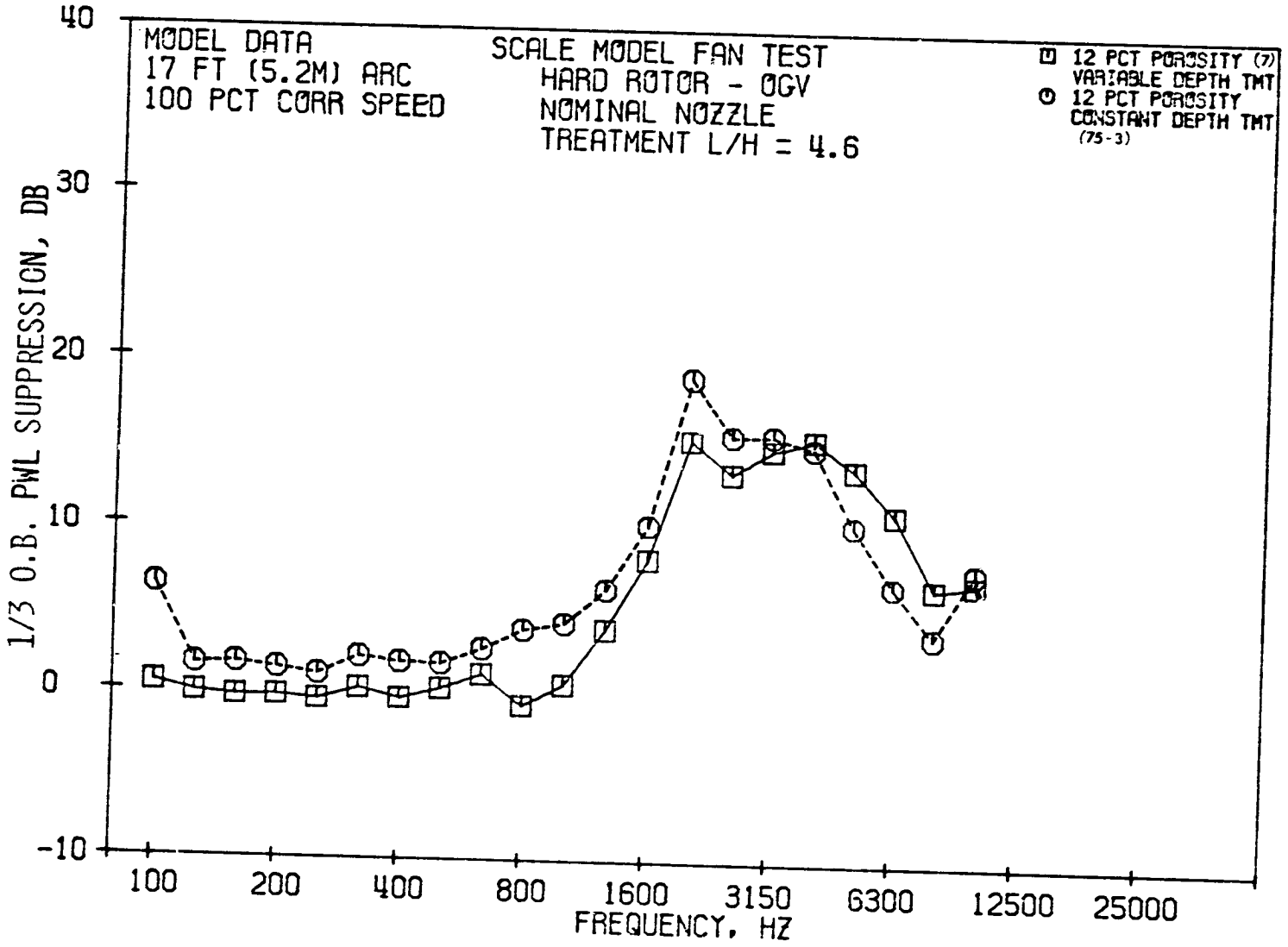

FIGURE 45 12 PERCENT POROSITY VARIABLE AND CONSTANT DEPTH TREATMENT PWL SUPPRESSION AT 100% $N/\sqrt{\theta}$

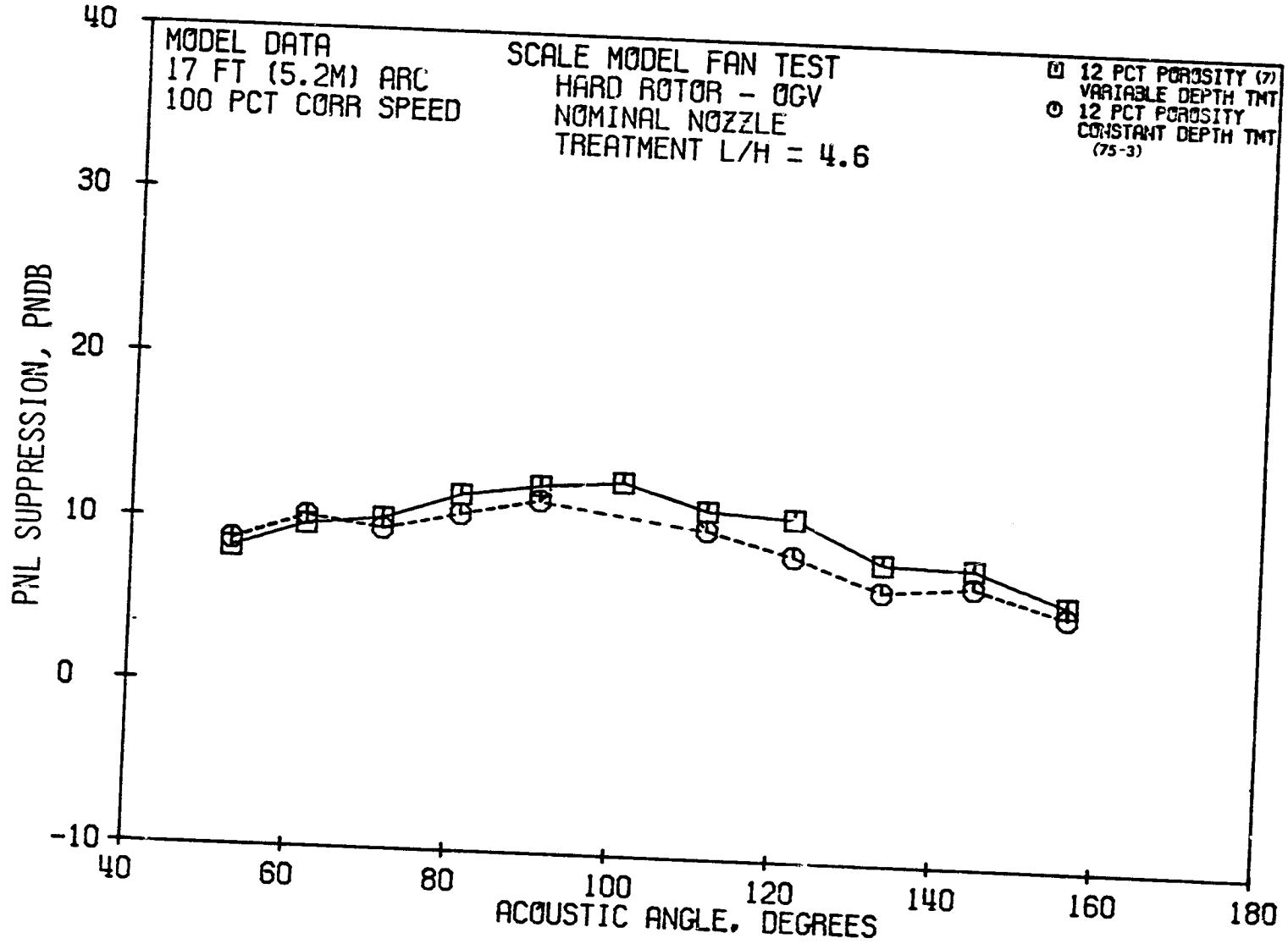

FIGURE 46 12 PERCENT POROSITY VARIABLE AND CONSTANT DEPTH TREATMENT PNL SUPPRESSION AT 100% $N/\sqrt{\theta}$

- NOMINAL NOZZLE
- HARD ROTOR-OGV
- 17 FT. (5.2 m.) ARC

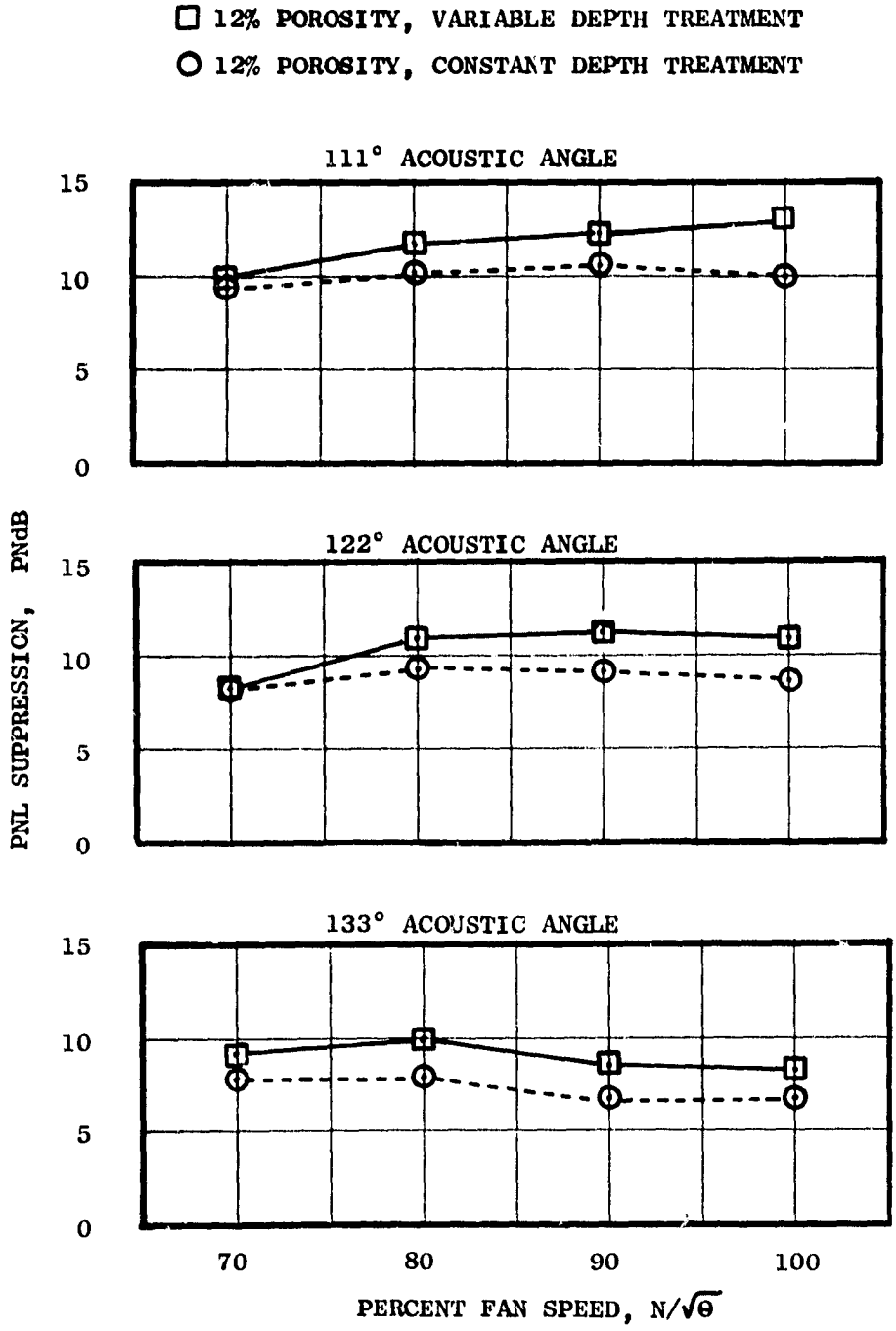

FIGURE 47 12 PERCENT POROSITY VARIABLE AND CONSTANT DEPTH TREATMENT PNL SUPPRESSION AS A FUNCTION OF FAN SPEED

2. 27 Percent Porosity Faceplate

Acoustic duct testing had indicated that the 27 percent faceplate, thin-to-thick configuration achieved significantly more suppression than the thick-to-thin design. Figures 48 to 51 show that the thin-to-thick 27% porosity configuration achieved better aft angle suppression than did the thick-to-thin design at frequencies of 3150 Hz to 10 KHz. At the lowest fan speed of 70% $N/\sqrt{\theta}$, frequencies from 1250 to 1600 Hz show the thin-to-thick configuration to be less effective. This trend does not continue at higher fan speeds, but is evident at all other aft angles at 70% $N/\sqrt{\theta}$. Figure 52 compares the suppression achieved by both configurations as a function of fan speed at frequencies of 2500, 3150, and 4000 Hz. The thin-to-thick design is essentially constant with fan speed and up to 5 dB better than the thick-to-thin design.

The 27 percent porosity configurations have been shown to be less effective than the 12 percent porosity configurations. In addition, the trends observed between variable depth and constant depth treatment were not the same. PWL suppression spectra show the 27 percent variable depth treatment to have higher peak suppression and wider bandwidth than constant thickness treatment. This is true for 100% $N/\sqrt{\theta}$ shown in Figure 53 and at 90% $N/\sqrt{\theta}$ (not shown). At 80% $N/\sqrt{\theta}$ the peak suppressions are equal with variable depth treatment giving wider bandwidth. The 70% $N/\sqrt{\theta}$ constant depth peak PWL suppression - as shown in Figure 54, is 3.5 dB better than the variable depth. On a PNL suppression basis, however, the variable depth, thin-to-thick treatment was consistently 2 PNdB more effective at all speeds at 111 and 122 degrees and 1 PNdB more effective at 133 degrees as shown in Figure 55.

The configurations discussed so far have had constant porosity faceplate on all four pairs of treatment panels. Two additional configurations, shown in Figure 56, were tested which varied porosity as well as treatment depth.

Figure 57 compares the 100% $N/\sqrt{\theta}$ suppressed PNL's of the 12-27-12-27 porosity variable depth design to the variable depth, thin-to-thick 12 percent design and to the 12 percent constant thickness design. The results indicate that the 12-27-12-27 percent porosity design gave from 0 to 1.5 PNdB vane suppression than variable depth, thin-to-thick treatment from 11 to 133 degrees. Similar results are observed at 90% $N/\sqrt{\theta}$ with 3.0 PNdB more suppression observed at 133 degrees in Figure 58. Examination of the spectra at 90% $N/\sqrt{\theta}$ and 133 degrees in Figure 59 where the maximum difference occurs indicates that additional suppression is achieved primarily from 1600 to 2500 Hz.

A PNL comparison of the two mixed porosity designs is presented in Figure 60 at 100% $N/\sqrt{\theta}$. There is no significant difference in suppression level between the two. Lower speeds show the same result.

The success of the mixed porosity designs is probably due to the fact that the mixed 12 and 27 percent porosities offer more nearly optimum resistence for each of the four panels. That the delta SPL's were most significant at 1600 to 2500 Hz supports this theory since the design frequency of the last 1.5 inch (3.8 cm) panel was 2200 Hz. From treatment theory, it is known that

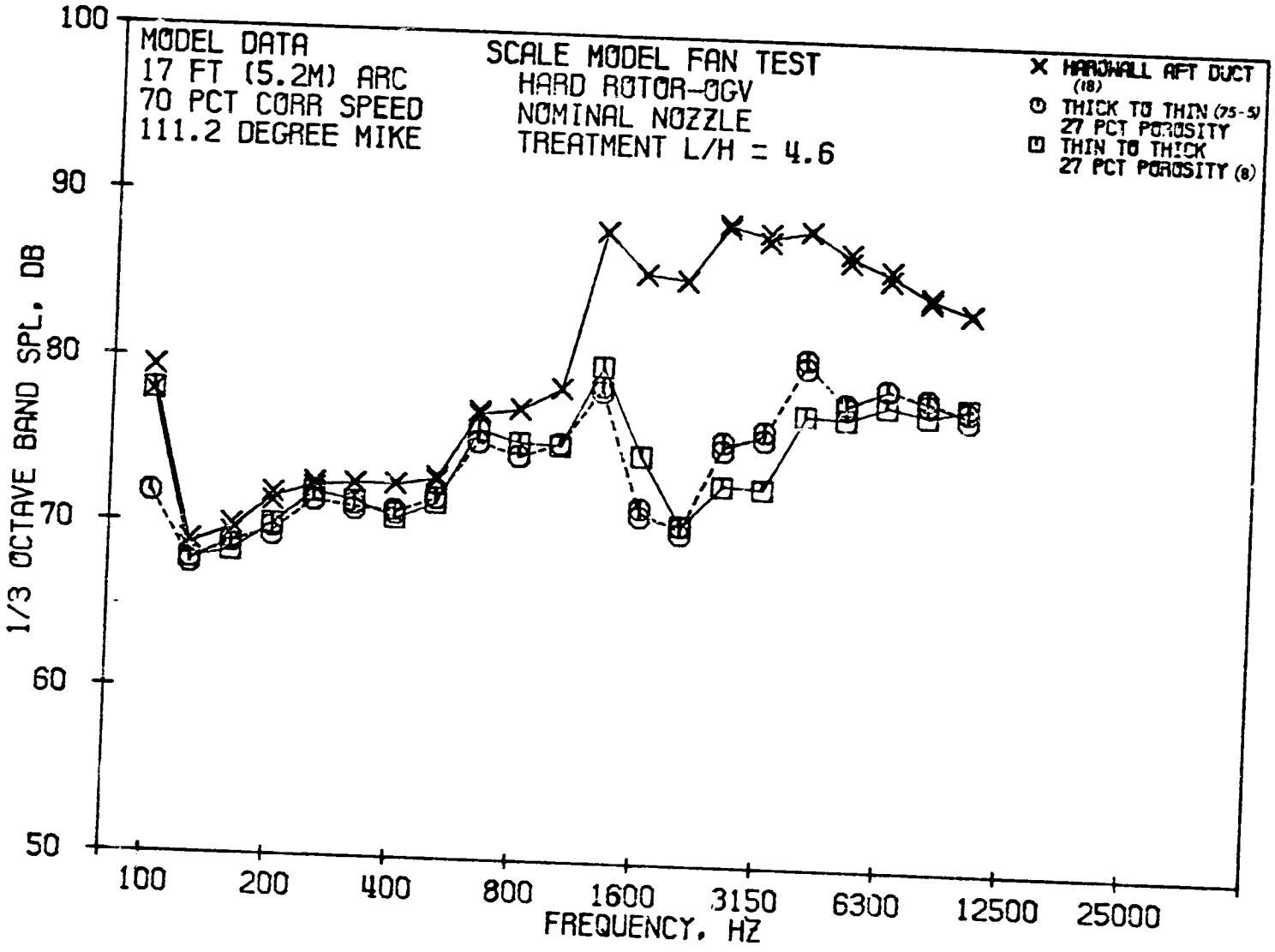

FIGURE 48 27 PERCENT POROSITY VARIABLE DEPTH TREATMENT SPL'S AT 70% $N/\sqrt{\theta}$

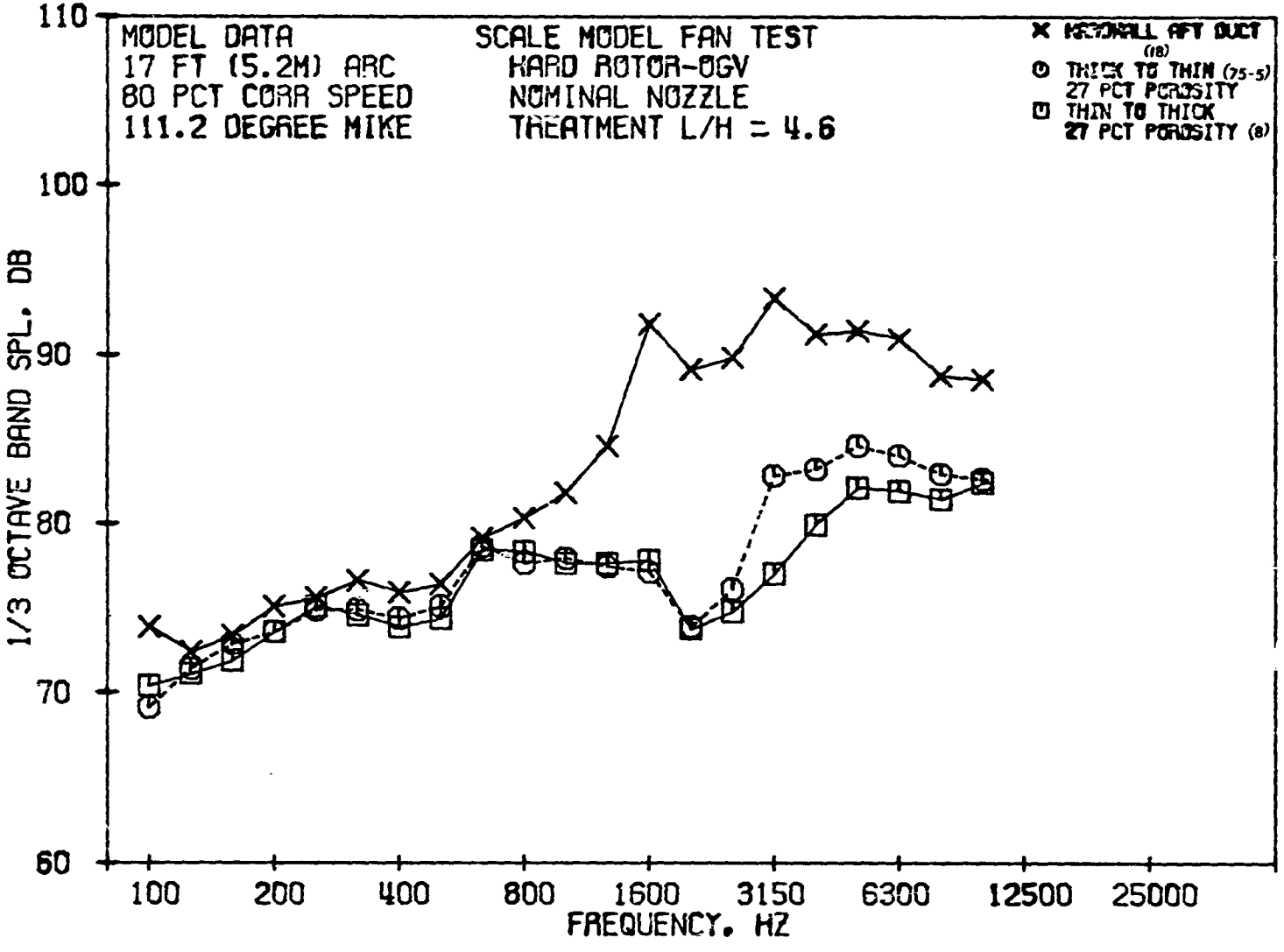

FIGURE 49 27 PERCENT POROSITY VARIABLE DEPTH TREATMENT SPL'S AT 80% $N/\sqrt{\theta}$

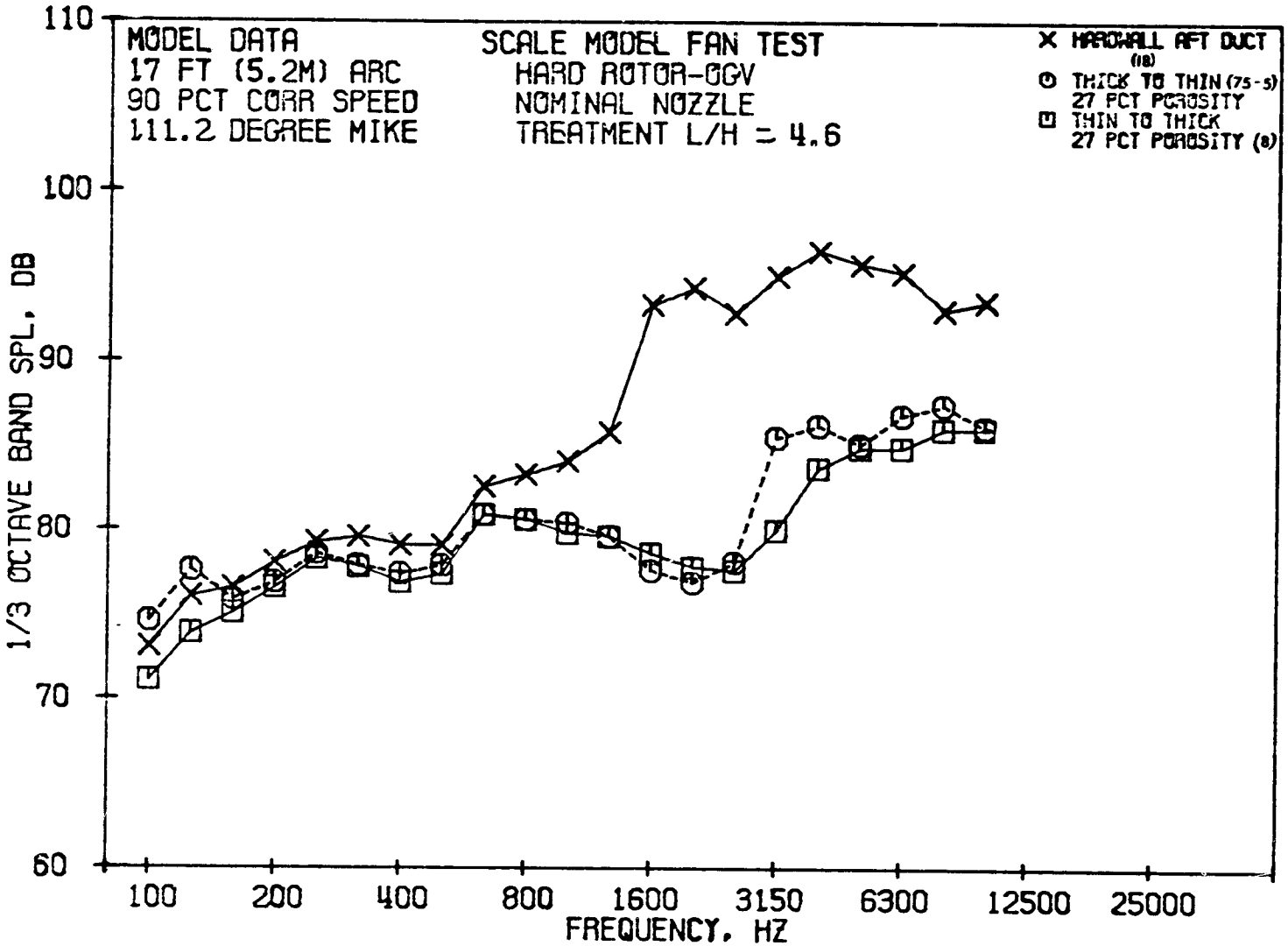

FIGURE 50 27 PERCENT POROSITY VARIABLE DEPTH TREATMENT SPL'S AT 90% $N/\sqrt{\theta}$

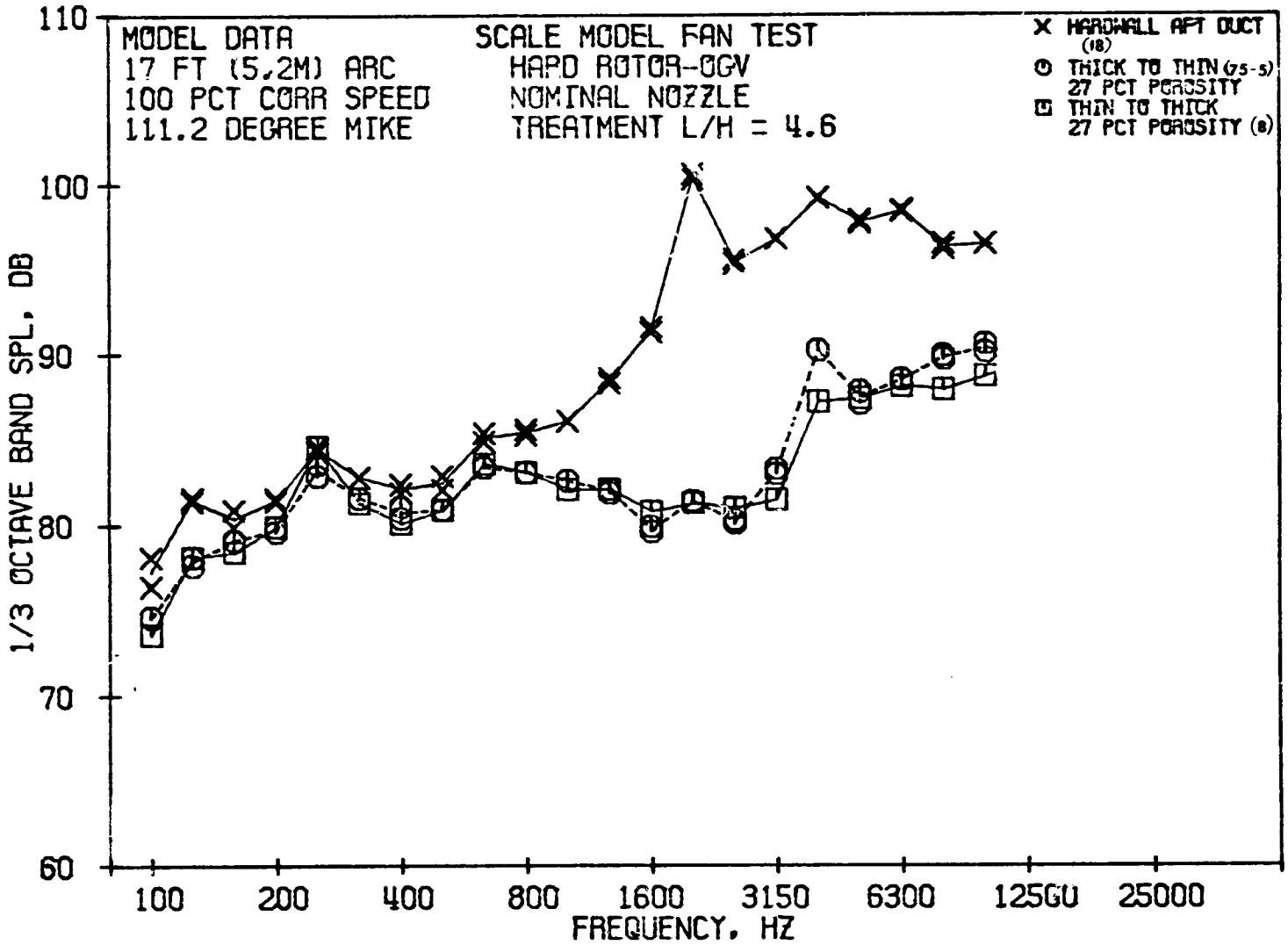

FIGURE 51 27 PERCENT POROSITY VARIABLE DEPTH TREATMENT SPL'S AT 100% $N/\sqrt{\theta}$

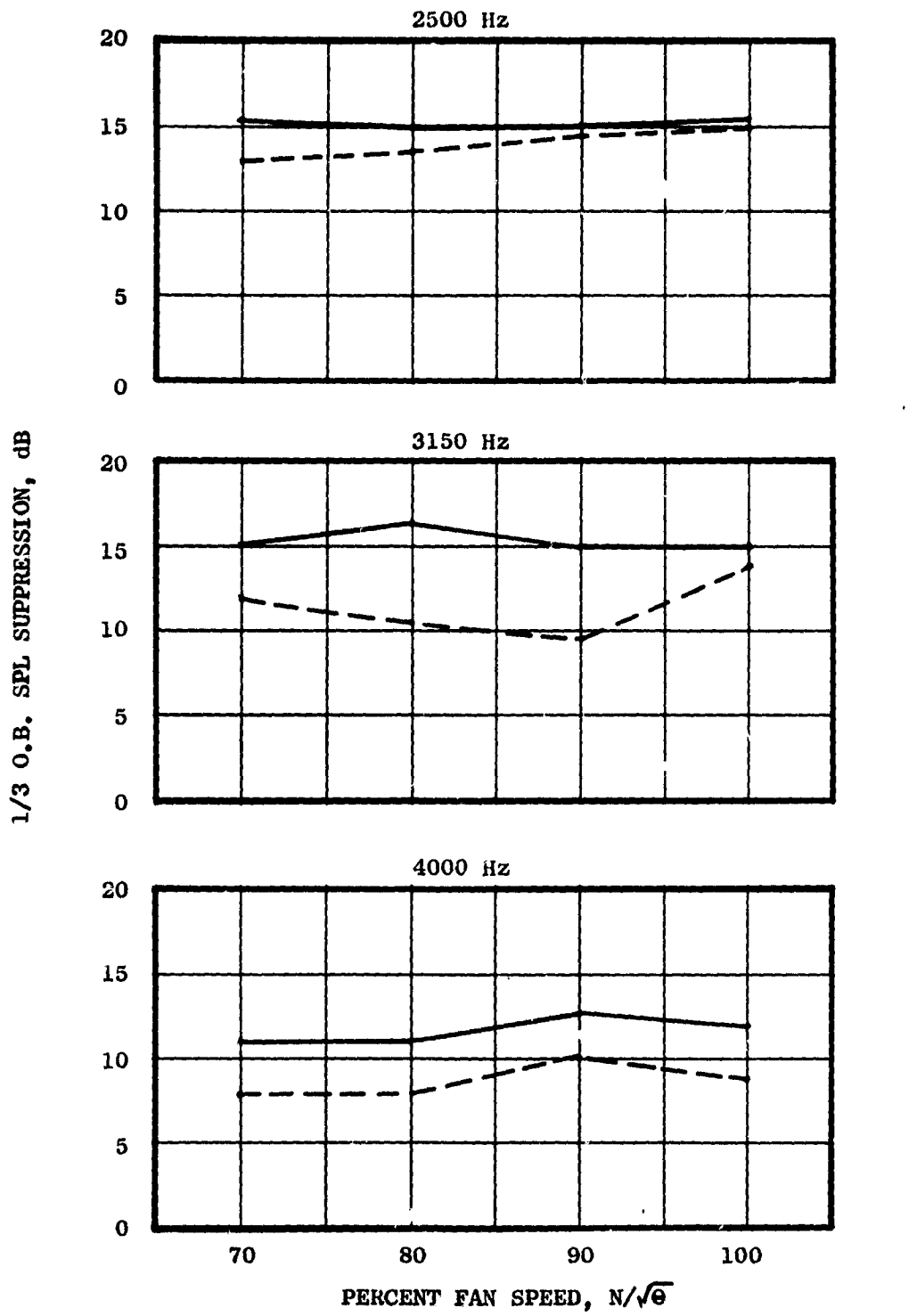

FIGURE 52 27 PERCENT POROSITY VARIABLE DEPTH TREATMENT SUPPRESSION AS A FUNCTION OF FAN SPEED

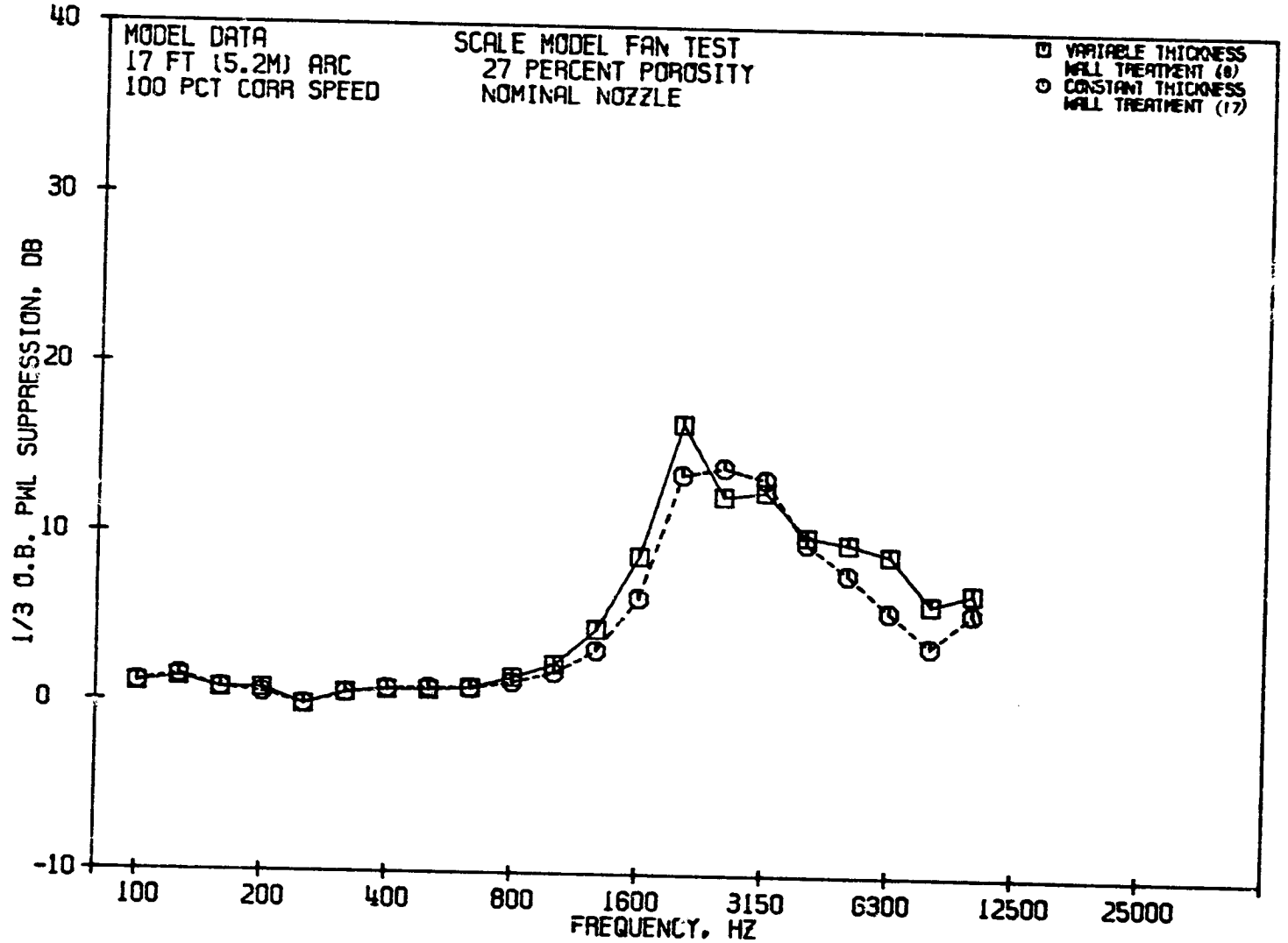

FIGURE 53 27 PERCENT POROSITY VARIABLE AND CONSTANT DEPTH TREATMENT PWL SUPPRESSION AT 100% $N/\sqrt{\theta}$

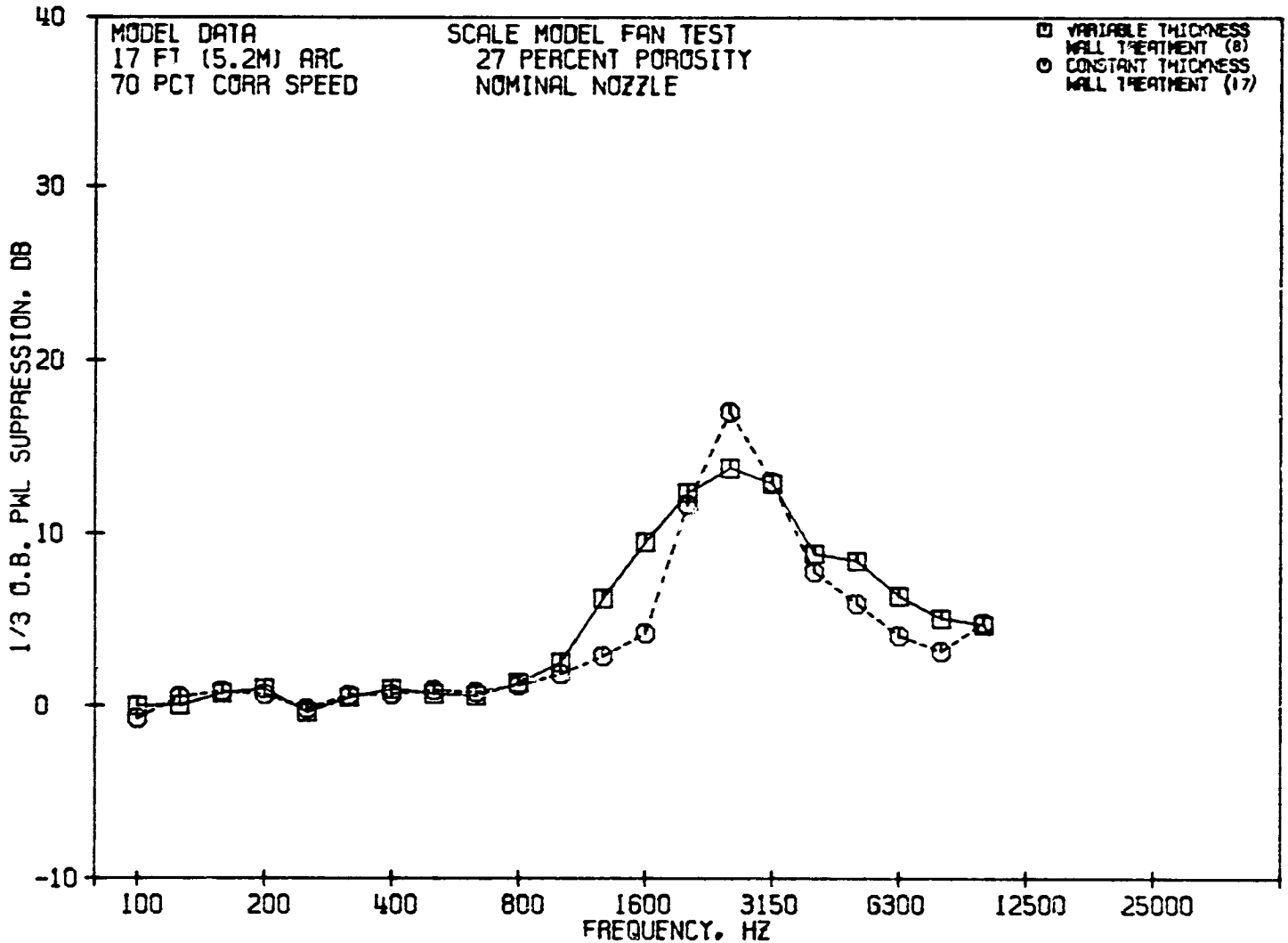

FIGURE 54 27 PERCENT POROSITY VARIABLE AND CONSTANT DEPTH TREATMENT PWL SUPPRESSION AT 70% $N/\sqrt{\theta}$

- NOMINAL NOZZLE
- HARD ROTOR-OGV
- 17 FT. (5.2 m.) ARC

□ 27% POROSITY, VARIABLE DEPTH TREATMENT (8)
○ 27% POROSITY, CONSTANT DEPTH TREATMENT (17)

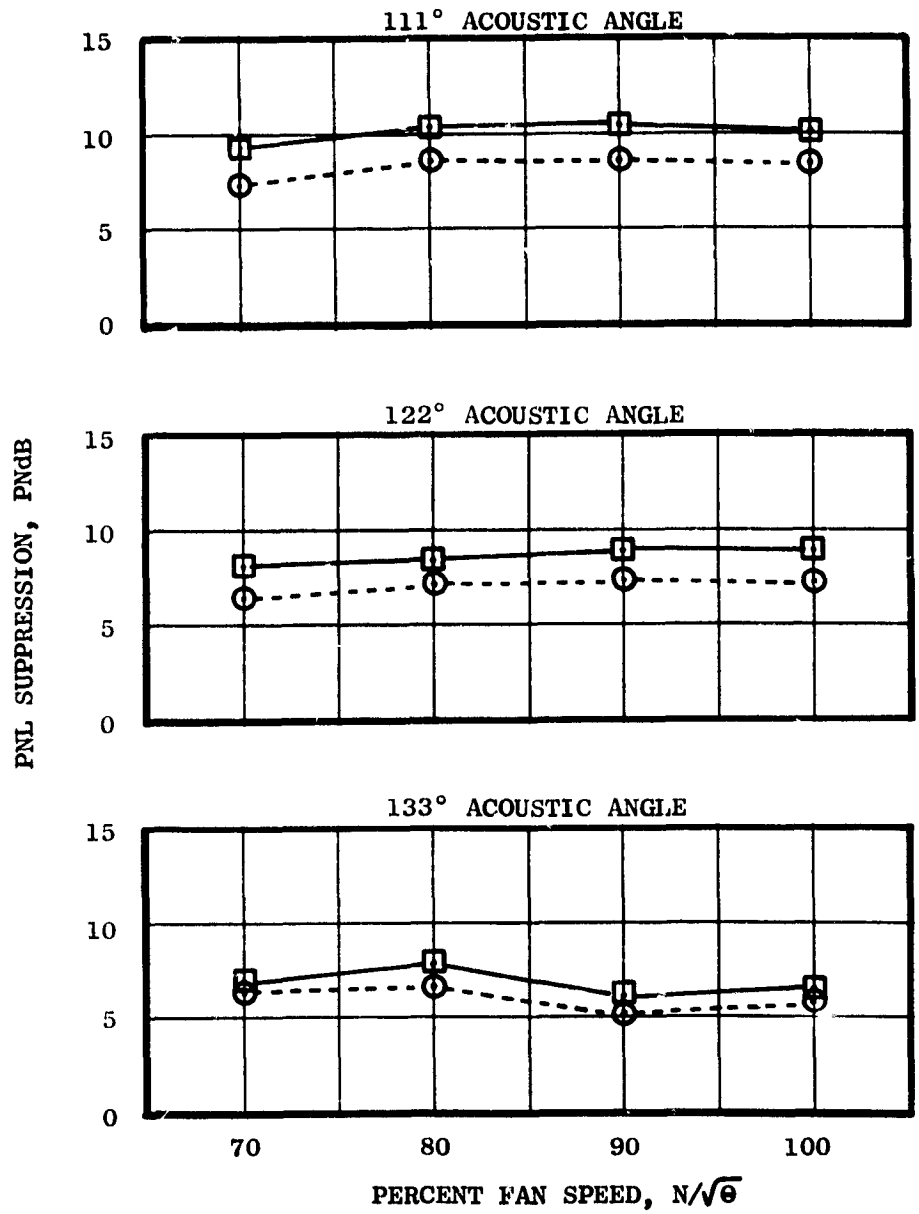

FIGURE 55 27 PERCENT POROSITY VARIABLE AND CONSTANT DEPTH TREATMENT PNL SUPPRESSION AS A FUNCTION OF FAN SPEED

- NOMINAL NOZZLE
- HARD ROTOR-OGV
- TREATMENT L/H = 4.6

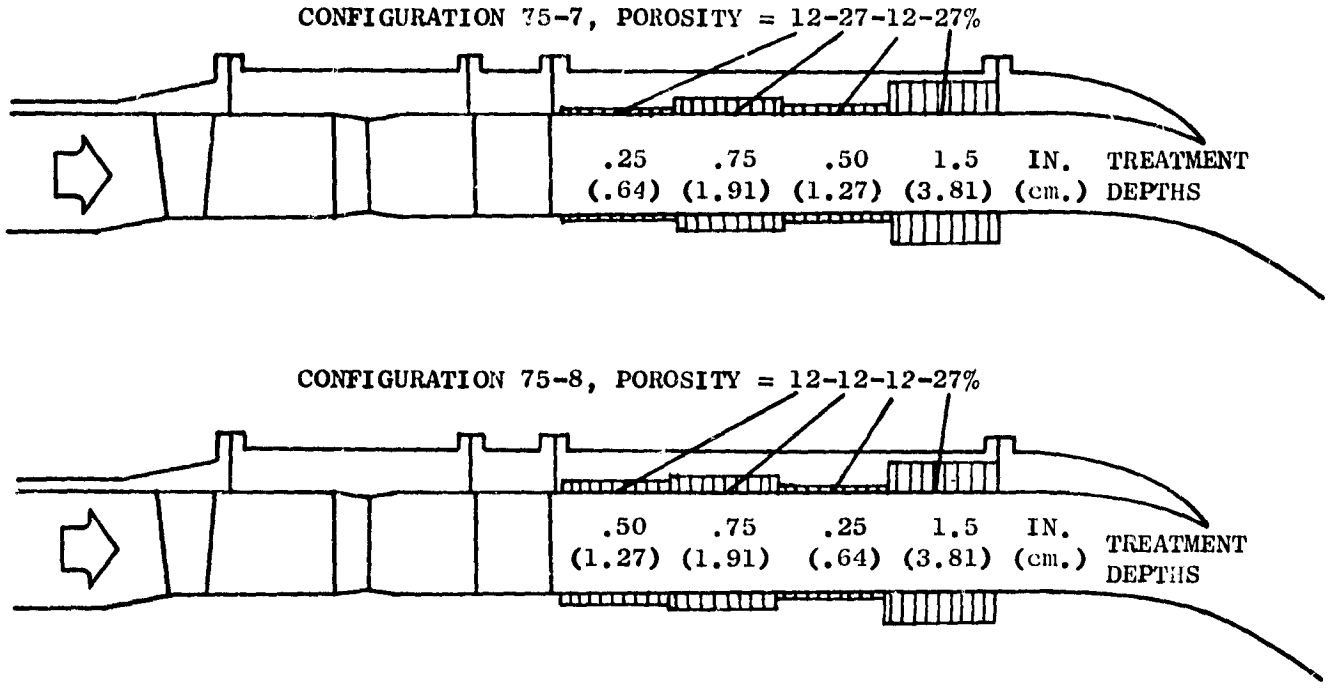

FIGURE 56 MIXED POROSITY CONFIGURATIONS

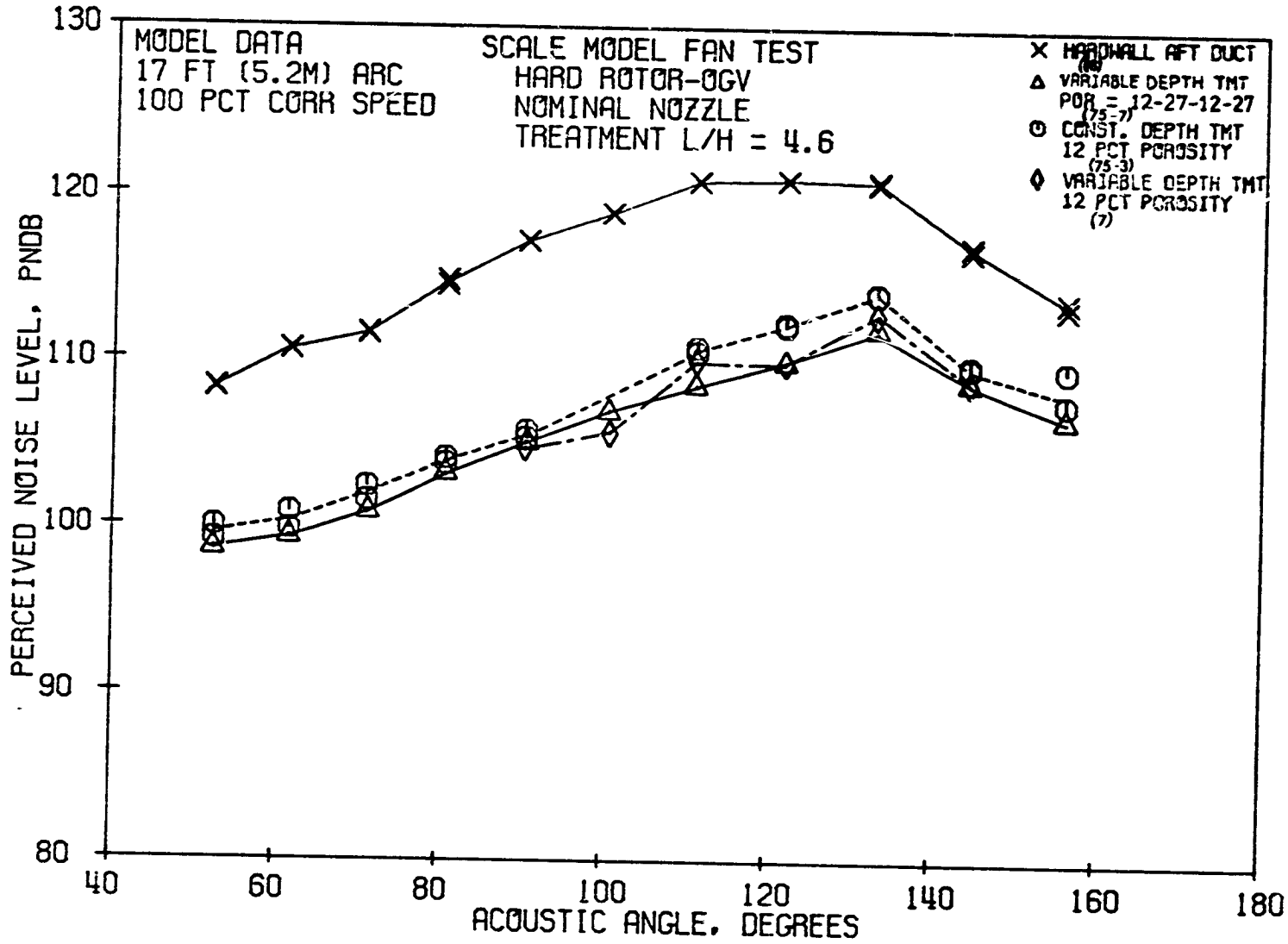

FIGURE 57 MIXED POROSITY SUPPRESSED PNL'S COMPARED TO VARIABLE DEPTH AND CONSTANT DEPTH AT 100% $N/\sqrt{\theta}$

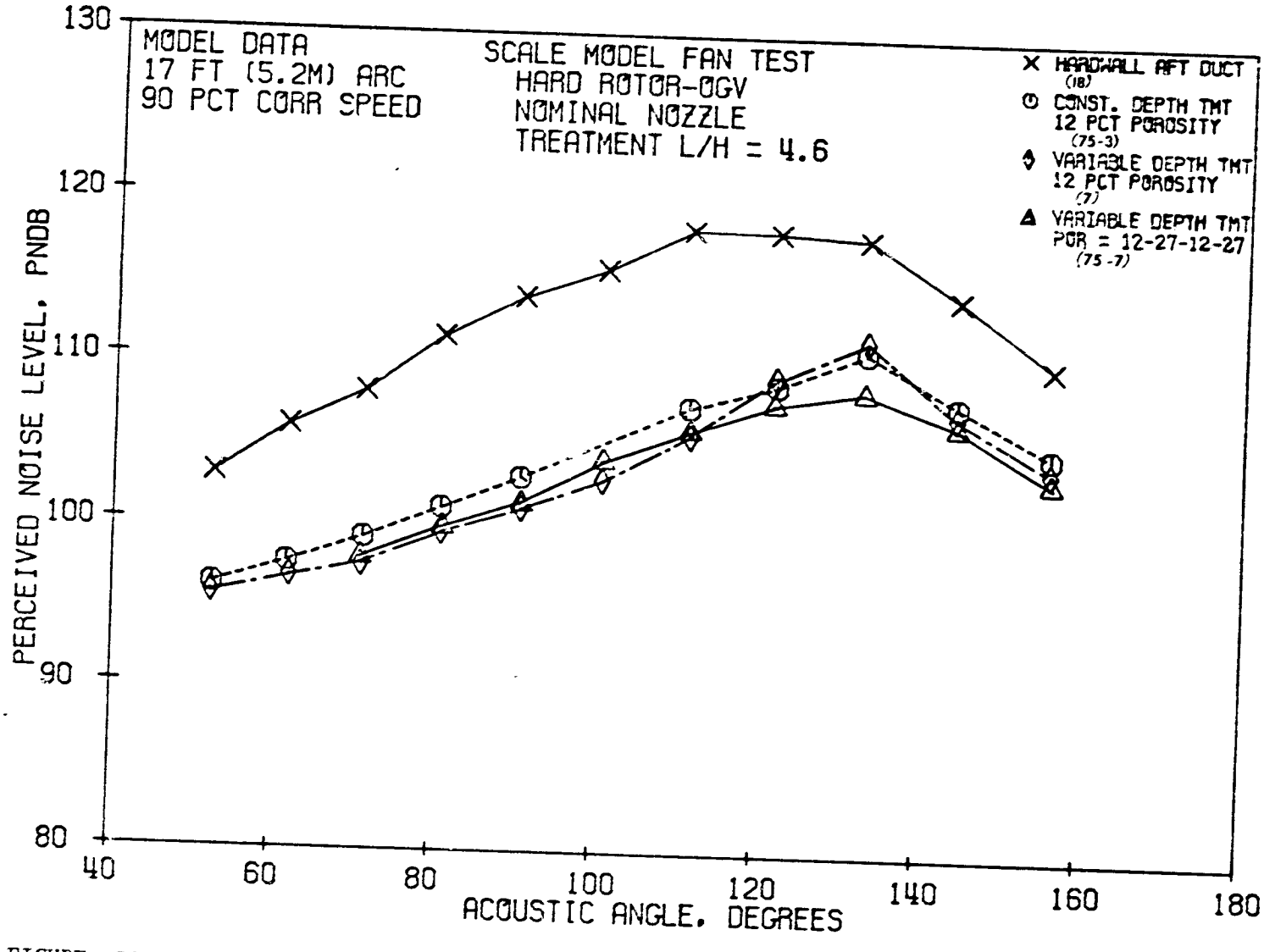

FIGURE 58 MIXED POROSITY SUPPRESSED PNL'S COMPARED TO VARIABLE DEPTH AND CONSTANT DEPTH PNL'S AT 100% $N/\sqrt{\theta}$

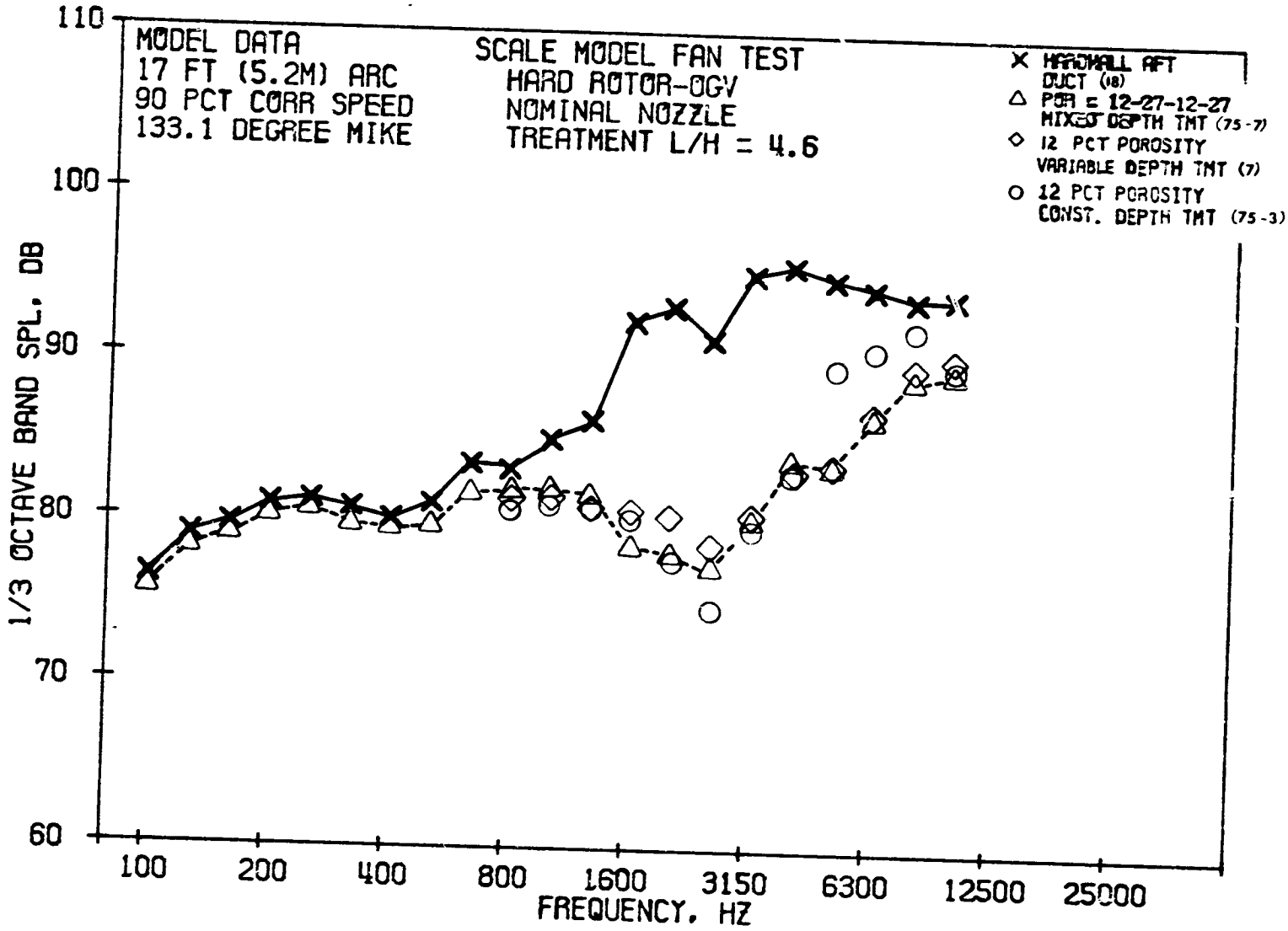

FIGURE 59 MIXED POROSITY SPL'S COMPARED TO VARIABLE DEPTH AND CONSTANT DEPTH SPL'S AT 90% $N/\sqrt{\theta}$

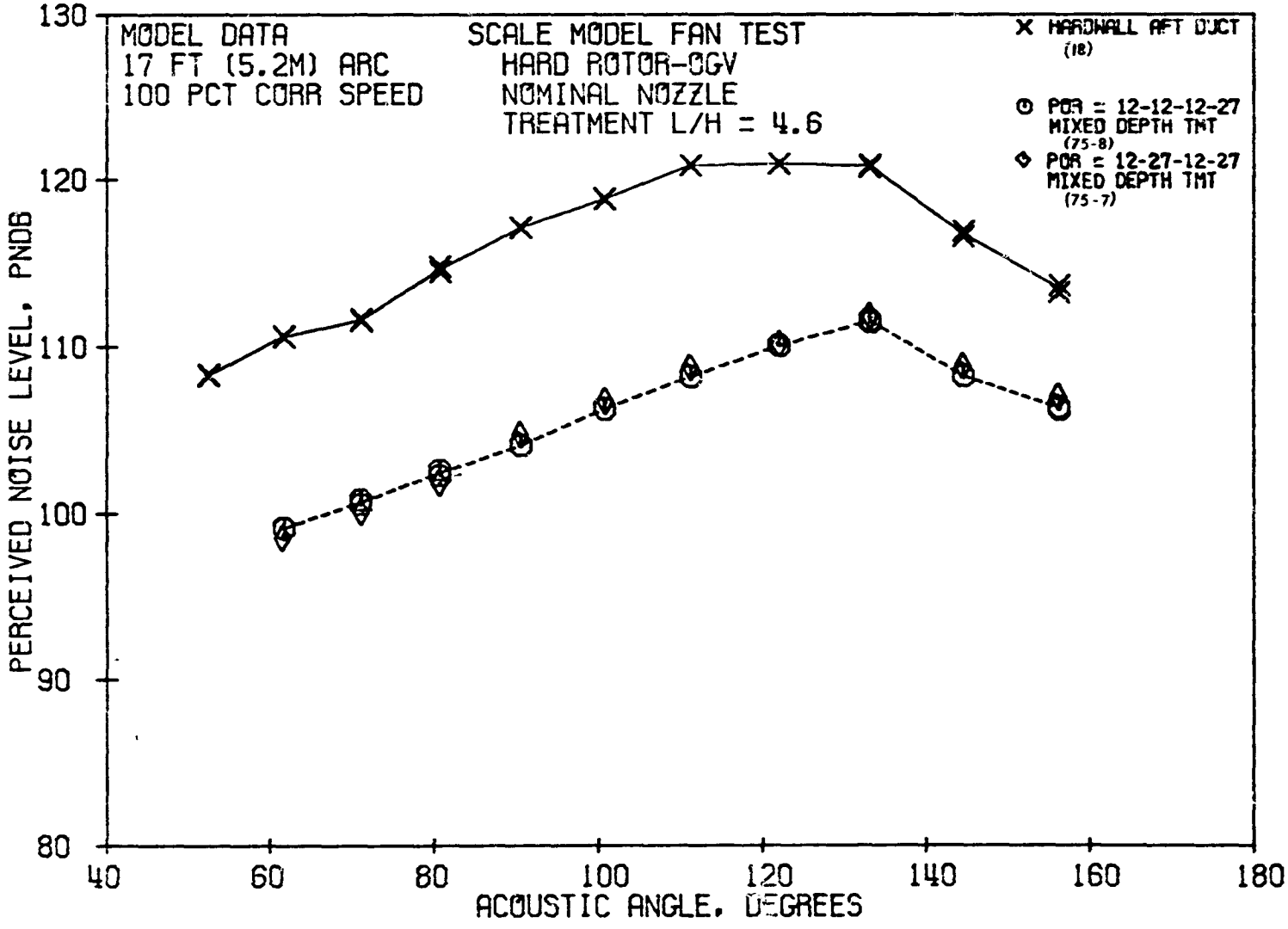

FIGURE 60 COMPARISON OF MIXED POROSITY PNL'S

a decrease in H/λ requires a decrease in resistance thus demanding a higher porosity. Thus, 27 percent porosity could give a resistance closer to the optimum value than does the 12 percent on the 1.5 thick (3.8 cm) panel of the variable depth configuration. Twelve percent may be closer to the optimum resistance of the forward panels which are tuned to higher frequencies.

C. Splitter Simulation

When a splitter is placed in an aft duct, the splitter is usually lined with constant thickness treatment, due to mechanical and aerodynamic flowpath constraints on the allowable thickness, while the duct walls have varying thickness treatment. Two configurations which had variable depth, thin-to-thick treatment on the outer flow path and constant depth treatment on the inner wall were tested to simulate a splitter model. In one case the porosity was 12 percent and in the second case 27 percent. These are shown schematically in Figure 61.

When the 12 percent porosity splitter model design is compared to the designs which had variable depth, thin-to-thick and constant thickness treatment on both the inner and outer panels, it achieved about the same PNL levels as the variable depth design. This is shown in Figure 62. The model PNL was down about 1 PNdB in the aft angles, however, the splitter design was consistently 1 to 2 PNdB better than the constant thickness design. Figure 63 shows the 100% $N/\sqrt{\theta}$, 122 degree SPL suppression levels which show the splitter model to fall between the other two in terms of both peak suppression and bandwidth.

A comparison of the PWL suppression achieved at 100% $N/\sqrt{\theta}$ for both the 12 and 27 percent porosity configuration in Figure 64 indicates that the 12 percent had higher peak suppression and wider bandwidth than did the 27 percent porosity. This is also clearly evident at 122 degrees for 100 and 70% $N/\sqrt{\theta}$ respectively in Figures 65 and 66. Although this was not the main intent of this test series, it is apparent that the 12 percent porosity configuration achieved more suppression.

D. Rotor-OGV Treatment

The test vehicle was designed to be tested with or without treatment between the rotor and OGV at 1.5 chord spacing. Only the outer flowpath was treated and the treatment used was slant cell single-degree-of-freedom with a cavity depth of 1.5 (3.8 cm) inches. Faceplate thickness was 0.019 inches (.48 mm) with hole diameters of 0.033 inches (.84 mm) and porosity of 28 percent open area. The treatment was tuned to 2200 Hz or the BPF at 110% $N/\sqrt{\theta}$ and had an L/H of 0.87.

As shown in Figure 67 the PWL suppression did peak at 2000 Hz and achieved 4 dB suppression. At all other frequencies except 6300 Hz, the suppression was less than 1 dB. The SPL directivity pattern of the 1/3-octave band which contains the BPF indicates 4 to 5 dB suppression at the BPF for

- NOMINAL NOZZLE
- HARD ROTOR-OGV
- TREATMENT L/H = 4.6

CONFIGURATION 18, HARDWALL

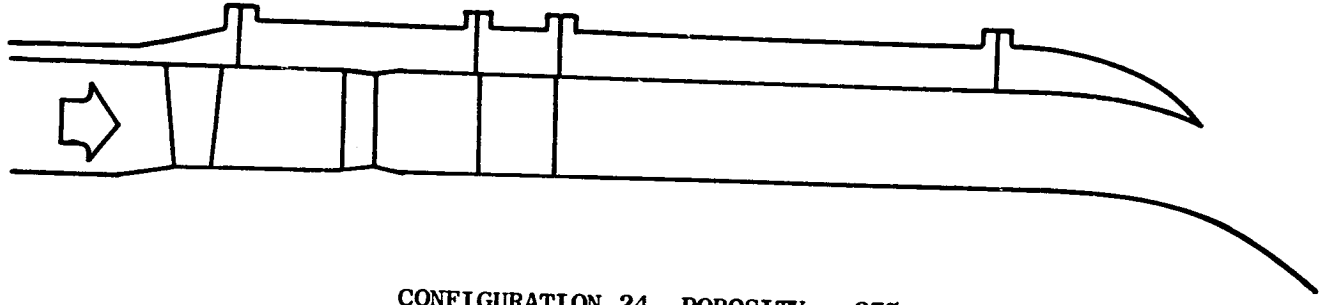

CONFIGURATION 24, POROSITY = 27%

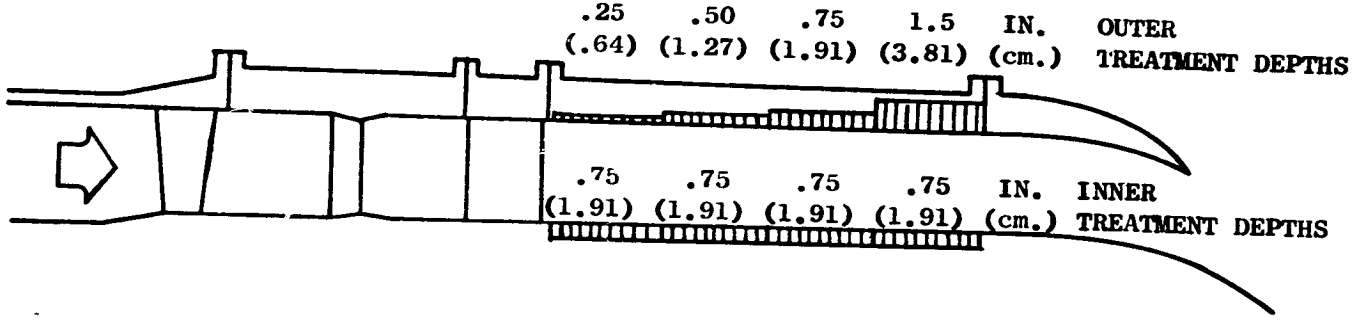

CONFIGURATION 75-4, POROSITY = 12%

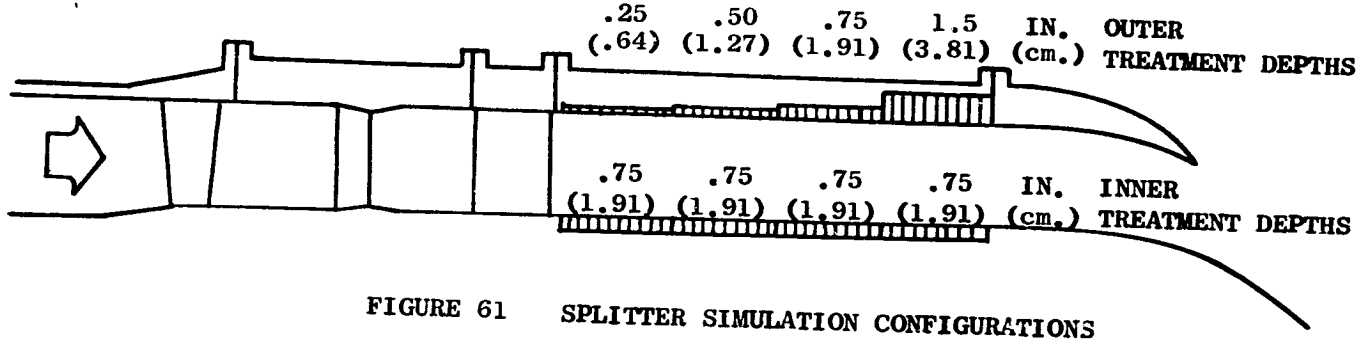

FIGURE 61 SPLITTER SIMULATION CONFIGURATIONS

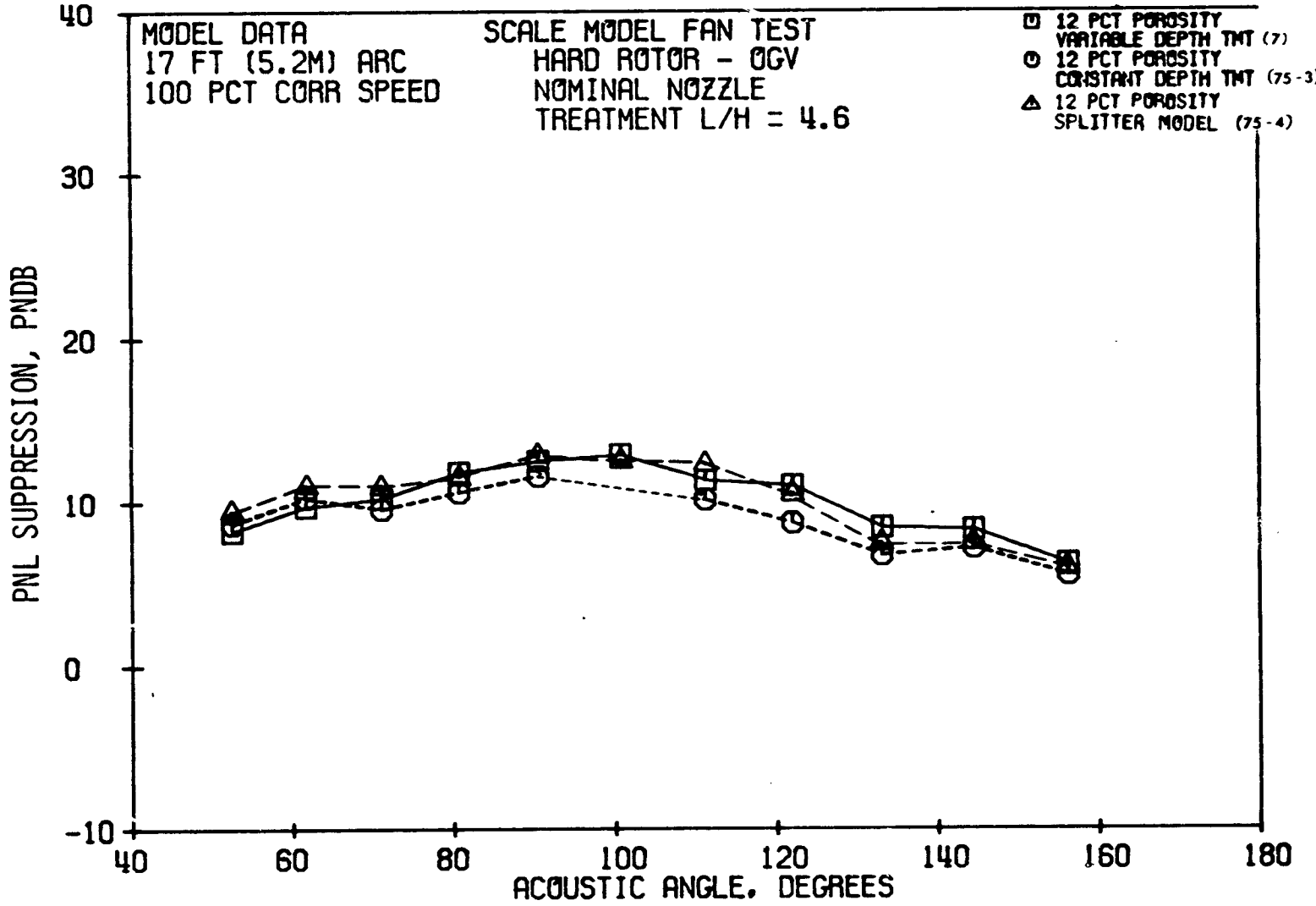

FIGURE 62 SPLITTER SIMULATION DESIGN PNL SUPPRESSIONS COMPARED TO VARIABLE AND CONSTANT DEPTH DESIGNS AT 100% $N/\sqrt{\theta}$

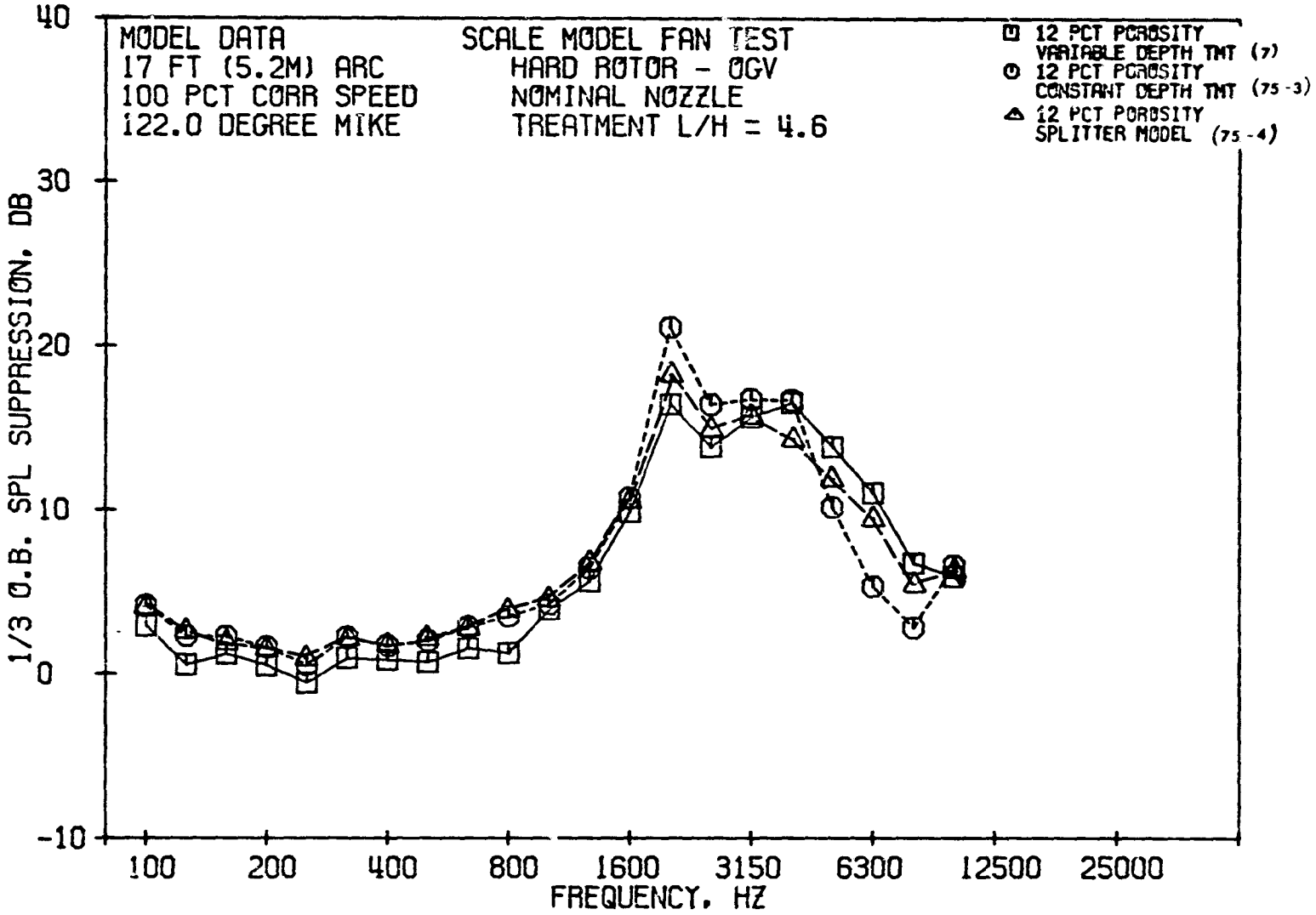

FIGURE 63 SPLITTER SIMULATION DESIGN SPL SUPPRESSION COMPARED TO VARIABLE AND CONSTANT DEPTH DESIGNS AT 100% $N/\sqrt{\theta}$

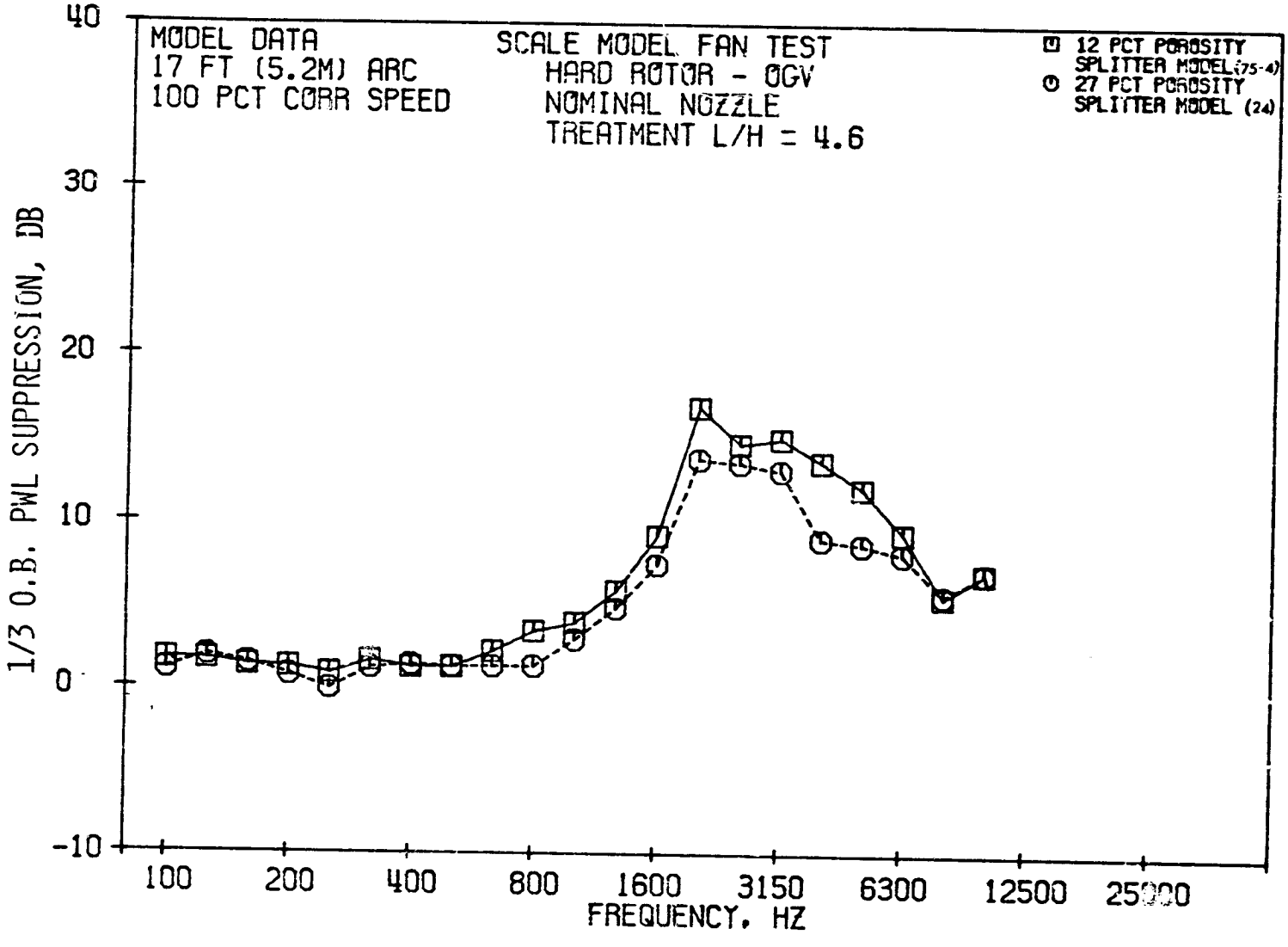

FIGURE 64 SPLITTER SIMULATION DESIGN PWL SUPPRESSION AT 100% $N/\sqrt{\theta}$

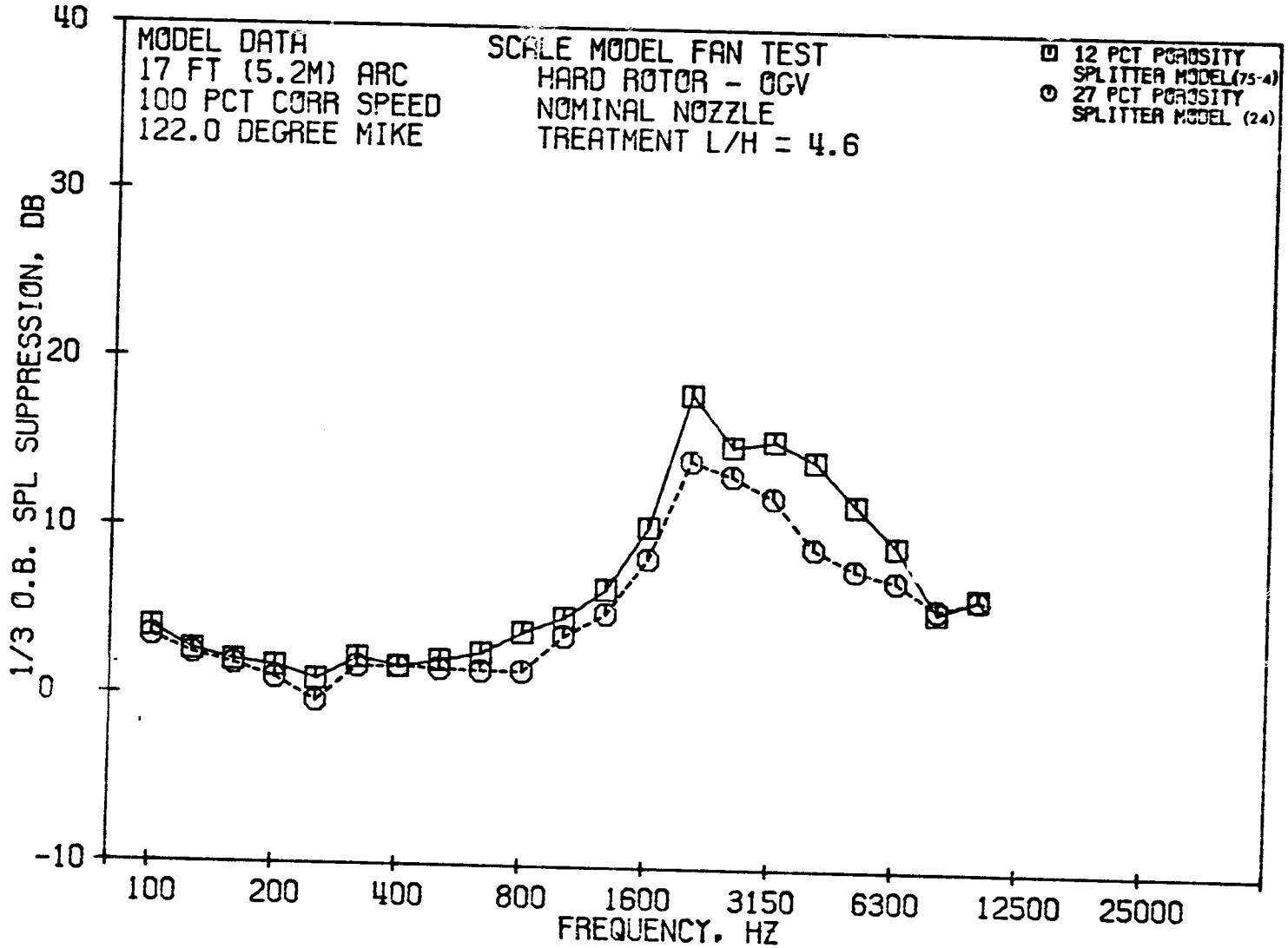

FIGURE 65 SPLITTER SIMULATION DESIGN SPL SUPPRESSION AT 100% $N/\sqrt{\theta}$

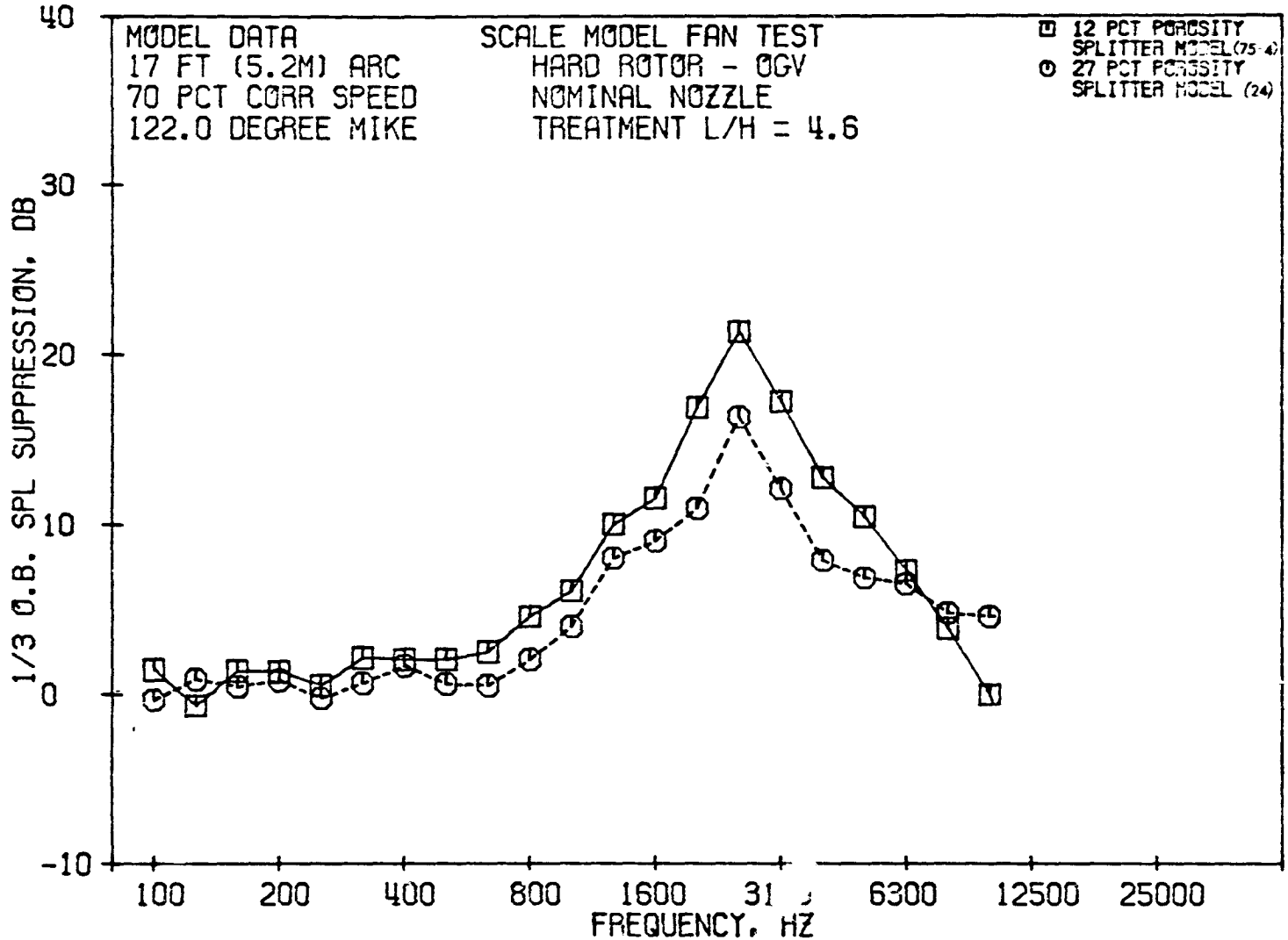

FIGURE 66 SPLITTER SIMULATION DESIGN SPL SUPPRESSION AT 70% $N/\sqrt{\theta}$

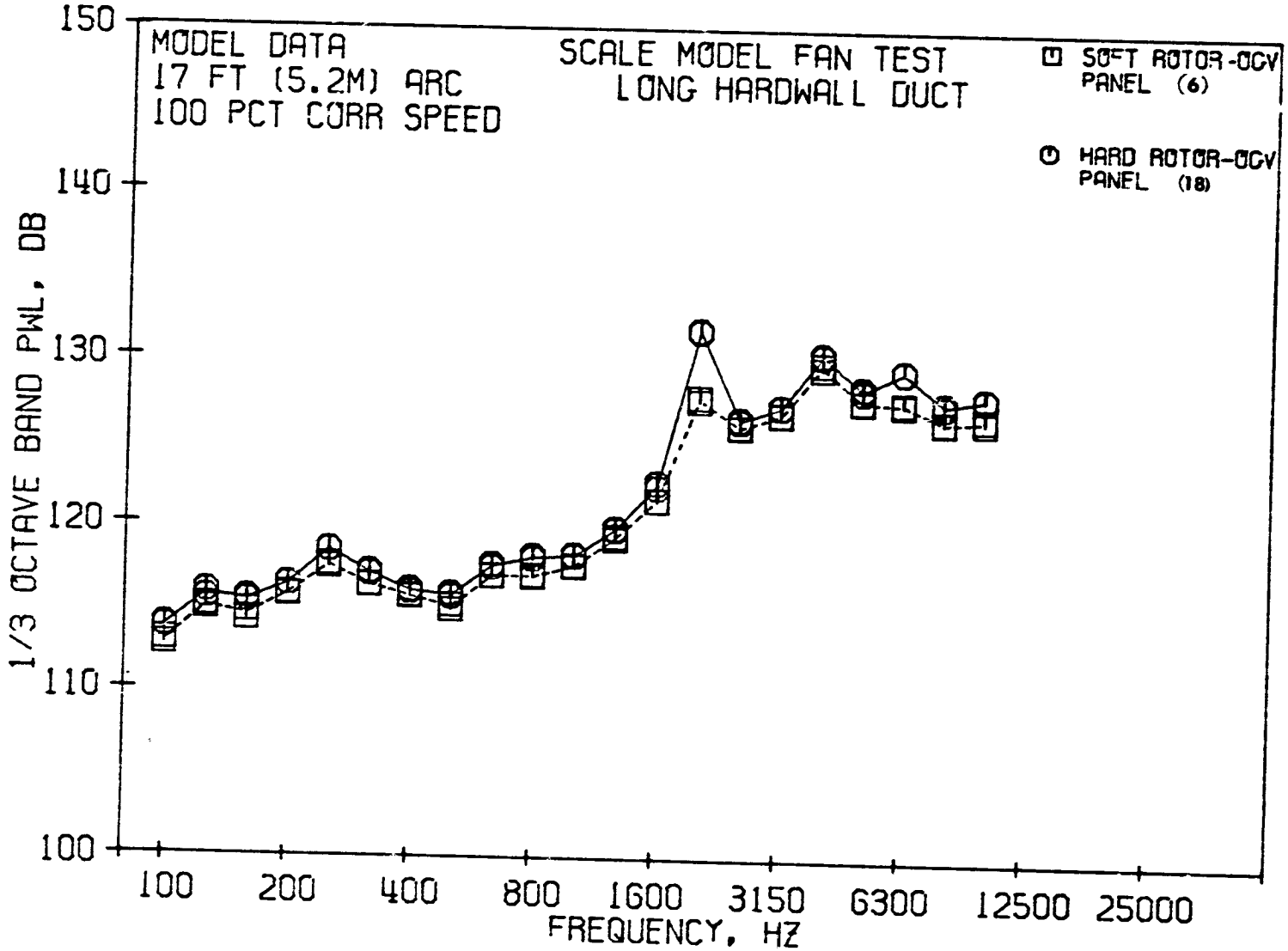

FIGURE 57 ROTOR-OGV PWL SUPPRESSION AT 100% $N/\sqrt{\theta}$

all angles due to rotor-OGV treatment as shown in Figure 68. On a PNL basis the gain is much less due to the small bandwidth. Figure 69 shows that about 1 PNdB suppression was achieved with the rotor-OGV treatment.

E. Treatment Area Effectiveness

Often in engine and model testing, treatment area is lost due to probe pads, static tap pads, close-out flanges, and blocked holes. To investigate the effect of loss in treatment area, a configuration was run with 20 percent of its area taped. This decreased the L/H from 4.6 to 3.68. Other than the taping of each panel, the configuration was identical to the 12 percent porosity, variable depth, thin-to-thick configuration. Both are shown schematically in Figure 70.

The reduction in PNL suppression level is summarized below for four fan speeds:

Reduction in PNL Suppression Level

% $N/\sqrt{\theta}$	111°	122°
70	0	-.3
80	+.6	+.7
90	-.3	+.6
100	-.6	0

These levels indicate very little effect of the taping on the suppression PNL's. A spectral comparison for 100% $N/\sqrt{\theta}$ at 122 degrees is shown in Figure 71 and shows that the taped design is about 1 dB less effective from the BPF to 10 kHz.

The difference in suppression with the taped design is less than one would expect for a 20 percent decrease in L/H. One possible explanation for this is that a higher rate of suppression is achieved with the impedance changes introduced by the circumferential taping. The attenuation with L/H is not linear because of the varying modal decay rates.

F. Treatment Regenerated Noise

Two types of comparisons are made to determine and evaluate flow noise effects on the variable depth treatment designs. The first type includes comparisons of measured suppressions for a particular configuration at different fan speeds and hence different flow Mach numbers. The second includes comparisons where the nozzle setting was varied from nominal to open and where the splitter was removed - both of which result in different duct Mach numbers. Figure 72 presents schematics of the configurations involved in these comparisons and Table III lists the duct Mach numbers for each configuration.

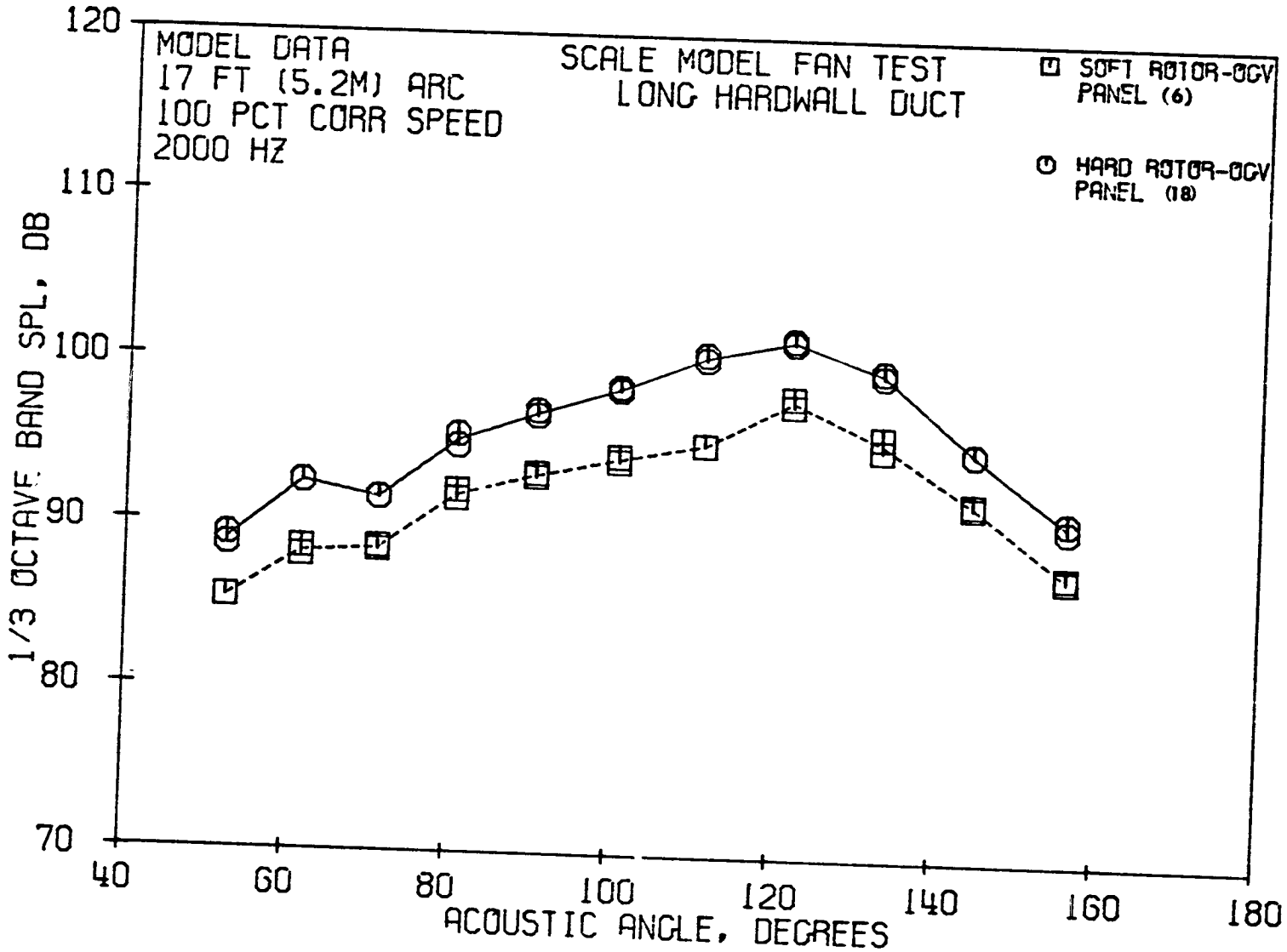

FIGURE 68 EFFECT OF ROTOR-OGV TREATMENT ON 1/3 OCTAVE BAND SPL BPF DIRECTIVITY AT 100% $N/\sqrt{\theta}$

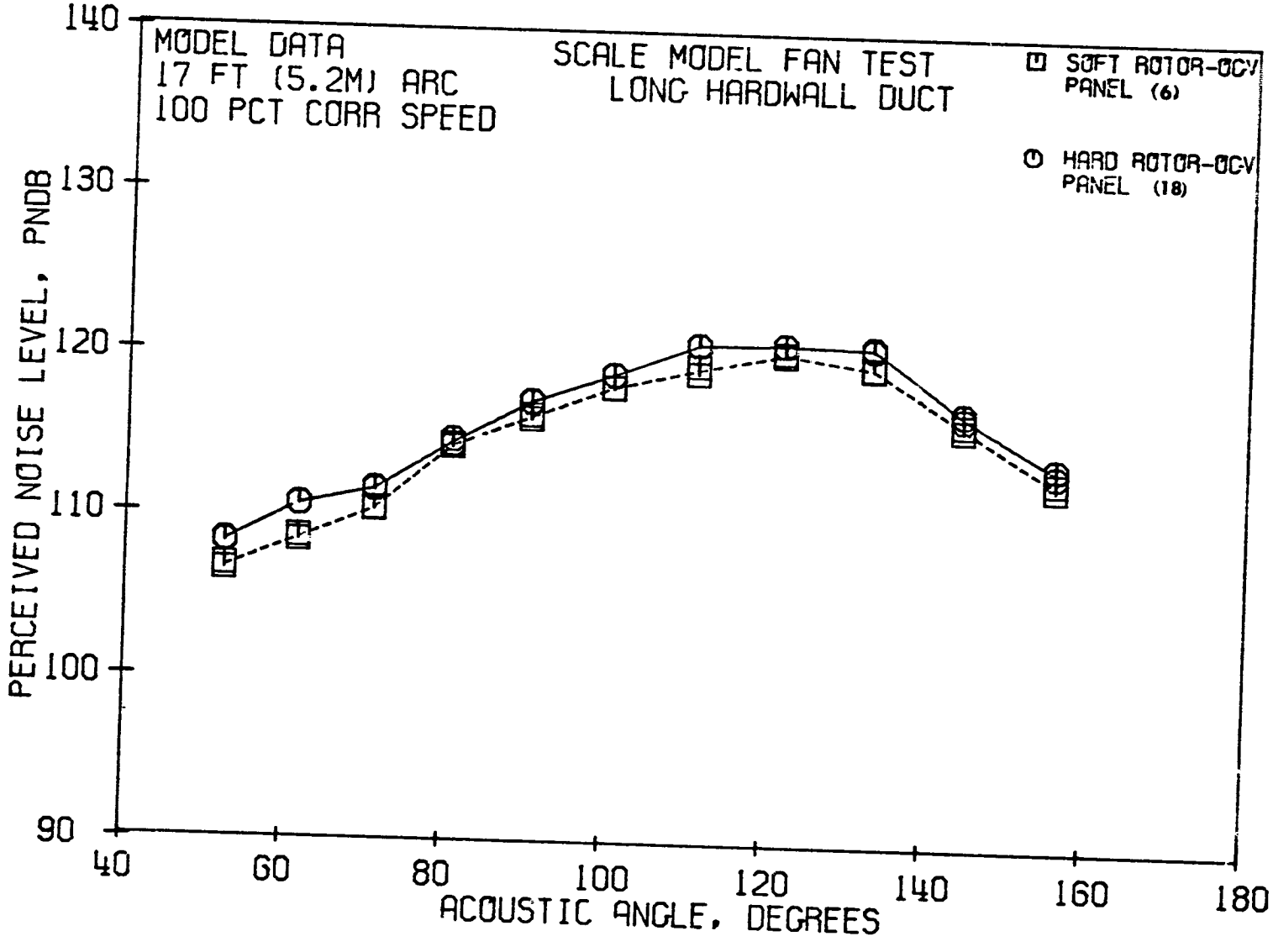

FIGURE 69 EFFECT OF ROTOR-OGV TREATMENT ON PNL DIRECTIVITY AT 100% $N/\sqrt{\theta}$

- NOMINAL NOZZLE
- HARD ROTOR-OGV
- POROSITY = 12%

CONFIGURATION 18, HARDWALL

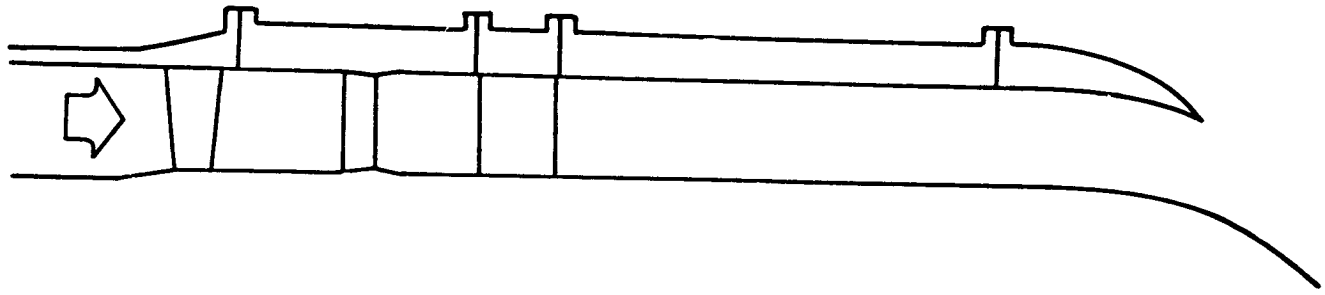

CONFIGURATION 7, TREATMENT L/H = 4.6

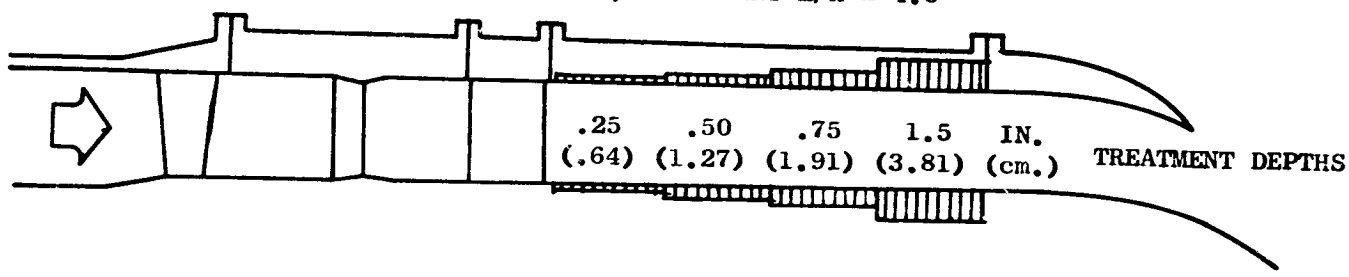

CONFIGURATION 75-9, TREATMENT L/H = 3.68

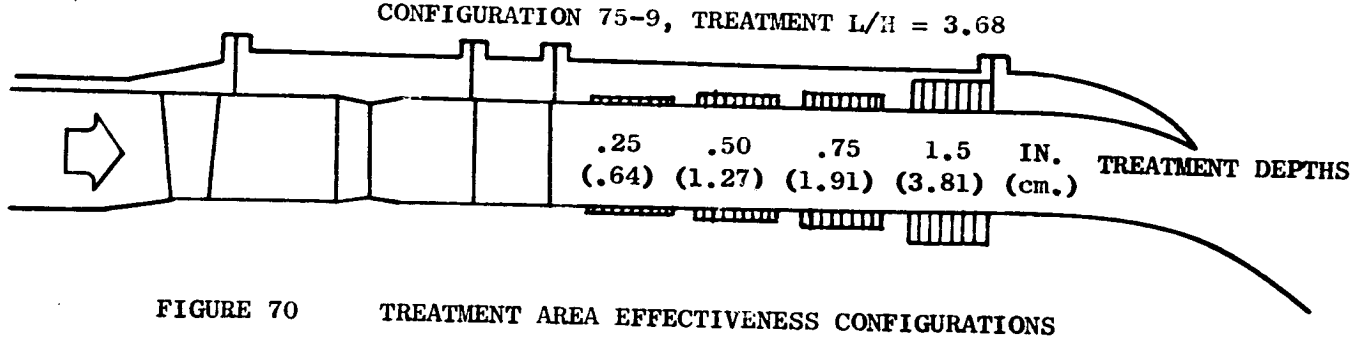

FIGURE 70 TREATMENT AREA EFFECTIVENESS CONFIGURATIONS

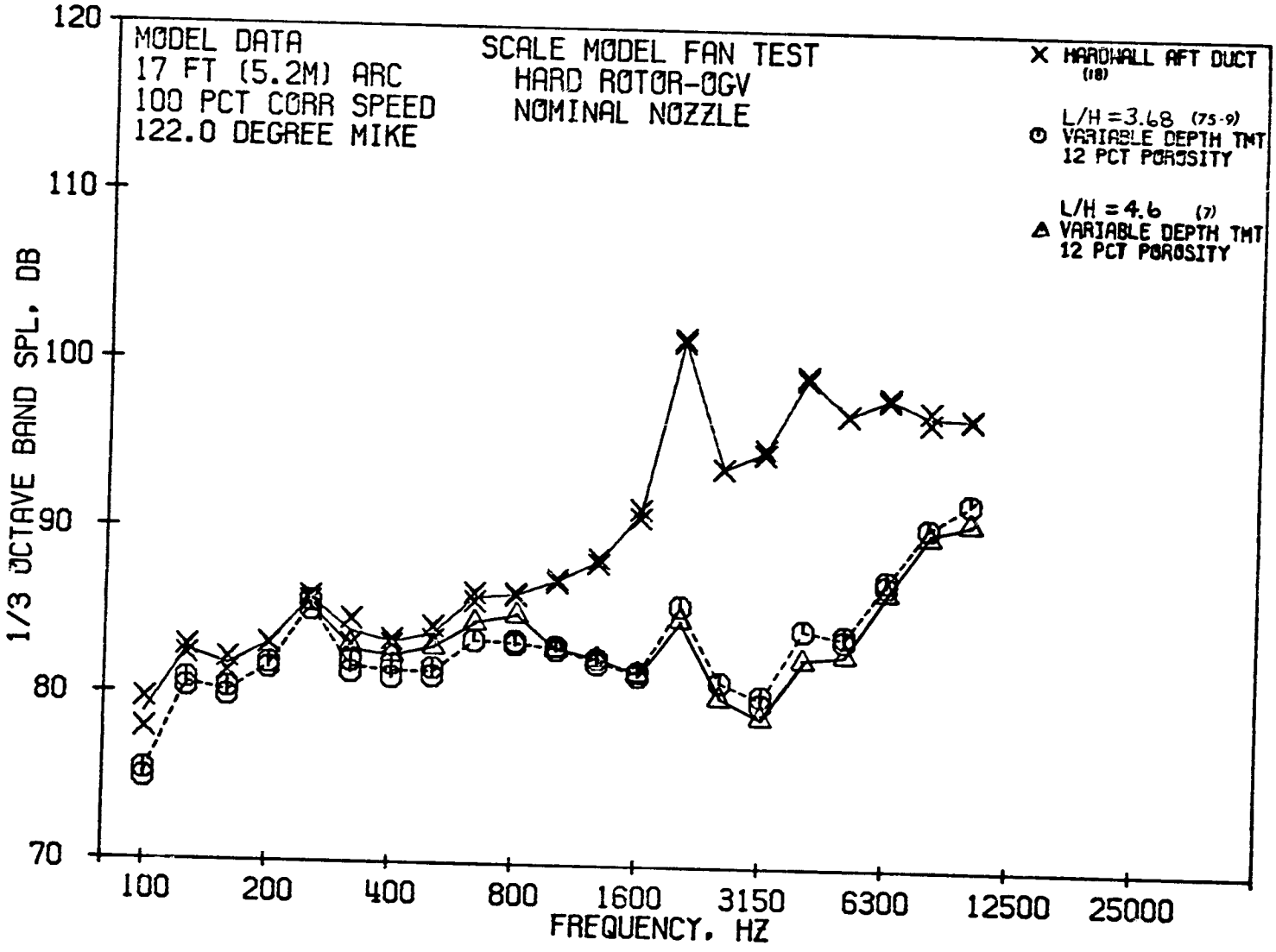

FIGURE 71 EFFECT OF TAPING ON TREATMENT EFFECTIVENESS

- HARD ROTOR-OGV
- TREATMENT L/H = 4.6

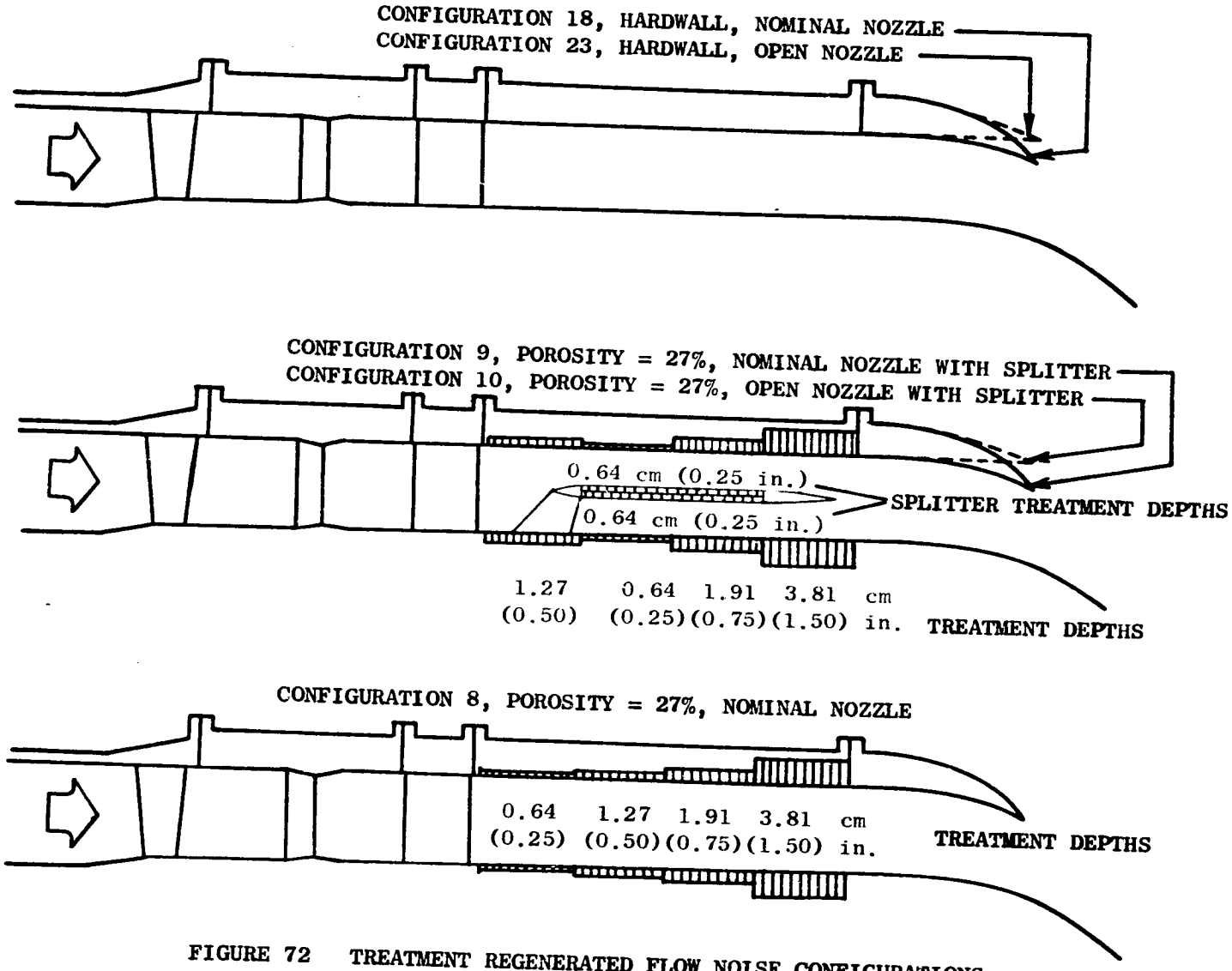

FIGURE 72 TREATMENT REGENERATED FLOW NOISE CONFIGURATIONS

Figure 73 compares the aft suppression achieved by three configurations - nominal nozzle without splitter, nominal nozzle with splitter, and open nozzle with splitter at 100% $N/\sqrt{\theta}$. For the same fan speed these three configurations represent an increase in the aft duct Mach number as previously indicated by Figure 22. There is a suppression increase evident above 4000 Hz due to installation of the splitter; however, further opening the nozzle did not result in any appreciable change in suppression except perhaps at 4000 Hz. If flow noise were a limiting item, then one would anticipate a decrease in suppression with the open nozzle plus splitter.

Aft suppression variation at 122 degrees for the nominal nozzle without splitter configuration is presented in Figure 74 and shows little change with fan speed. In fact, the peak suppression is achieved at 2000 Hz at 100% $N/\sqrt{\theta}$. Part of this may be due to the fact that the BPF at 100% $N/\sqrt{\theta}$ falls in the 2000 Hz 1/3-octave band; however, other frequencies show no degradation of suppression with fan speed and corresponding Mach number increase.

The variation of 122 aft degree suppression with fan speeds is presented in Figure 75 for the nominal nozzle with splitter configuration. There is no significant change between 70 and 100% $N/\sqrt{\theta}$. As before, there is little difference between the suppressions achieved with the 100% $N/\sqrt{\theta}$ or highest duct Mach number generally being the best. This trend continues at high frequencies as the nozzle is opened with the splitter installed as shown in Figure 76. There is an indication in Figure 76 at 2500 to 5000 Hz that the suppression achieved at 100% $N/\sqrt{\theta}$ is less than that at lower speeds. Apparently, the duct Mach numbers were not high enough to generate flow noise levels which significantly degraded suppression levels.

A flow noise related phenomenon was observed in all configurations which were tested with 12 percent porosity faceplate. The phenomenon was observed at the lower fan speeds and was visible as a sharp tone at 12500 Hz. Figures 77 and 78 at 70 and 80% $N/\sqrt{\theta}$, respectively, show this tone. Reference 7 discusses these tones which are generated by the interaction of the vortex wave, "psuedo sound", and the actual wave. They are the result of flow pulsations or eddies synchronized by the sound occurring at the edges of the face sheet perforations. The frequency at which the tone is generated is given by the expression

$$f = \frac{n\ c\ q\ M\ (1+M)}{L\ (1+M - qM)}$$

where
- f - frequency of tone
- n - integer (in practice n = 1 or 2)
- q - flow speed factor, fraction of freestream Mach number at which eddies propagate
- M - freestream Mach number
- c - speed of sound
- L - perforation spacing in the direction of flow.

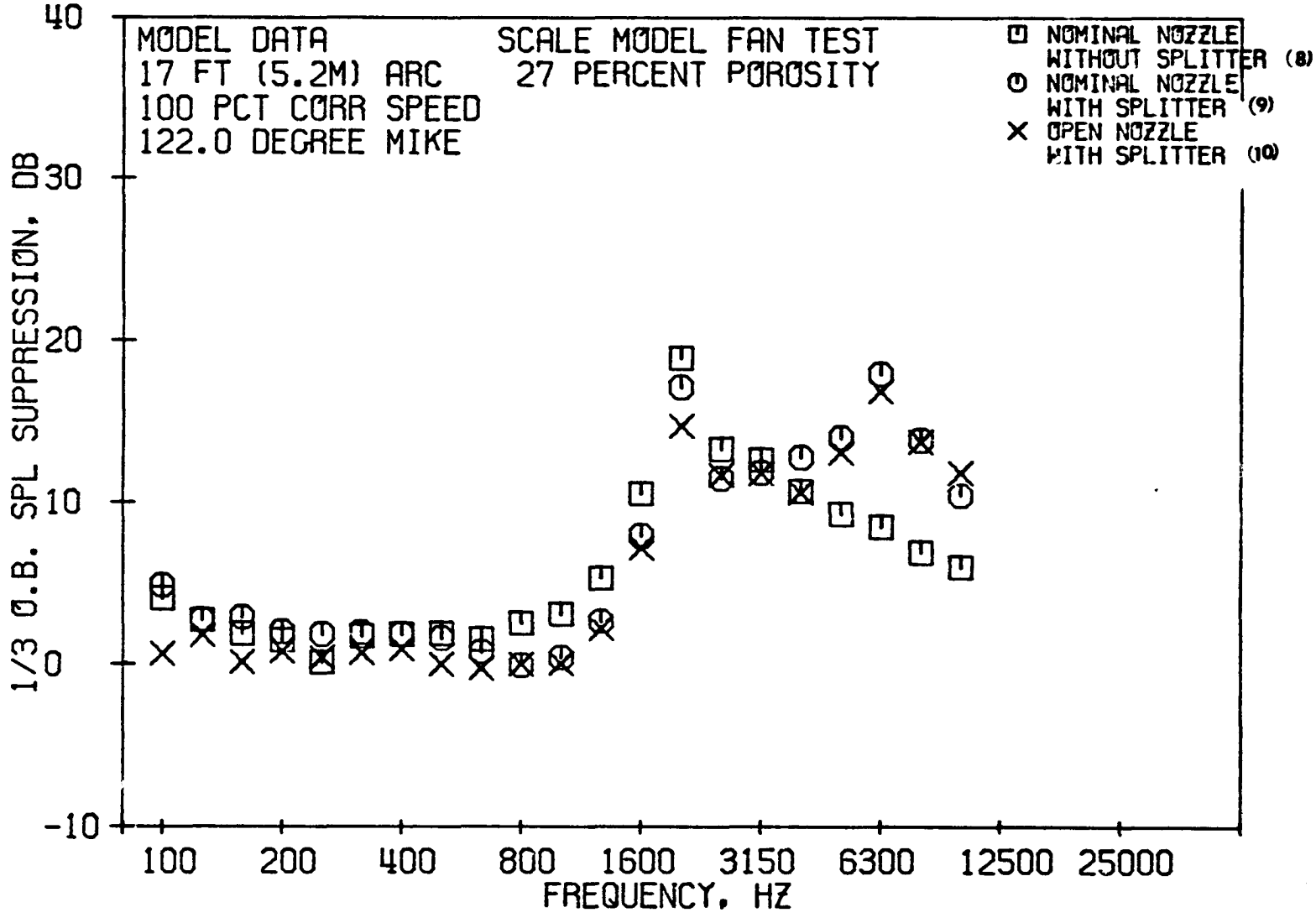

FIGURE 73 AFT SUPPRESSION AT 100% $N/\sqrt{\theta}$

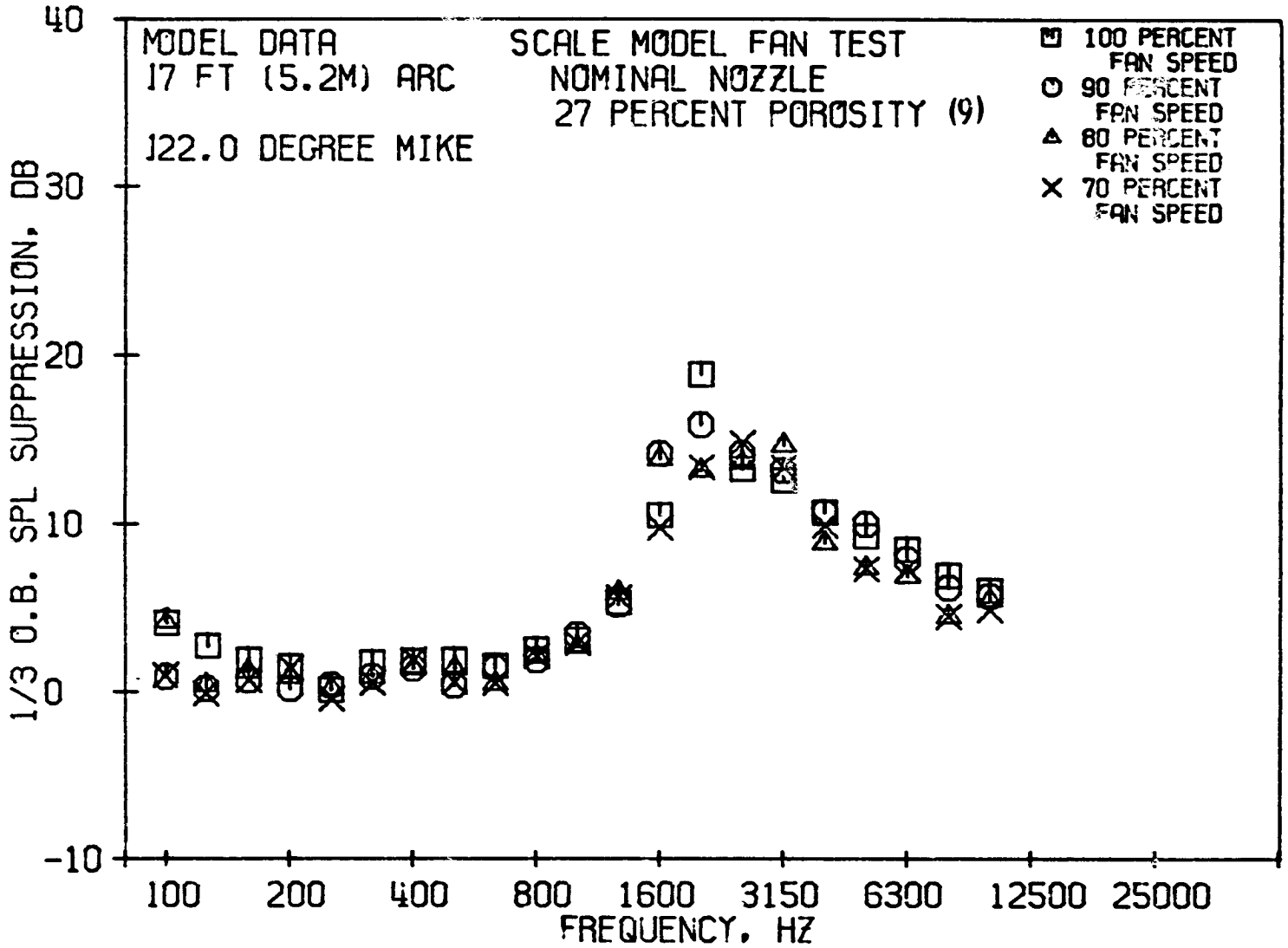

FIGURE 74 AFT SUPPRESSION CHANGE WITH FAN SPEED, NOMINAL NOZZLE WITHOUT SPLITTER

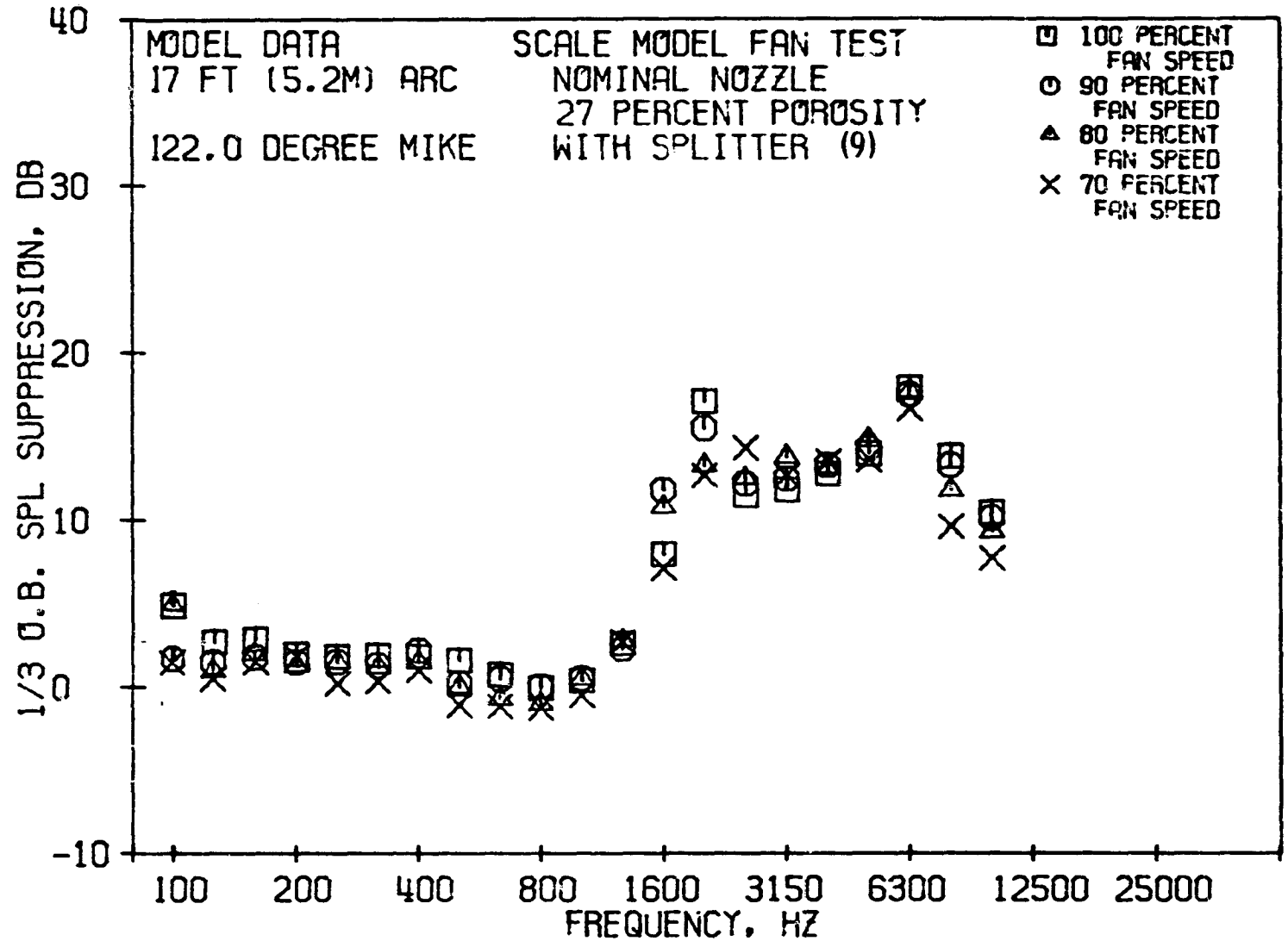

FIGURE 75 AFT SUPPRESSION CHANGE WITH FAN SPEED, NOMINAL NOZZLE WITH SPLITTER

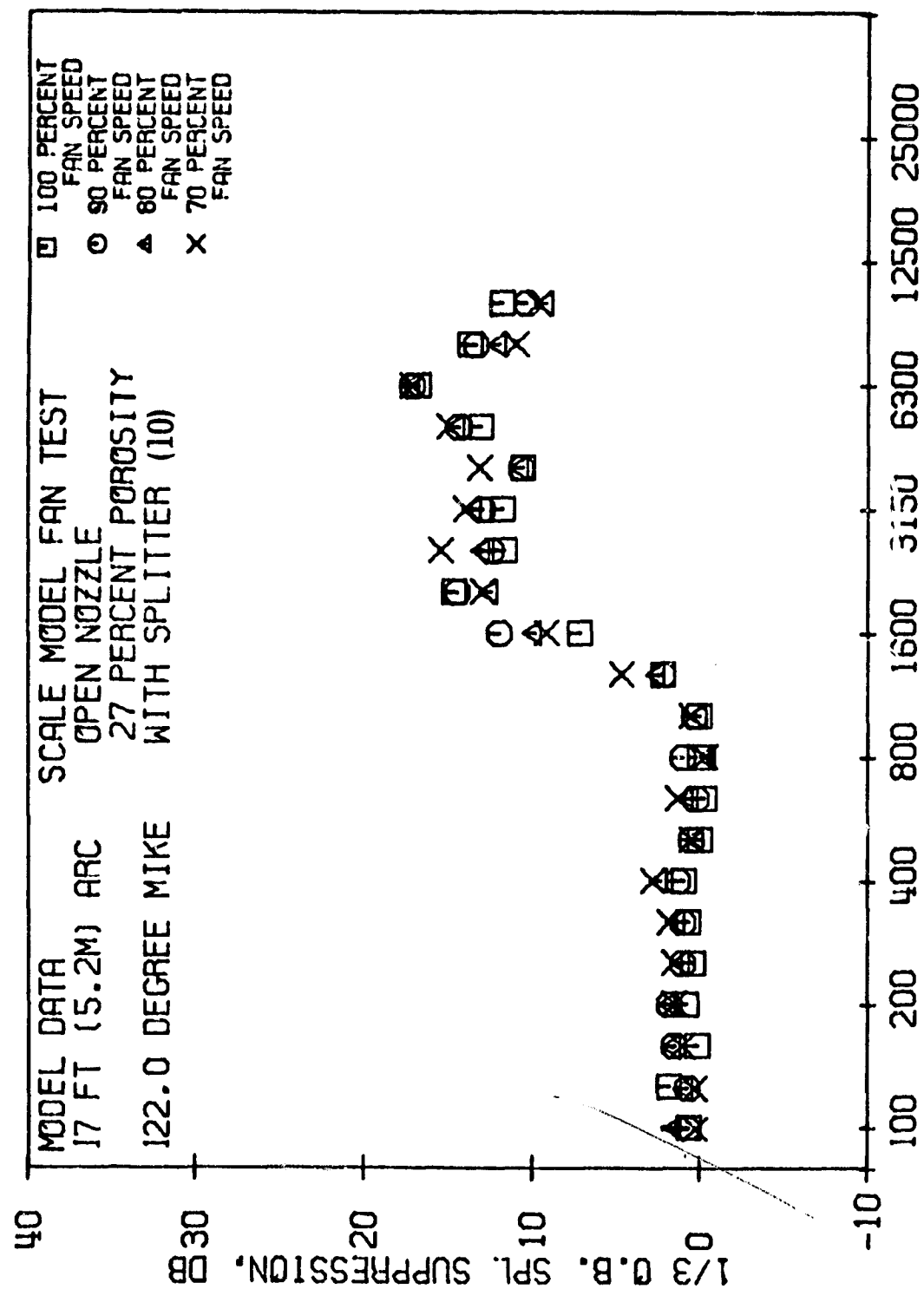

FIGURE 76 AFT SUPPRESSION CHANGE WITH FAN SPEED, OPEN NOZZLE WITH SPLITTER

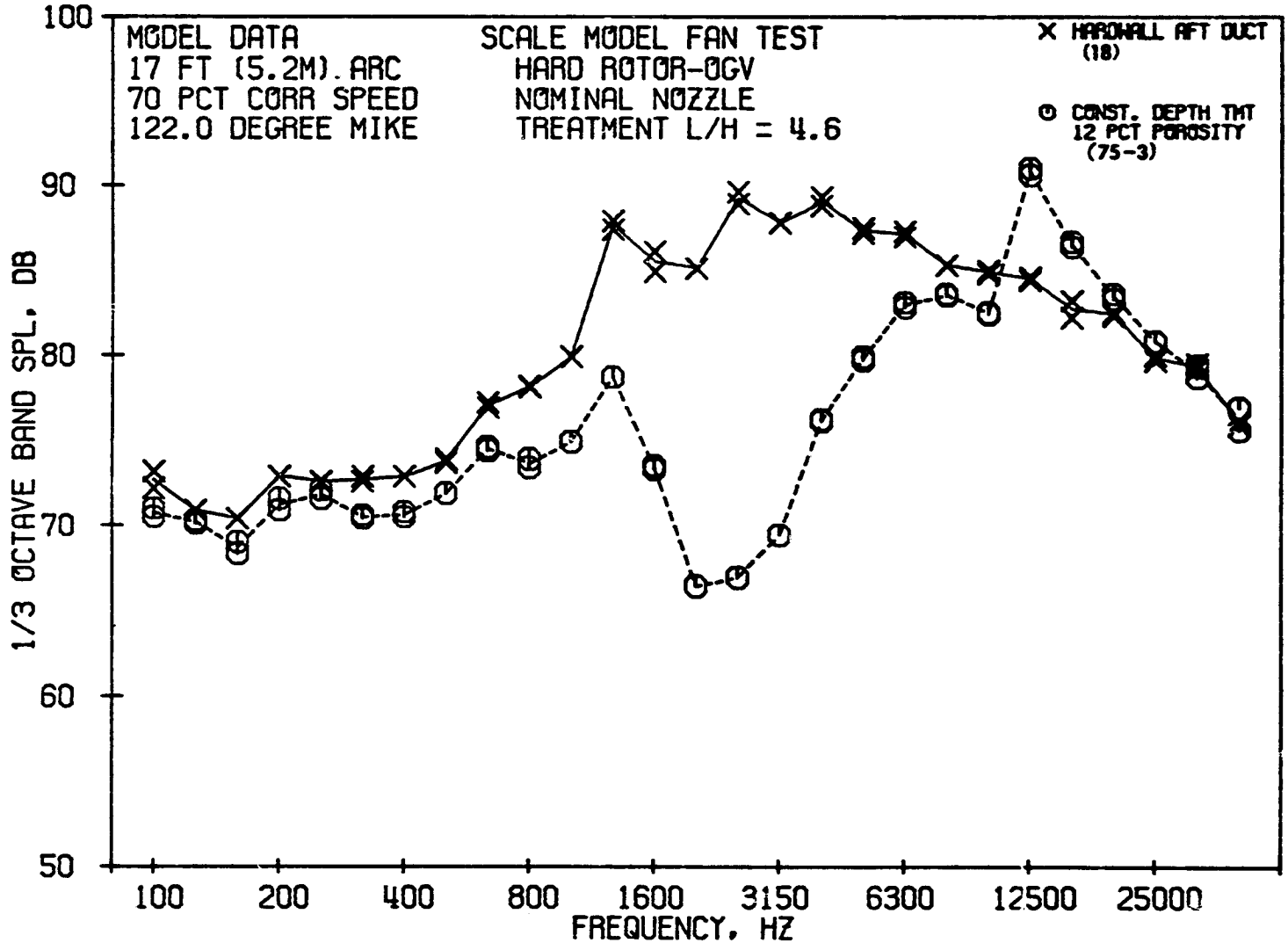

FIGURE 77 12 PERCENT POROSITY CONSTANT DEPTH SPL'S AT 70% $N/\sqrt{\theta}$

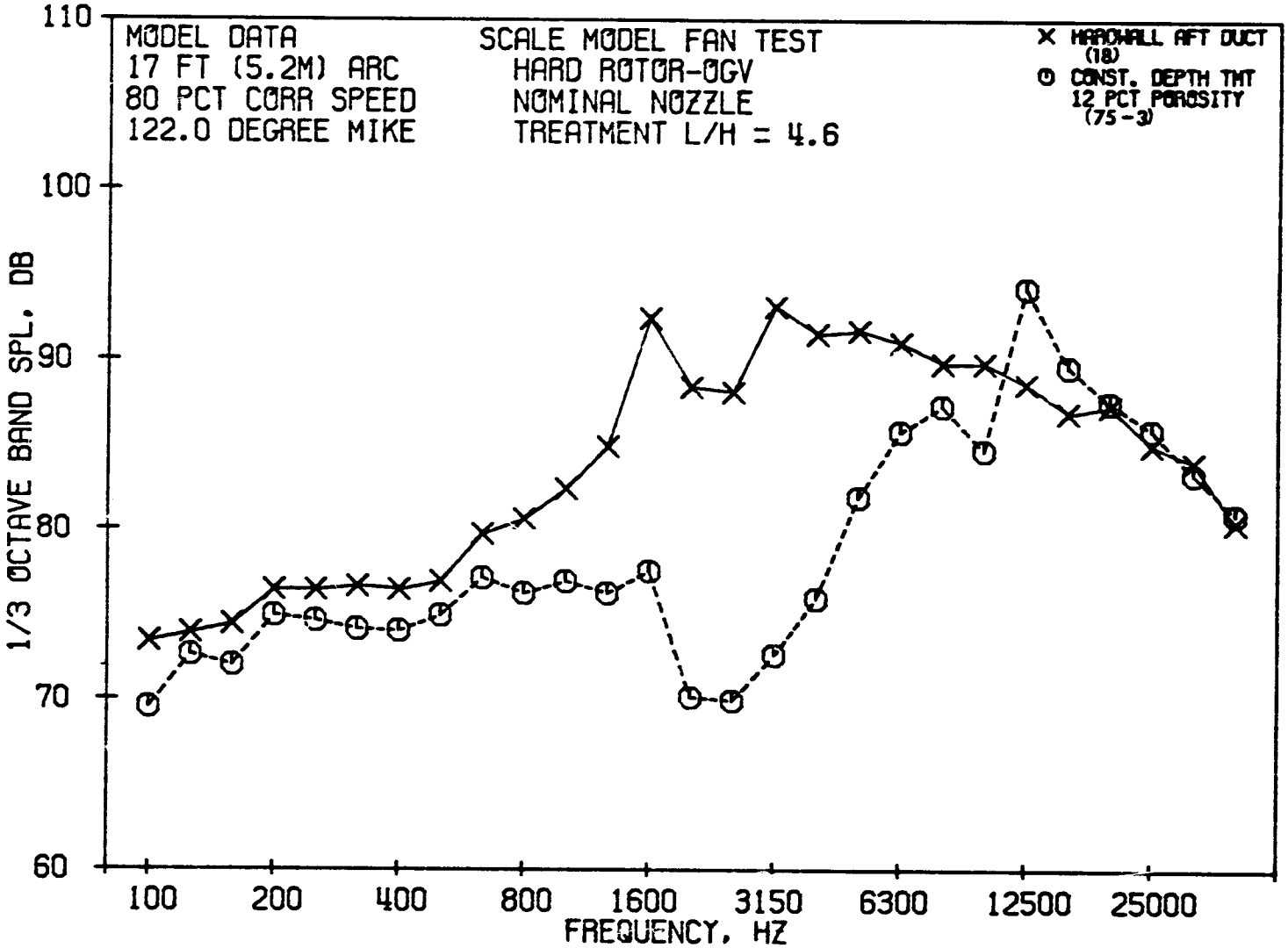

FIGURE 78 12 PERCENT POROSITY CONSTANT DEPTH SPL'S AT 80% $N/\sqrt{\theta}$

Using the above theory for the 12 percent porosity faceplate with L = 0.16 inches (0.41 cm) and q = 0.47, a frequency of 13500 Hz is obtained which is within the 12500 Hz 1/3-octave band. At speeds above 80% $N/\sqrt{\theta}$, the tone is not visible. For the 27 percent porosity configurations, a tone at 34000 Hz would be predicted.

This phenomena will be investigated further when narrowbands are processed. The key point is that these tones could influence the data - especially when scaled to full size engine levels - and should be evaluated for each treatment design.

SECTION IX

CONCLUSIONS

- Second harmonic tone reductions were achieved at close (one-half chord) spacing at a vane-blade ratio of 1.87. No significant differences in second harmonic noise level were observed at 1.5 chord spacing.
- At wide rotor-stator spacings the noise levels appear to be controlled by rotor-turbulence interaction noise, not rotor-stator noise.
- Variable depth treatment panels achieved somewhat wider bandwidth suppressions than a constant thickness treatment.
- Configurations designed to simulate variable depth wall treatment opposite constant thickness splitter treatment indicate no significant loss in suppression for such an arrangement.
- Variations in aft duct Mach number up to about 0.53 indicated no significant contribution of treatment regenerated flow noise which would degrade suppression levels.
- No significant change in fan broadband noise level was observed by lowering the Mach number through the vane row; however, any changes may be masked by rotor turbulence noise.
- Rotor-OGV frame treatment achieved 4 to 5 dB BPF tone suppression at all angles.
- The measured suppression loss (-.6 to 0 PNdB at 100% $N/\sqrt{\theta}$) due to treatment area blockage was less than one would predict for 20 percent loss in treatment length.
- With a constant or variable depth treatment configuration, twelve percent porosity gave more suppression (1 to 2 PNdB) than 27 percent porosity.

SECTION X

NOMENCLATURE

Symbol or Abbreviation	Definition	Units
BPF	Blade passing frequency	Hz
c	Speed of sound	ft/sec (m/sec)
c	Chord	in. (cm)
C_p	Static pressure coefficient	---
f	Frequency	Hz
H	Duct height	ft (m)
L	Distance between holes Treatment length	ft (m) ft (m)
M	Mach number	--
n	Integer (1 or 2)	--
N	Fan speed	RPM
OGV	Outlet guide vane	--
PNL	Perceived noise level	PNdB
ΔP_s	Hub static pressure rise between rotor and stator	psia (N/m^2)
P_s	Static Pressure	psia (N/m^2)
$\overline{P_t}$	Mass weighted discharge pressure	psia (N/m^2)
PWL	Sound power level, re 10^{-13} watts	dB
q	Fraction of freestream Mach number	--
SPL	Sound pressure level, re .0002 microbar	dB
t_m	Maximum vane thickness	in. (cm)
δ	Relative absolute pressure	
λ	Wavelength	ft (m)
θ	Relative absolute temperature	

SECTION XI

REFERENCES

1. Lewis, Jr., G.W., and Tysl, E.R.; Overall and Blade-Element Performance of a 1.20 Pressure-Ratio Fan Stage at Design Blade Setting Angle, NASA TM X-3101, September 1974.

2. Mani, R., "Discrete Frequency Noise Generation from an Axial Flow Fan Blade Row," Paper 69-GE-12, ASME, presented at Applied Mechanics and Fluids Engineering Conference, June 16-18, 1969.

3. Cumpsty, N.A. and Lowrie, B.W., "The Cause of Tone Generation by Aero-Engines at High Subsonic Tip Speeds and the Effect of Forward Speed," ASME Paper 73-WA/GT-4, November 1973.

4. Hanson, D.B., "Spectrum of Rotor Noise Caused by Atmospheric Turbulence," J. Acous. Soc, Am., 56, 1, July 1974.

5. A. Silverstein, S. Katzoff, and W.K. Bullivant, "Downwash and Wake Flow Behind Plain and Flapped Airfoils," NACA Tech. Rep. No. 651 (1939)

6. Roundhill, J.P. and Shaut, L.A., "Model and Full Scale Test Results Relating to Fan Noise In-Flight Effects," AIAA Paper 75-465, March 1975.

7. Meyer, F. and Neumann, E., Physical and Applied Acoustics, Academic Press, 1972, New York.